

Final Technical Report
Research Project T9233, Task 41
Seismic Vulnerability—Alaskan Way Viaduct II

**SEISMIC VULNERABILITY OF THE ALASKAN
WAY VIADUCT: SED TYPICAL UNIT**

by

Paul Knaebel
Graduate Research Assistant
Department of Civil Engineering
University of Washington

Marc O. Eberhard
Assistant Professor
Department of Civil Engineering
University of Washington

Jaime De la Colina
Research Associate
Department of Civil Engineering
University of Washington

Washington State Transportation Center (TRAC)
University of Washington,
University District Building
1107 NE 45th Street, Suite 535
Box 354802
Seattle, Washington 98105-4631

Washington State Department of Transportation
Technical Monitor
Timothy M. Moore
Senior Structural Engineer

Prepared for
Washington State Transportation Commission
Department of Transportation
and in cooperation with
U.S. Department of Transportation
Federal Highway Administration

July 1995

TECHNICAL REPORT STANDARD TITLE PAGE

1. REPORT NO. WA-RD 363.3	2. GOVERNMENT ACCESSION NO.	3. RECIPIENT'S CATALOG NO.	
4. TITLE AND SUBTITLE SEISMIC VULNERABILITY OF THE ALASKAN WAY VIADUCT: SED TYPICAL UNIT		5. REPORT DATE July 1995	
		6. PERFORMING ORGANIZATION CODE	
7. AUTHOR(S) Paul Knaebel, Marc O. Eberhard and Jaime De la Colina		8. PERFORMING ORGANIZATION REPORT NO.	
9. PERFORMING ORGANIZATION NAME AND ADDRESS Washington State Transportation Center (TRAC) University of Washington, Box 354802 University District Building; 1107 NE 45th Street, Suite 535 Seattle, Washington 98105-4631		10. WORK UNIT NO.	
		11. CONTRACT OR GRANT NO. Agreement T9233, Task 41	
12. SPONSORING AGENCY NAME AND ADDRESS Washington State Department of Transportation Transportation Building, MS 7370 Olympia, Washington 98504-7370		13. TYPE OF REPORT AND PERIOD COVERED Final technical report	
		14. SPONSORING AGENCY CODE	
15. SUPPLEMENTARY NOTES This study was conducted in cooperation with the U.S. Department of Transportation, Federal Highway Administration.			
16. ABSTRACT <p>An engineering team from the University of Washington (UW) evaluated the seismic vulnerability of the Alaskan Way Viaduct, located in Seattle, Washington. This report presents the evaluation of a typical three-bay unit that was designed by The City of Seattle Engineering Department (SED). The evaluation team performed response-spectrum analyses and nonlinear analyses for the fixed-base condition. The team considered a widely used soft-soil spectrum and worst-case, site-specific spectra. Wherever possible, the UW team evaluated the vulnerability for each failure mode following procedures proposed by the Applied Technology Council and by researchers at the University of California, San Diego.</p> <p>The evaluation team found that the vulnerability of the Alaskan Way Viaduct exceeds that of bridges built to current standards. The vulnerability is a result of a combination of two factors: (1) the design ground motion would strongly excite the viaduct; and (2) many of the structural components lack the ductility required by current standards. The following deficiencies were identified as the most critical.</p> <ul style="list-style-type: none"> • The lower-story columns have inadequate transverse reinforcement, and could fail in shear before they develop their flexural capacity. • The first- and second-story joints have inadequate confinement reinforcement, and during strong ground motions, they could experience a diagonal-tension failure. • If the base of the lower-story columns develop their flexural capacity, the footings could fail in shear. 			
17. KEY WORDS Bridge, earthquakes, evaluation, reinforced concrete		18. DISTRIBUTION STATEMENT No restrictions. This document is available to the public through the National Technical Information Service, Springfield, VA 22616	
19. SECURITY CLASSIF. (of this report) None	20. SECURITY CLASSIF. (of this page) None	21. NO. OF PAGES 144	22. PRICE

DISCLAIMER

The contents of this report reflect the views of the authors, who are responsible for the facts and the accuracy of the data presented herein. The contents do not necessarily reflect the official views or policies of the Washington State Transportation Commission, Department of Transportation, or the Federal Highway Administration. This report does not constitute a standard, specification, or regulation.

TABLE OF CONTENTS

<u>Section</u>	<u>Page</u>
Summary	ix
Chapter 1: Introduction	1
1.1 Context	1
1.2 Scope of Report	3
Chapter 2: Description of the Seattle Section	5
2.1 On Site Inspection	8
2.2 Framing of Typical Unit	10
2.3 Reinforcement of Typical Unit	13
Girders	13
End Bent	14
Interior Bent	14
Pile-Supported Footings	15
2.4 Material Properties	15
Chapter 3: Linear, Dynamic Analysis	17
3.1 Description of Structural Model	17
3.2 Gravity Analysis	19
3.3 Modal Analysis	22
3.4 Response-Spectrum Analysis	24
Transverse Direction	25
Longitudinal Direction	29
3.5 Flexural Capacity-to-Demand Ratios	29
Transverse Direction	31
Longitudinal Direction	33
Chapter 4: Nonlinear, Static Analysis	35
4.1 Description of Analysis	35
4.2 Transverse Direction Response	38
Interior Frame Response	38
Exterior Frame Response	44
4.3 Longitudinal Direction Response	48
4.4 Plastic-Hinge Analysis	49
4.5 Comparison with the WSDOT Unit	55
Chapter 5: Flexural Ductility	57
5.1 ATC-6-2 Evaluation	57
5.2 Priestley et al. (1992) Evaluation (UCSD)	60
Equivalent Elastic Strength, V_E	60
Base-Shear Demand, V_D	64
Global Capacity-to-Demand Ratios	66
5.3 Global Ductility Demands	67

TABLE OF CONTENTS (Continued)

<u>Section</u>	<u>Page</u>
Chapter 6: Shear	69
6.1 ATC-6-2 Evaluation.....	70
Transverse Direction	72
Longitudinal Direction	74
6.2 Priestley et al. (1994) Evaluation (UCSD).....	75
6.3 Combined Evaluation.....	76
Chapter 7: Anchorage	79
7.1 ATC-6-2 Evaluation.....	79
Columns	81
Transverse Beams	83
Longitudinal Girders	83
7.2 Priestley et al. (1992) Evaluation (UCSD).....	84
Columns	87
Transverse Beams	87
Longitudinal Girders	88
7.3 Combined Assessment	88
Chapter 8: Splices	91
8.1 ATC-6-2 Evaluation.....	92
8.2 Priestley et al. (1992) Evaluation (UCSD).....	95
8.3 Combined Assessment	96
Chapter 9: Joints	97
9.1 Effective Joint Areas	97
9.2 Evaluation	99
Chapter 10: Pile-Supported Footings	103
10.1 Pile Forces	105
10.2 Flexure	107
10.3 Shear.....	108
10.4 Column-to-Footing Joints	109
Chapter 11: Recommendations	111
11.1 Vulnerabilities	111
Column Shear Failure	111
Anchorage Failure	112
Splice Failure	112
Joint Shear Failure	113
Footing Failure	113

TABLE OF CONTENTS (Continued)

<u>Section</u>	<u>Page</u>
Chapter 11: Recommendations (Continued)	
11.2 Retrofit Priorities.....	113
11.3 Comparison with Typical WSDOT Unit	114
Columns	115
Joints	115
Lower-Story Lap Splices	115
Footings.....	116
Upper-Story Lap Splices	116
Acknowledgments	117
References	119
Appendix A: Structural Drawings of Typical Section	
Appendix B: Calculations of ATC-6-2 Flexural C/D Ratios	
Appendix C: Calculations of all other ATC-6-2 C/D Ratios	

LIST OF FIGURES

<u>Figure</u>		<u>Page</u>
1.1	Aerial Photograph of the Alaskan Way Viaduct	2
2.1	Single- to Double-Deck Transition (Bents 53 through 63)	6
2.2	Pedestrian Undercrossing Near Bent 87	7
2.3	Shear Cracks in Outrigger Beam at Bent 56.....	9
2.4	1.5 Inch Expansion Gap Between Units	11
2.5	Deck Framing of the Typical SED Unit	12
3.1	Three-dimensional Finite Element Model of the Typical SED Unit	18
3.2	Gravity Moment and Shear Diagrams - Exterior Frame	20
3.3	Gravity Moment and Shear Diagrams - Interior Frame	21
3.4	Gravity Moment and Shear Diagrams - Longitudinal Direction	23
3.5	ATC-6 Response Spectrum (0.25g).....	25
3.6	Seismic Moment and Shear Diagrams - Exterior Frame	26
3.7	Seismic Moment and Shear Diagrams - Interior Frame	28
3.8	Seismic Moment and Shear Diagrams - Longitudinal Direction.....	30
3.9	Column Analysis Locations.....	31
3.10	Flexural C/D Ratios for Transverse Frames	32
3.11	Flexural C/D Ratios for a Longitudinal Frame	33
4.1	Locations of Column Segment Ends	36
4.2	Lateral Force-Displacement Relations - Transverse Direction	39
4.3	Moment Diagrams for Interior, Transverse Beams	40
4.4	Moment Diagrams for Interior, Transverse Columns.....	42
4.5	Flexural Capacity/Demand Ratios for Interior Frames	43
4.6	Moment Diagrams for Exterior, Transverse Beams	45
4.7	Moment Diagrams for Exterior, Transverse Columns	46
4.8	Flexural Capacity/Demand Ratios for Exterior Frames	47
4.9	Lateral Force-Displacement Relationships for Longitudinal Frames.....	48
4.10	Moment Diagrams for Exterior, Longitudinal Girders.....	50
4.11	Moment Diagrams for Longitudinal Columns	51
4.12	Flexural Capacity/Demand Ratios for Longitudinal Frame	52
4.13	Plastic-Hinging Mechanisms 1 through 3.....	53
5.1	ATC-6-2 C/D Ratios for Transverse Confinement, r_{cc}	59
5.2	Site-specific Response Spectrum.....	61
5.3	Base Shear-Displacement Curves - Transverse Direction	63
6.1	Variation of Shear Resistance with Ductility	70
6.2	Shear C/D Ratios for Transverse Frames	73
6.3	Shear C/D Ratios for Longitudinal Frame	74
8.1	Lap Splices for Interior, Lower-Story Columns	92
9.1	Effective Joint Areas and Designations - Transverse Direction	98
9.2	Effective Joint Areas and Designations - Longitudinal Direction	99
10.1	Footing Configurations and Plan Dimensions	104
10.2	Typical SED Unit Footing	105

LIST OF TABLES

<u>Table</u>	<u>Page</u>
3.1 Computed Modal Properties	22
3.2 Story Drifts and Drift Ratios.....	27
4.1 Assumed Material Properties.....	37
4.2 Summary of Plastic-Analysis Results.....	54
4.3 Summary of Nonlinear Analyses.....	55
5.1 Computed Displacements	65
5.2 Equivalent Elastic Base-Shear Strengths.....	66
5.3 Global Capacity-to-Demand Ratios.....	66
5.4 Global Ductility Demands	67
6.1 Priestley et al. (1994) Shear Evaluation for Columns	77
7.1 Required Embedment Lengths	82
7.2 ATC-6-2 Anchorage Evaluation for Column Bars into Cap Beams	82
7.3 ATC-6-2 Anchorage Evaluation for Transverse Beams.....	82
7.4 ATC-6-2 Anchorage Evaluation for Longitudinal Girders	83
7.5 Priestley et al. (1992) Anchorage Evaluation	86
8.1 ATC-6-2 Column Splice C/D Ratios, r_{cs}	94
8.2 Priestley et al. (1992) Splice Evaluation.....	96
9.1 Joint-Shear C/D Ratios	101
10.1 Pile Forces - Assuming Connections Have Tensile Capacity	106
10.2 Pile Forces - Assuming Connections Have No Tensile Capacity.....	107
10.3 Footing Flexural C/D Ratios - Transverse Direction.....	108
10.4 Footing Shear C/D Ratios - Transverse Direction	109
10.5 Column-To-Footing Joint Shear C/D Ratios	110
11.1 Priority Ratings For Retrofit Measures.....	114

SUMMARY

At the request of the Washington State Department of Transportation (WSDOT), an engineering team from the University of Washington (UW) evaluated the seismic vulnerability of the Alaskan Way Viaduct. The viaduct is a 2.2-mile long, reinforced concrete structure that runs parallel to the shore of Elliot Bay in Seattle, Washington. The viaduct was selected for detailed evaluation for the following reasons: (1) it is an important link in the region's transportation network; (2) it is underlain by loose, hydraulic fills; (3) its reinforcement details do not satisfy current code requirements; and (4) its geometry is similar to double-deck structures that were damaged during the 1989 Loma Prieta Earthquake. An overview of the Alaskan Way Viaduct evaluation is provided by Kramer and Eberhard (1995).

This report presents the evaluation of a typical three-bay unit that was designed by The City of Seattle Engineering Department (SED). A companion report by Eberhard et al. (1995) discusses the vulnerability of the typical unit that WSDOT designed, and a third report by Kramer et al. (1995) considers the viaduct's geotechnical hazards. The results of the geotechnical study provided the structural team with estimates of ground motions and liquefaction potential for the various site profiles.

The evaluation team performed linear response-spectrum analyses and nonlinear static analyses for the fixed-base condition. The pinned-base condition was not considered because the columns did not have longitudinal reinforcement splices at the base of the column. The response-spectrum analyses were computed with a three-dimensional model of the typical unit. The team considered a soft-soil spectrum (ATC-6, 1981) and worst-case, site-specific spectra. Two-dimensional, nonlinear analyses were performed for typical longitudinal and transverse frames. Wherever possible, the UW team evaluated the vulnerability for each failure mode following two procedures. These procedures included those proposed; by the Applied Technology Council (ATC-6-2, 1983); by Priestley et al. (1992); by Priesley et al. (1994); and by Thewalt and Stojadinvic (1992).

The evaluation team found that the vulnerability of the Alaskan Way Viaduct exceeds that of bridges built to current standards. The vulnerability is a result of a combination of two factors: (1) the ground motions are likely to strongly excite the viaduct; and (2) many of the structural components are likely to behave in a brittle manner. The following deficiencies were identified as the most critical.

- The lower-story columns have inadequate transverse reinforcement, and would fail in shear before they developed their flexural capacity.
- The first- and second-story joints have inadequate confinement reinforcement, and during strong ground motions, they could experience a diagonal-tension failure.
- If the base of the lower-story columns develop their flexural capacity, the footings could fail in shear.

The typical SED and WSDOT units have similar span lengths, widths, heights, column sizes, weights, mode shapes, and periods of vibration. However, their seismic deficiencies are not identical because the reinforcement details and horizontal framing configuration differ. The SED and WSDOT typical units differ in the following ways:

- The lower-story column bars were lap-spliced at the column base in the WSDOT unit, but not in the SED unit. As a consequence, the WSDOT columns are more likely to lose their flexural capacity at the base.
- The columns of the SED unit have significantly higher flexural capacities than those of the WSDOT unit. As a result, the SED columns are less likely to fail in flexure, but they are more likely to fail in shear than the WSDOT columns.
- The column bars of the WSDOT unit are anchored into the footings with outward hooks. In contrast, the column bars of the SED unit are welded to steel frames that are embedded into the footings.

Some of the deficiencies of the SED and WSDOT units are similar:

- The upper- and lower-story joints of both the SED and WSDOT units are vulnerable to diagonal-tension failure.
- The footings of both the SED and WSDOT units are vulnerable to shear failure.

CHAPTER 1

INTRODUCTION

1.1 CONTEXT

The Alaskan Way Viaduct, shown in Figure 1.1, is an elevated, reinforced concrete structure that follows the shoreline of Elliott Bay in downtown Seattle. In the 1950s, the Alaskan Way Viaduct was the main north-south arterial for the City of Seattle. The viaduct was constructed to relieve congestion from Seattle's streets, especially that caused by heavy truck traffic. Today the Alaskan Way Viaduct is still an important link in Seattle's transportation network. Approximately 86,000 vehicles use the viaduct each day.

The Alaskan Way Viaduct was designed by two agencies; the northern two thirds was designed by the City of Seattle Engineering Department (SED) in 1950, and the southern one third was designed by the Washington State Department of Transportation (WSDOT) in 1956. The SED-designed section starts in the north as a single-level bridge, and after one-half mile, it changes into a double-deck bridge. The SED section continues south as a double-deck bridge for three quarters of a mile, at which point the WSDOT-designed section begins. The WSDOT section remains a double-deck structure until it approaches the southern abutment, where the viaduct reverts to a single-deck structure.

The Alaskan Way Viaduct was built during the 1950s when seismic concerns were minimal. Many bridges that were built during that time have details that are inadequate to resist seismic loadings. For example, their columns often have inadequate transverse reinforcement for confinement and shear resistance, lap splice and anchorage lengths for reinforcement are sometimes too small, and footings typically have no top reinforcement.

The viaduct was built along Seattle's waterfront because the land was flat and because the waterfront was nearly vacant. Most businesses had moved to the south and to Harbor Island where newer facilities were built. Unfortunately, the soil conditions beneath



Figure 1.1. Aerial Photograph of the Alaskan Way Viaduct

the viaduct are poor and may compound its seismic vulnerability. The location of the existing waterfront was once part of Elliott Bay. Humans have reshaped the waterfront many times since the late 1800s to better accommodate maritime industries. The shoreline where the northern portion of the viaduct now exists was built up and extended into Elliott bay in the early 1900s. The southern portion of the viaduct rests on top of mud flats from the Duwamish River that were covered over with fill. Much of the fill material came from surrounding hills that were leveled off with water hoses, and the fill was transported to Elliott bay as a slurry through wood-stave pipes (Hershman et al., 1981). This loose, saturated fill that underlies the viaduct has a high potential for liquefaction and may amplify long-period ground motions. A team of geotechnical researchers at the University of Washington has investigated these possibilities, and the results are presented in a separate report (Kramer et al., 1995).

Recently, WSDOT began a program to evaluate the seismic vulnerability of Washington State bridges built before 1984 and retrofit them (McLean, 1994). WSDOT determined that the Alaskan Way Viaduct required special attention because of its importance in Seattle's transportation system. Two preliminary studies of the viaduct's seismic vulnerability were performed: one by WSDOT (Dodson et al., 1990) and one by the University of Washington (Brown et al., 1992). Both studies concluded that a more detailed evaluation was needed because of the bridges complex structure and surrounding soil conditions.

1.2 SCOPE OF REPORT

This report presents the results of a detailed evaluation of a typical SED unit. The results of an evaluation of the typical WSDOT unit were presented in a separate report (Eberhard et al., 1995). The procedures that were followed in the evaluation of the WSDOT unit were also followed in this study. The first procedure was presented by the Applied Technology Counsel in a report titled "Seismic Design Guidelines For Highway

Bridges, ATC-6-2" (ATC, 1983). The second procedure was developed at the University of California, San Diego (UCSD) by Priestley, Seible, and Chai (1992).

The SED unit was evaluated in both the transverse and longitudinal directions. The base was assumed to be fixed in all cases. The response spectrum from Section 5.2.2 of "Seismic Design Guidelines For Highway Bridges ATC-6" (ATC, 1981) was used in the ATC-6-2 evaluation. The response spectrum was constructed by assuming a soil type III and a peak ground acceleration of 0.25g. This was the same spectrum that was used in the evaluation of the typical WSDOT unit (Eberhard et al., 1995). A site-specific response spectrum was also developed by the Geotechnical researchers at the University of Washington (Kramer et al., 1995). Both the ATC-6 and site-specific response spectra were used in the Priestley et al. (1992) evaluation.

Chapter 2 describes the typical SED unit's geometry, reinforcing layout, and material properties. The unit's details are provided in Appendix A. Observations made from a brief on-site inspection are also presented in Chapter 2. Chapter 3 discusses the three-dimensional, linear, dynamic analysis used in the ATC-6-2 evaluation. It includes a description of the model, results of the gravity and dynamic analysis, and computations of the flexural capacity-to-demand ratios. Chapter 4 discusses the two-dimensional, nonlinear, static analysis used in the Priestley et al. (1992) evaluation. Chapters 5 through 10 discuss the results of the ATC-6-2 and the Priestley et al. (1992) evaluations for various failure modes. These modes include confinement, anchorage, lap-splice, joint, and footing failures. Finally, recommendations are presented in Chapter 11.

CHAPTER 2

DESCRIPTION OF THE SEATTLE SECTION

The Seattle section begins in the north at the Battery Street Tunnel and continues south 1.3 miles. The Seattle section starts as a single-deck structure (bents 1 thru 53), changes into a double-deck structure (bents 53 thru 63), and remains a double-deck structure to its end (bents 63 thru 121).

The double-deck portion of the Seattle section is constructed mainly of three-bay units. Adjacent units are separated by a 1.5-inch gap. Each unit is independent of the others, except that the end columns of adjacent units share a common footing. Two typical three-bay units make up the majority of the Seattle section's double-deck structure. Both typical SED units have the same deck and footing elevations, and both have similar framing systems. They differ in total span length (184-foot versus 222-foot) and in member sizes. The 184-foot unit was chosen for the detailed evaluation because it closely resembles the typical WSDOT unit. Comparisons could then be made between the SED and WSDOT units.

The Seattle section has some atypical features along its length. The viaduct changes from a single-deck to a double-deck structure between bents 53 and 63 (Figure 2.1). The geometry of this transition zone is extremely complex. Another atypical feature is short cantilever sections that provide clearance for pedestrian under-crossings (Figure 2.2). The Seattle section has two pedestrian under-crossings: one between bents 69 and 70, and one between bents 87 and 88. The Seattle section's double-deck structure has one curved section. The curved section is 406 feet long with an 800-foot radius. It consists of one curved 184-foot unit and one curved 222-foot unit. There are also numerous deck widenings for on- and off-ramps.

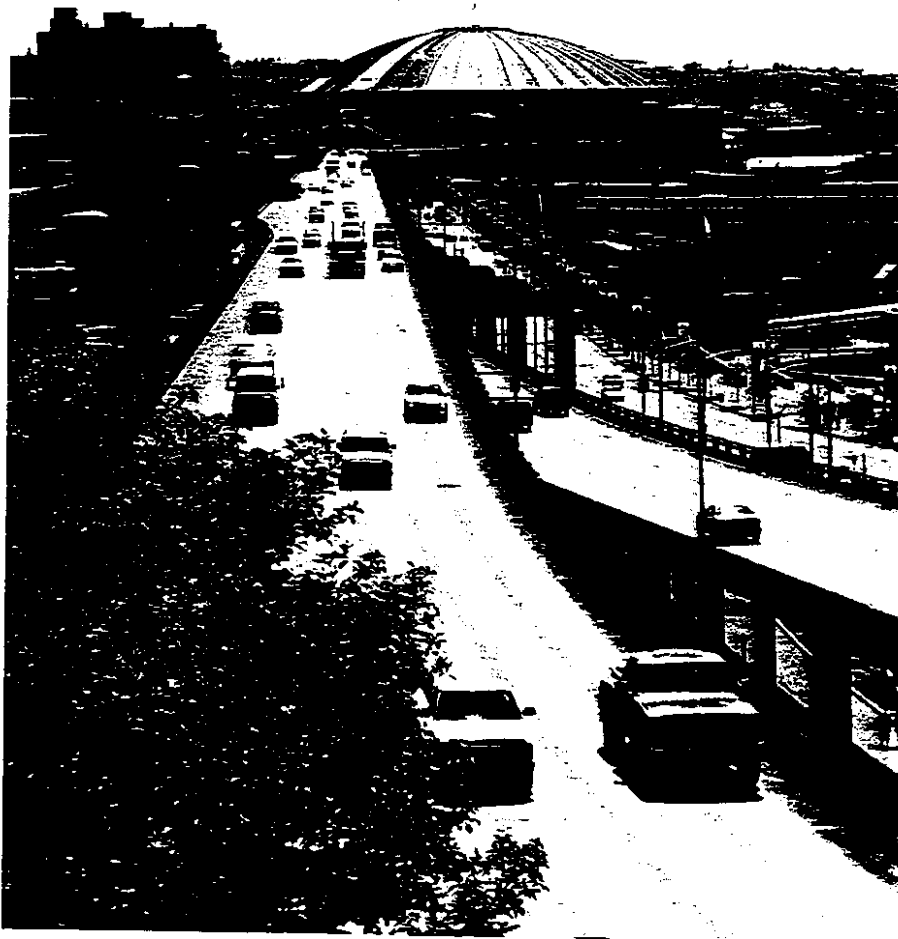


Figure 2.1. Single- to Double-Deck Transition (Bents 53 thru 63)



Figure 2.2. Pedestrian Undercrossing Near Bent 87

2.1 ON SITE INSPECTION

The researchers walked the length of the bridge to evaluate its present condition and search for damage. With a few exceptions, the present condition of the bridge is still very good, even after 40 years of weathering, heavy use, and one moderate earthquake (1965).

Many cracks were visible in the Seattle section. Most of the cracks were minor and expected. Some severe cracking was observed in outrigger beams that were used in the single-deck to double-deck transition zones and where columns were moved outward to avoid obstructions. Most outrigger beams had significant shear cracks. Figure 2.3 shows the extensive shear cracking at bent 56, which is located in the single- to double-deck transition zone.

Other shear cracks were present in crossbeams at the column bents. Shear cracks extended down and outward from conduit holes towards the columns at 45-degree angles. Most end-bent and some interior-bent crossbeams had such cracks.

Some column joints also had shear cracks where crossbeams were connected. These cracks extended from the outside of the longitudinal girders and upward at approximately 45 degrees. The pedestrian under-crossing between bents 87 and 88 provided a unique opportunity to view the face of an end column opposite an exterior girder. These faces are normally not visible because the end columns of abutting frames are only 1.5 inches apart. One column at the under-crossing had similar joint shear cracks in the face opposite the exterior girder. These cracks may have resulted from the shear generated by unbalanced moments from both the exterior girder and the cross beam. If similar cracks were present at other end bents, they could not be accessed.

Some exterior girders had vertical cracks at their ends where they connected to the columns. These cracks ran the full depth of the girders and continued up into the slabs. The cause of these cracks is unknown.

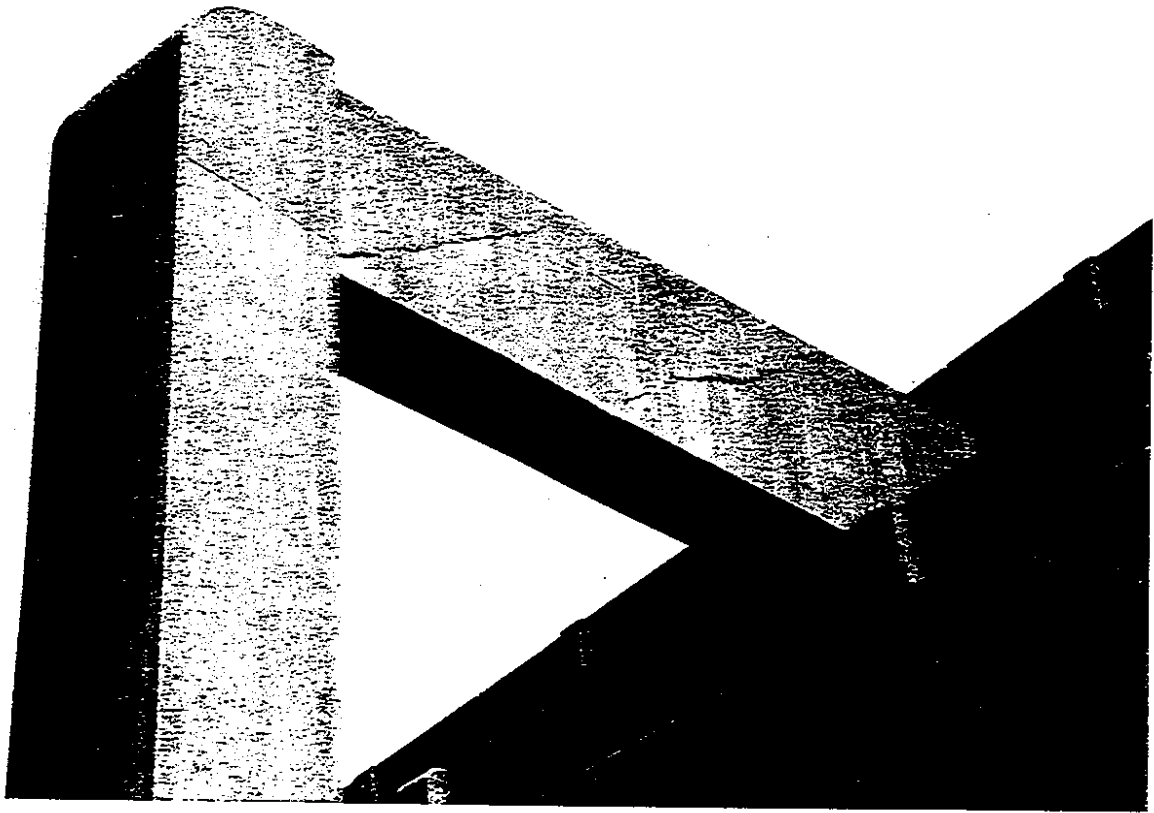


Figure 2.3. Shear Cracks in Outrigger Beam at Bent 56

The footings and column bases are underground and were not accessible for inspection.

2.2 FRAMING OF TYPICAL UNIT

The three-span unit between bents 109 and 112 was selected for the detailed evaluation. Appendix A contains the plans for this unit.

The overall appearance of the typical 184-foot SED unit is similar to the WSDOT unit. The typical unit has three continuous longitudinal bays with spans of 57 feet, 70 feet, and 57 feet. The typical unit is 47 feet wide from center-to-center of the columns. The roadway is 40 feet wide with 2.8-foot curbs on both sides. Figure 2.4 shows the 1.5-inch gap that separates adjacent units from each other. A common footing shared by the end columns of adjacent units is the only structural element connecting abutting sections.

The elevations of roadway decks and footings are the same for both typical WSDOT and SED units, with one exception; the end bent footings in the SED unit are 3 feet lower than those in the WSDOT unit. Therefore, the end columns in the SED unit are 3 feet longer. The cross-sectional dimensions for the end bent columns are the same as those for the WSDOT unit, 4 feet in the transverse direction and 2 feet in the longitudinal direction. The interior bent columns are 4 feet square; 6 inches bigger in the longitudinal direction than those of the WSDOT unit.

Figure 2.5 shows the typical SED unit's deck framing. Large transverse beams span between columns at the column bents. The beams at the exterior bents are approximately half the width of those at the interior bents. Ten small transverse stringers, three in each end bay and four in the interior bay, are evenly spaced between the cross-beams. Large exterior girders span between columns in the longitudinal direction. The girders' inside, vertical faces are flush with the inside faces of the columns, and the girders' centerlines are offset 16 inches from the columns' centerlines. Two large, haunched girders and one small stringer along the bridge's centerline are evenly spaced

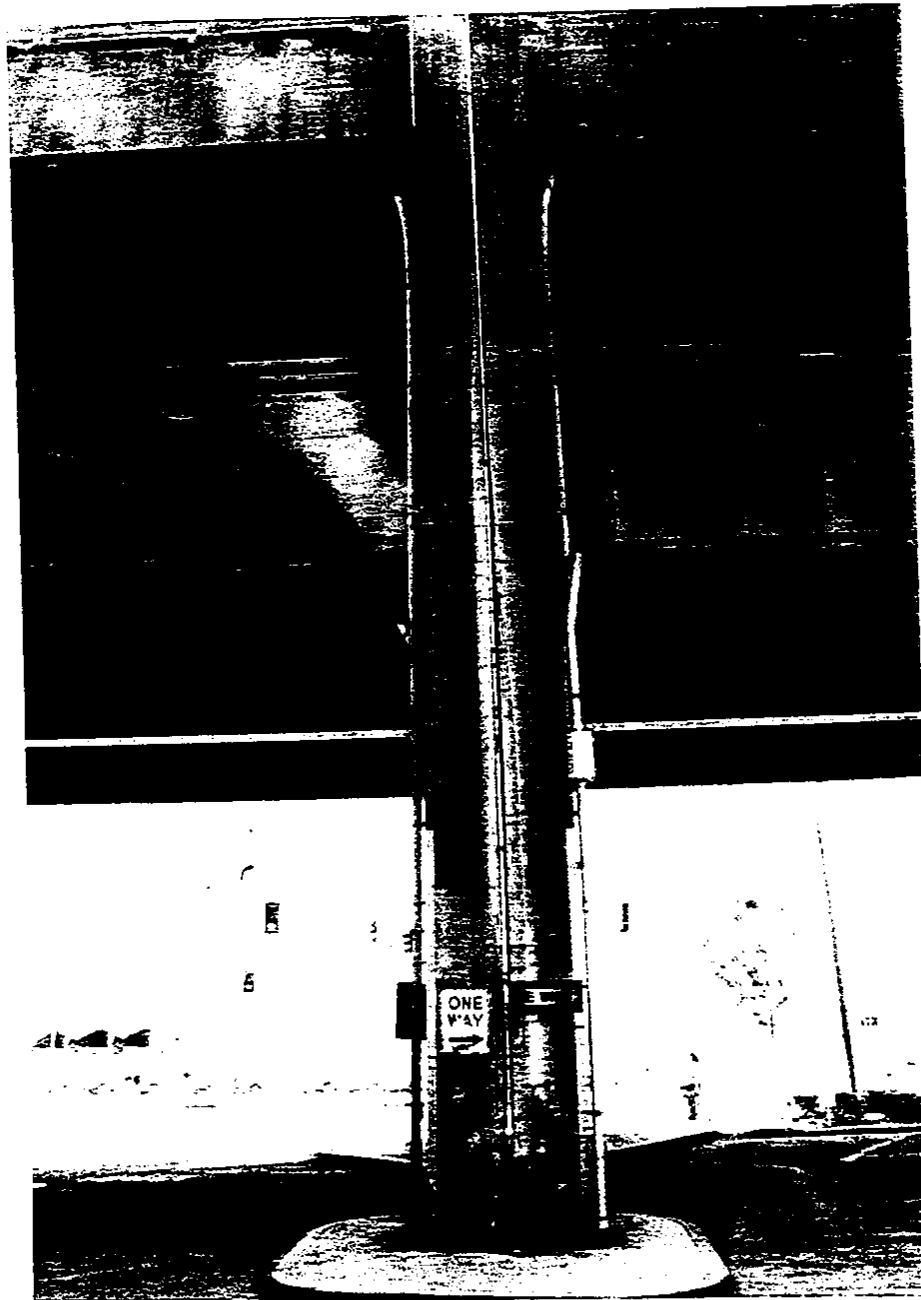


Figure 2.4. 1.5 Inch Expansion Gap Between Units

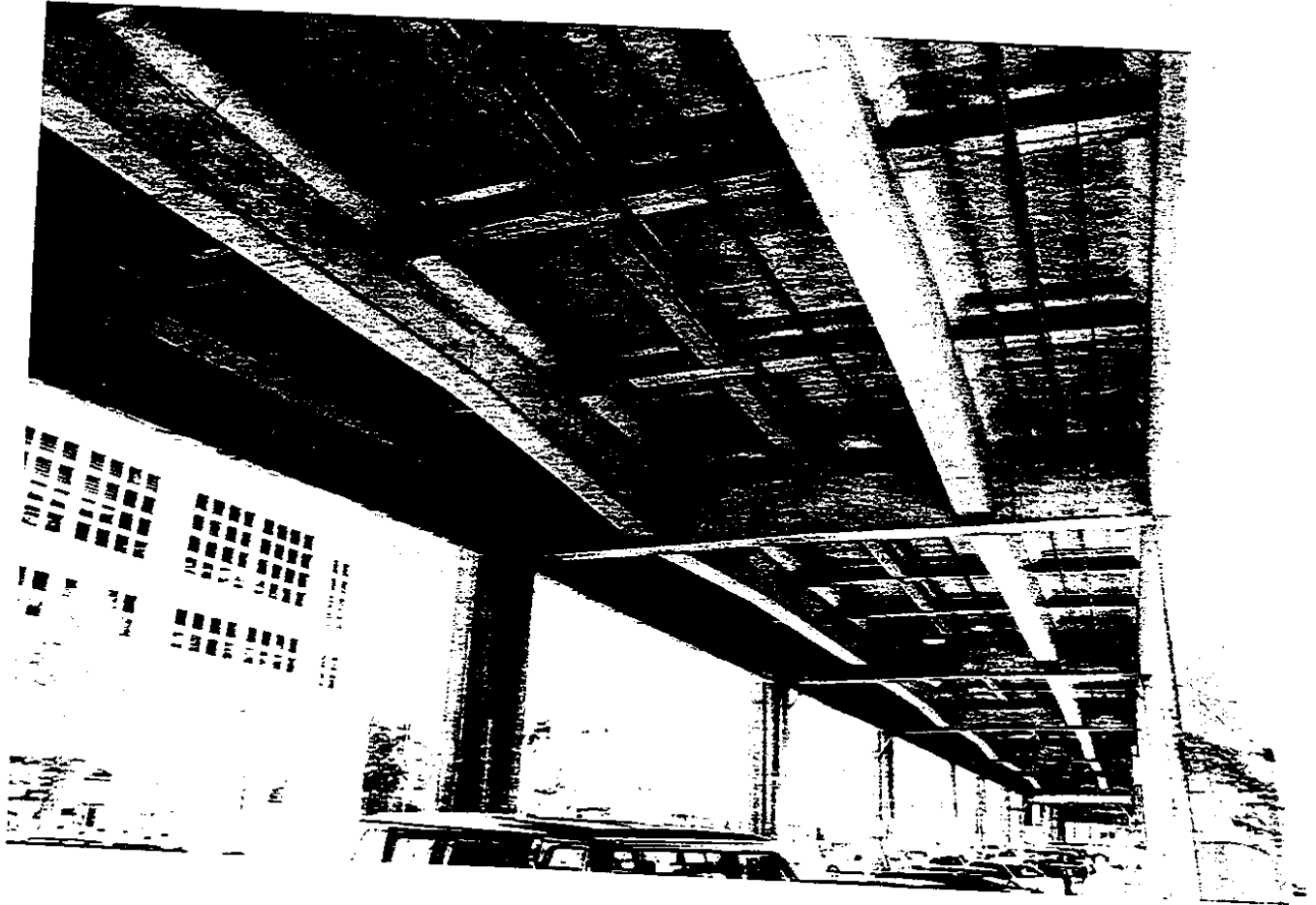


Figure 2.5. Deck Framing of the Typical SED Unit

between the exterior girders. The interior girders have a thickened haunch section at both interior bents. Both SED and WSDOT units have 6.5-inch thick slabs.

The main difference between the horizontal framing systems for the SED and WSDOT units is how deck load is transferred to the columns. The SED unit relies on interior longitudinal girders to transfer most of the deck load to the beams at the column bents. In contrast, the WSDOT unit relies on intermediate transverse beams, spaced evenly between the columns, to transfer most the deck load to the exterior longitudinal girders.

Columns are supported by a footing and pedestal combination. The footing is 2-1/2 feet thick, and the pedestal is 2 feet thick for a total thickness of 4-1/2 feet. The horizontal dimensions vary depending on location. The footings are supported on 14-inch diameter, cast-in-place concrete piles, which are embedded 12 inches into the footings.

2.3 REINFORCEMENT OF TYPICAL UNIT

The main longitudinal reinforcement for frame members consists of square deformed bars for the SED unit, in comparison to the round deformed bars for the WSDOT unit. Transverse reinforcements, such as stirrups and ties, are typically round bars. Top and bottom 5/8-inch diameter round bars reinforce the slabs in both directions.

Girders

The reinforcement for a typical exterior girder is shown in plan sheet 8 in Appendix A. All longitudinal bars are 1 inch square. At the ends of the girders all three top bars have large, 90-degree hooks into the columns, and two of four bottom bars have small, 180-degree hooks. The lower exterior girders have three additional 1-inch square bars in the top at the intermediate supports. Stirrups are made of 1/2-inch diameter bars and are spaced a constant 3 feet between supports. No stirrups are used at the joints.

The typical interior girder reinforcement is shown in plan sheet 3 in Appendix A. The majority of bars are 2 inches square, with a few 1-inch and 1.5-inch square bars. Both

the top and bottom bars have 180-degree hooks at the girder ends. Stirrups are made of 5/8-inch diameter bars and are spaced 8 inches at the end supports and 2.3 feet at mid-span of the end bays. Double stirrups are used near the supports.

End Bent

Plan sheets 4 and 5 in Appendix A show the typical end bent reinforcement. The vertical column bars are 2-inch and 1.5-inch square bars. At the bottom they are welded to a "grillage," a structural steel frame made of heavy angle iron that is embedded 3.75 feet into the footing. This differs from the WSDOT unit, in which the bars are hooked outwards in the footing. The reinforcement ratio at the base of exterior columns is 2.9 percent and drops to 2.2 percent 5 feet above the footings. The ratio increases to 2.9 percent at the joints. The vertical bars are weld spliced away from the column ends, and the splices are staggered 2 feet. This is an important difference from the WSDOT unit, in which the bars are lap spliced at the column ends, and the splices are not staggered. The transverse reinforcement consists of hoops spaced continuously at 12 inches, and they are made of 1/2-inch diameter bars. The hoops are overlapped at one corner with 90-degree bends at the ends.

The longitudinal reinforcement for the end bent cross-beams are mainly 2-inch square bars, with a few 7/8-inch, 1-inch, 1.25-inch and 1.5-inch square bars. The top bars have large, 90-degree hooks at the ends of the beams, while the bottom bars are not hooked. Stirrups are made of 5/8-inch diameter bars, spaced 3 feet at mid-span of the beams, and they are made of 3/4-inch diameter bars, spaced 7.5 inches near the ends of the beams.

Interior Bent

The typical interior bent reinforcement is shown in plan sheets 6 and 7 in Appendix A. All the vertical bars are 2 inch square except at the mid-height of the lower columns, where eight of twelve bars are 1 inch square. The bars are again welded to a "grillage" embedded in the footing. The reinforcement ratio is greatest at the base of the interior

columns (4.2 percent). At 4 feet above the footings, the ratio drops to 3.5 percent, and it drops again at 7 ft above the footing to 1 percent. The ratio increases to 3.5 percent at the joints, and to 2.1 percent at the mid-height of the upper story columns. At two locations in the lower-story columns, 7 feet above the footings and 7 feet below the first-story joints, eight of twelve vertical bars are spliced with 2.5-foot lap splices. The other four bars, the four corner bars, are weld spliced at the mid-height of the upper- and lower-story columns. The hoops are again made of 1/2-inch diameter bars. They are spaced 12 inches and alternate between square and octagonal shapes.

The transverse beams are reinforced mainly with 2-inch square bars, with a few 1.25-inch and 1.5-inch square bars. The top bars are hooked at the ends of the beams, but the bottom bars are not. Single stirrups made of 5/8-inch diameter bars spaced 3 feet are used at mid-span, and double stirrups made of 3/4-inch diameter bars spaced 6 inches are used near the ends of the beams.

File-Supported Footings

The footings have only bottom reinforcement in both directions, with bar sizes ranging from 7/8-inch diameter round to 1.5-inch square. All bars are hooked 180 degrees at the ends. The footings have no vertical reinforcement, top steel, or steel connections to the piles.

2.4 MATERIAL PROPERTIES

Heavy framing members such as columns, beams, and girders were specified to be made of class "ES" concrete with a nominal compressive strength of 4200 psi. Slabs and light framing members were specified to be made of class "AS" concrete, and footings made of class "E" concrete. Both class "AS" and "E" concretes have a specified nominal compressive strength of 3600 psi. All reinforcing steel was specified to be Structural Grade with a yield strength of 33 ksi.

Following the procedures used in the evaluation of the WSDOT unit, concrete strengths used in calculations were assumed to be 1.5 times the specified strengths, and the steel strength was assumed to be 1.1 times the specified strength. The elastic modulus for concrete, E , was assumed to be equal to $57,000\sqrt{f' c}$.

CHAPTER 3

LINEAR, DYNAMIC ANALYSIS

To implement the ATC-6-2 assessment procedure, the ratio of the flexural capacity to the flexural demand had to be computed at critical locations. Although bridge components are likely to yield during strong earthquakes, the ATC-6-2 document requires that flexural demands be computed with linear analyses. Section 3.1 describes the three-dimensional, finite-element model used to perform linear analyses; Section 3.2 presents the results of gravity analysis; Section 3.3 presents the results of modal analyses; and Section 3.4 reports the results of response-spectrum analyses.

The flexural capacity-to-demand (C/D) ratio at each location is important because it is related to the flexural ductility demand. A flexural C/D ratio of less than 1.0 indicates that yielding is possible and that the region is a location of potential "plastic hinging." These ratios are reported in Section 3.5.

3.1 DESCRIPTION OF STRUCTURAL MODEL

The SAP90 finite-element program (Wilson and Habibullah, 1988) was used to perform three-dimensional, linear analyses of the typical SED unit. Figure 3.1 shows the three-dimensional, finite-element model. Prismatic frame elements represented the columns, girders, beams, and stringers. The roadway slabs were modeled with four-node shell elements that combined membrane and plate bending behavior. The nodes were located at the bridge's physical joints. This discretization resulted in a uniform mesh for the shell elements with plan dimensions equal to 11 feet by 13 feet. Additional nodes were added where the column steel reinforcement changed significantly. All members were modeled at their centerlines. Rigid links enforced compatibility at joints where member centerlines did not intersect. The column bases were fixed for all analyses.

The beam and column reinforcement changes frequently along the members' lengths. Consequently, it would have been tedious to compute the transformed-section

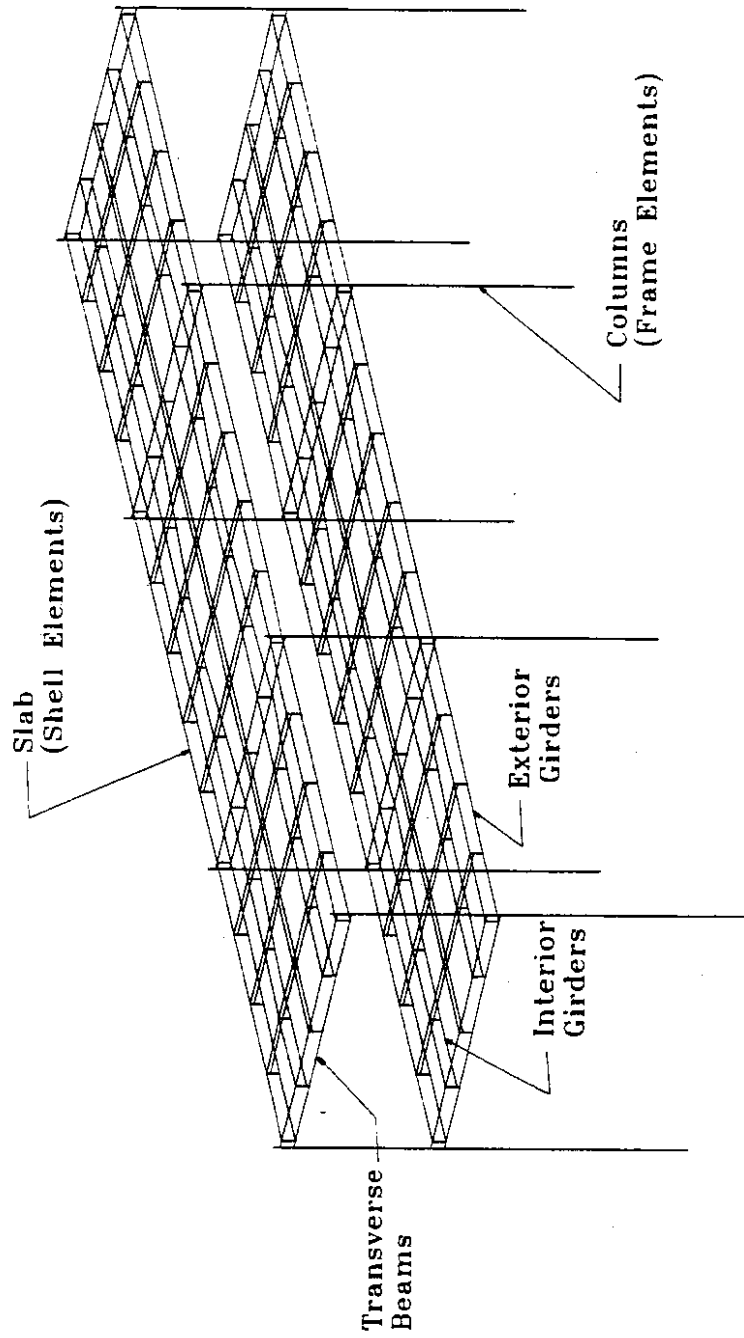


Figure 3.1. Three-dimensional Finite Element Model of the Typical SED Unit

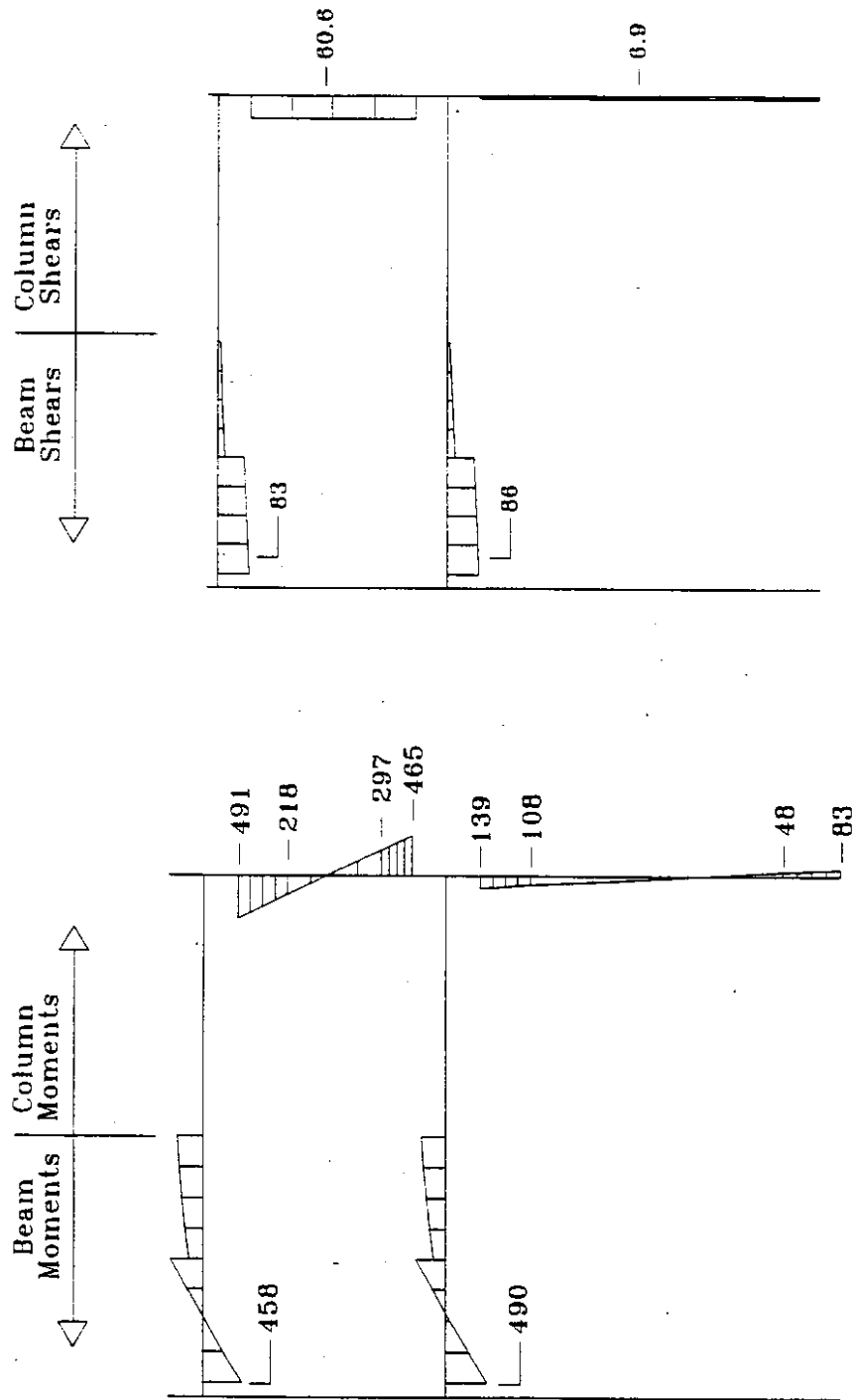
properties for each cross-section. As an approximation, the transformed-section moments of inertia were assumed to be half that of the gross-section. This approximation was also made for the WSDOT unit (Eberhard et al., 1995). Column stiffnesses at the joints were increased by a factor of 8.

As recommended by Priestley et al. (1992), the concrete's compressive strength was assumed to be 1.5 times the specified compressive strength. Although the specified strength varied between 3600 psi and 4200 psi, the researchers assumed for simplicity that the specified compressive strength was 3600 psi everywhere. A sensitivity analysis by Ryter (1994) showed that linear analysis is not sensitive to variations in concrete compressive strength.

The concrete unit weight used was 150 pcf. The weights of curbs and fillets were not included in the finite-element model. This omission helped offset the duplication of member weights at joints. A detailed calculation found the weight of the SED unit to be 4950 kips, which compared well with the weight computed by the finite-element program (5180 kips; 5-percent higher than the detailed calculation). In comparison, the WSDOT unit weighed 4800 kips.

3.2 GRAVITY ANALYSIS

A gravity analysis was performed using the three-dimensional, linear model. The moment and shear diagrams for the exterior and interior transverse frames are shown in Figures 3.2 and 3.3. The plotted beam moments include three contributions: (1) the moment in the beam element at the column face, (2) moments from the slab elements, and (3) moments due to coupled axial forces between the beam and slab elements. The shapes of the diagrams were similar to those of the WSDOT unit in that the moments were much larger in the upper-story than in the lower-story columns. Because the upper-story columns were shorter and stiffer than the lower-story columns, they attracted more of the beam moments. The column moments were much larger in the SED unit than in the



b) Gravity Shears (Kips)

a) Gravity Moments (Kip-ft)

Figure 3.2. Gravity Moment and Shear Diagrams - Exterior Frame

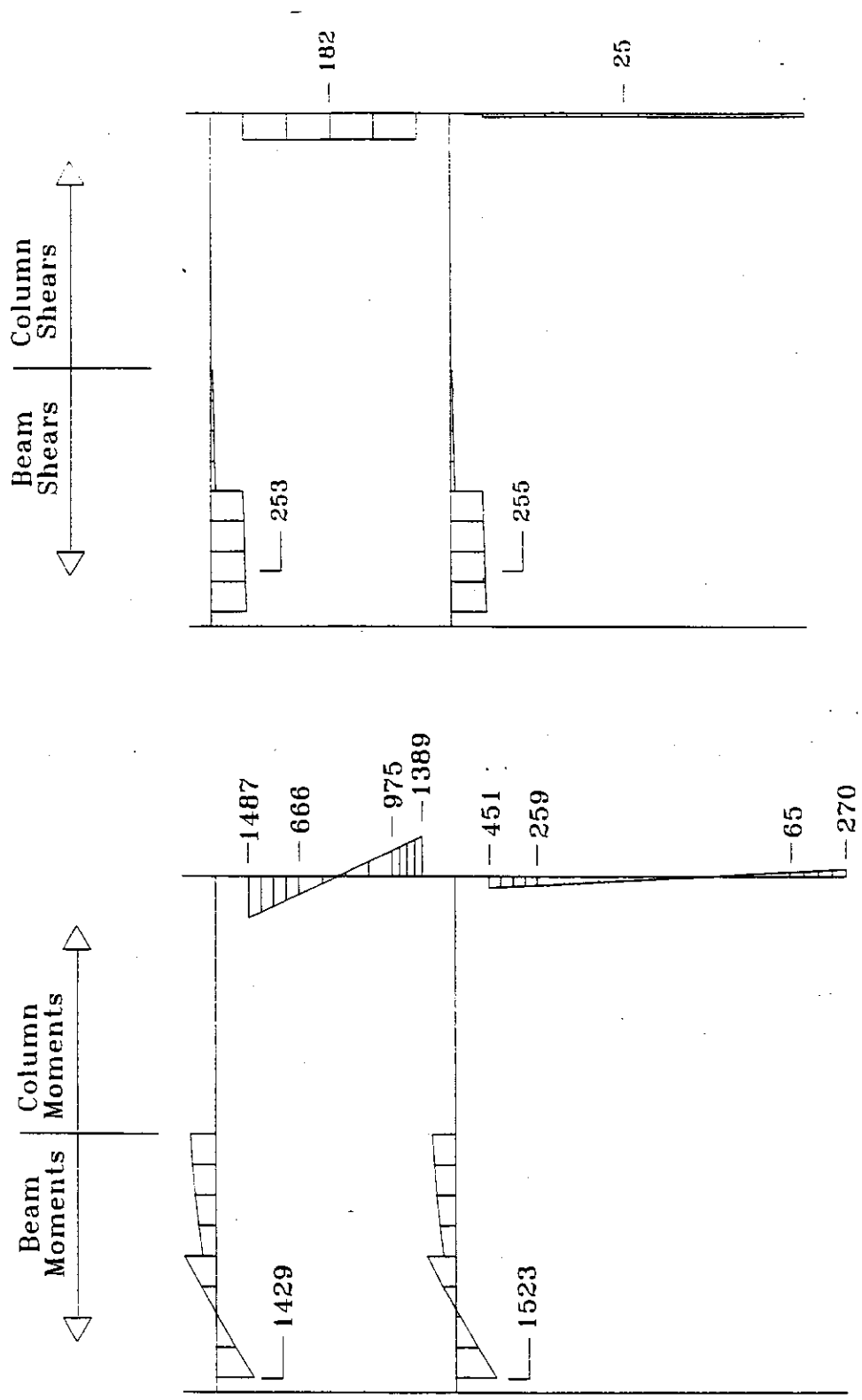


Figure 3.3. Gravity Moment and Shear Diagrams - Interior Frame

WSDOT unit; the exterior transverse frame moments were twice as large, and the interior frame moments were 2.5 times as large. This difference was a consequence of the differences in framing systems. The SED unit uses interior, longitudinal girders to transfer deck loads to cross beams at the column bents. The WSDOT unit uses intermediate, transverse cross beams between column bents to transfer deck loads to exterior, longitudinal girders. It follows that the transverse gravity moments were higher in the SED unit than in the WSDOT unit.

The moment and shear diagrams for a longitudinal frame are shown in Figure 3.4. Again, the shapes of the diagrams were similar to those for the WSDOT unit. As expected, the moments in the exterior girders were smaller in the SED unit than in the WSDOT unit because of the different framing systems.

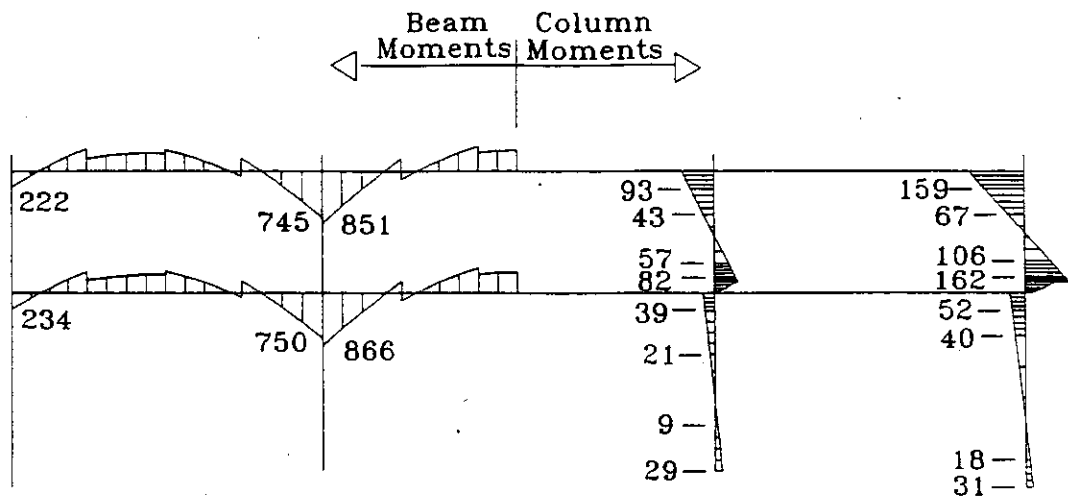
3.3 MODAL ANALYSIS

The results of the modal analysis performed by SAP90 are presented in this section. The first three mode shapes for the SED unit were the same as the WSDOT unit's. The first mode consisted of swaying motion in the longitudinal direction, the second mode consisted of swaying motion in the transverse direction, and the third mode was dominated by torsional motion about the center of the unit.

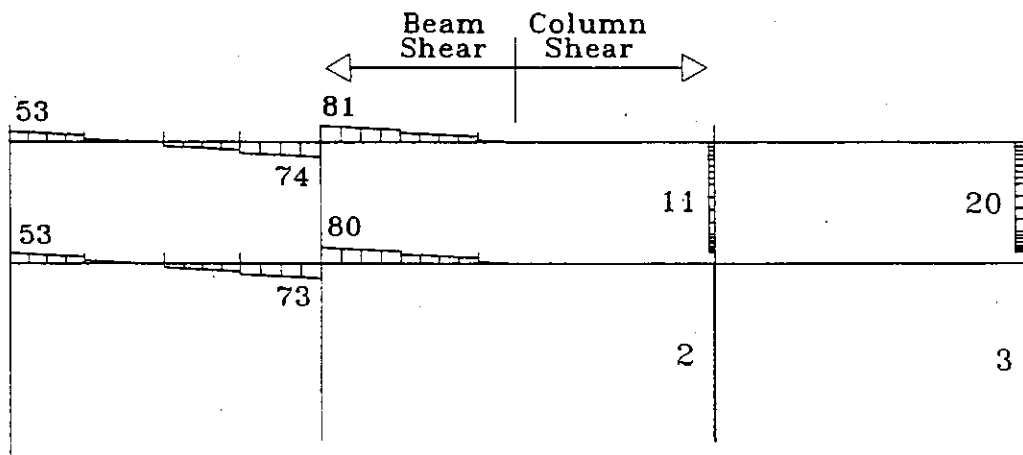
The modal properties are listed in Table 3.1. The period for mode 1 was slightly less in the SED unit than in the WSDOT unit. This difference was attributed to the higher

Table 3.1. Computed Modal Properties

	Units	Mode 1	Mode 2	Mode 3	Mode 4
Period	sec	0.86	0.77	0.71	0.22
Spectral Acceleration	g	0.50	0.54	0.57	0.43
Effective Mass (transverse)	% of wt.	-	95.3	-	-
Effective Mass (longitudinal)	% of wt.	95.4	-	-	-



a) Gravity Moments (Kip-ft)



b) Gravity Shears (Kips)

Figure 3.4. Gravity Moment and Shear Diagrams - Longitudinal Direction

stiffness of the SED unit's interior columns in the longitudinal direction. The SED unit's interior columns are 6 inches deeper in the longitudinal direction. The period for mode 2 was nearly the same for both units.

Ninety-five percent of the mass was effective in the first two modes for each direction, which was 4 percent less than in the WSDOT unit. The difference resulted from adding additional nodes to the SED unit's lower story columns. The WSDOT unit's lower-story columns had been modeled using single frame elements. The finite-element program lumped the element masses at the nodes. Masses lumped at restrained nodes were ignored in the analysis. In the WSDOT unit, half the mass of the lower-story columns was lost in the analysis. Since the lost mass did not contribute to the response for modes 1 and 2 anyway because of its proximity to the restraints, the participating mass was unaffected by the mass lumping. However, the effective mass (the ratio of the participating mass to the total mass) increased because the total mass decreased. By adding additional nodes to the SED unit's lower-story columns, less of the column's total mass was lost at the restrained nodes, and therefore, the effective mass was less. This was verified by removing the additional nodes and modeling the SED unit's lower-story columns with single elements. By doing this, the effective mass increased to 99 percent.

3.4 RESPONSE-SPECTRUM ANALYSIS

Spectral analyses were performed in both the transverse and longitudinal directions. The response spectrum, shown in Figure 3.5, was derived from Section 5.2.2 of "Seismic Design Guidelines For Highway Bridges, ATC-6" (ATC, 1981). The response spectrum was constructed by assuming a soil type III and a peak ground acceleration of 0.25g. SAP90 used the Complete Quadratic Combination (CQC) method to combine modal responses. To be consistent with the analysis of the WSDOT unit, 5 percent damping was used in the analysis.

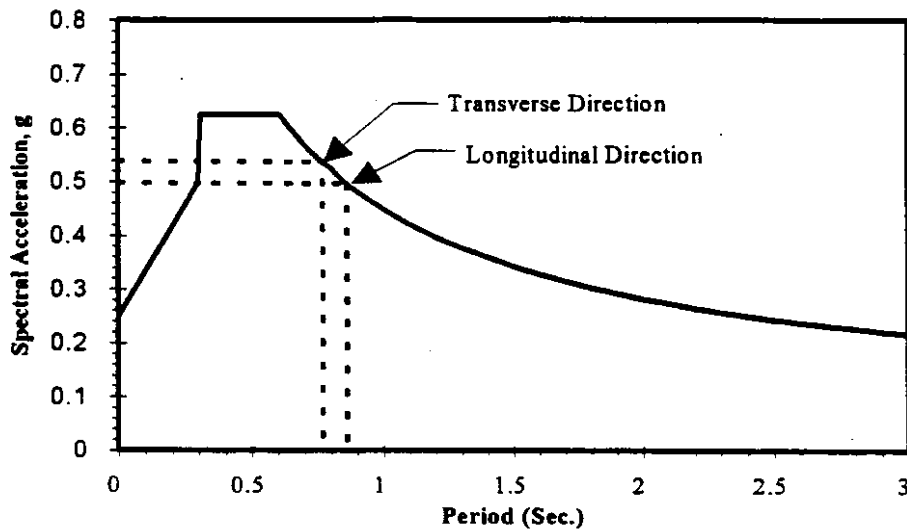
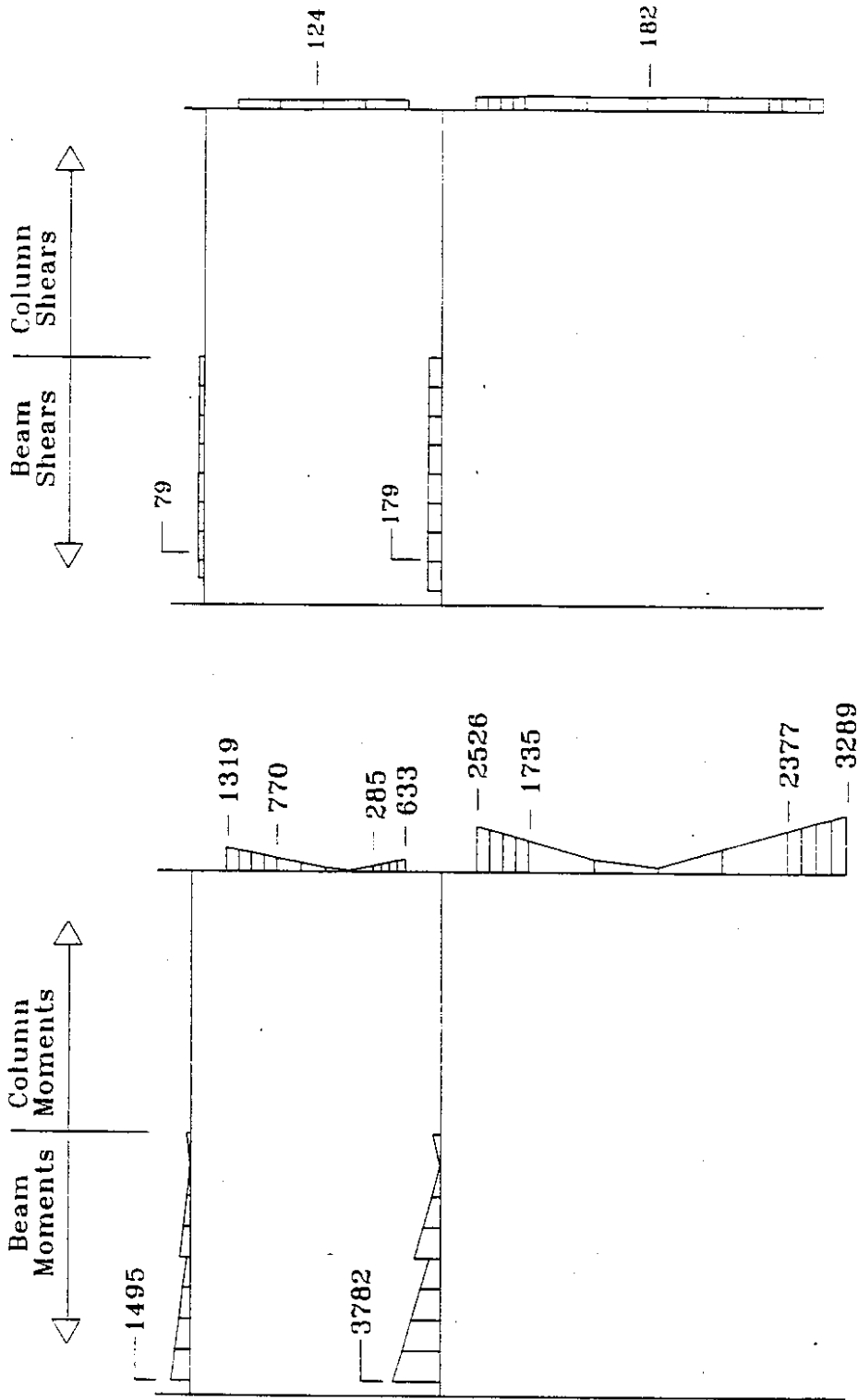


Figure 3.5. ATC-6 Response Spectrum (0.25g)

The spectral accelerations for modes 1 and 2 were nearly the same as in the WSDOT unit. Both were approximately 0.5g. The relative drift ratios listed in Table 3.2 were also nearly the same as in the WSDOT unit. All the ratios were less than 1 percent.

Transverse Direction

Figure 3.6 shows the moments and shears for an exterior transverse frame. Because the CQC method does not give the directions of forces, all forces were plotted with the same sign. The moments were largest at the ends of the lower-story columns and at the ends of the lower-story beam. The column moments were smallest at the bottom of the upper-story columns.



a) Seismic Moments (Kip-ft)

b) Seismic Shears (Kips)

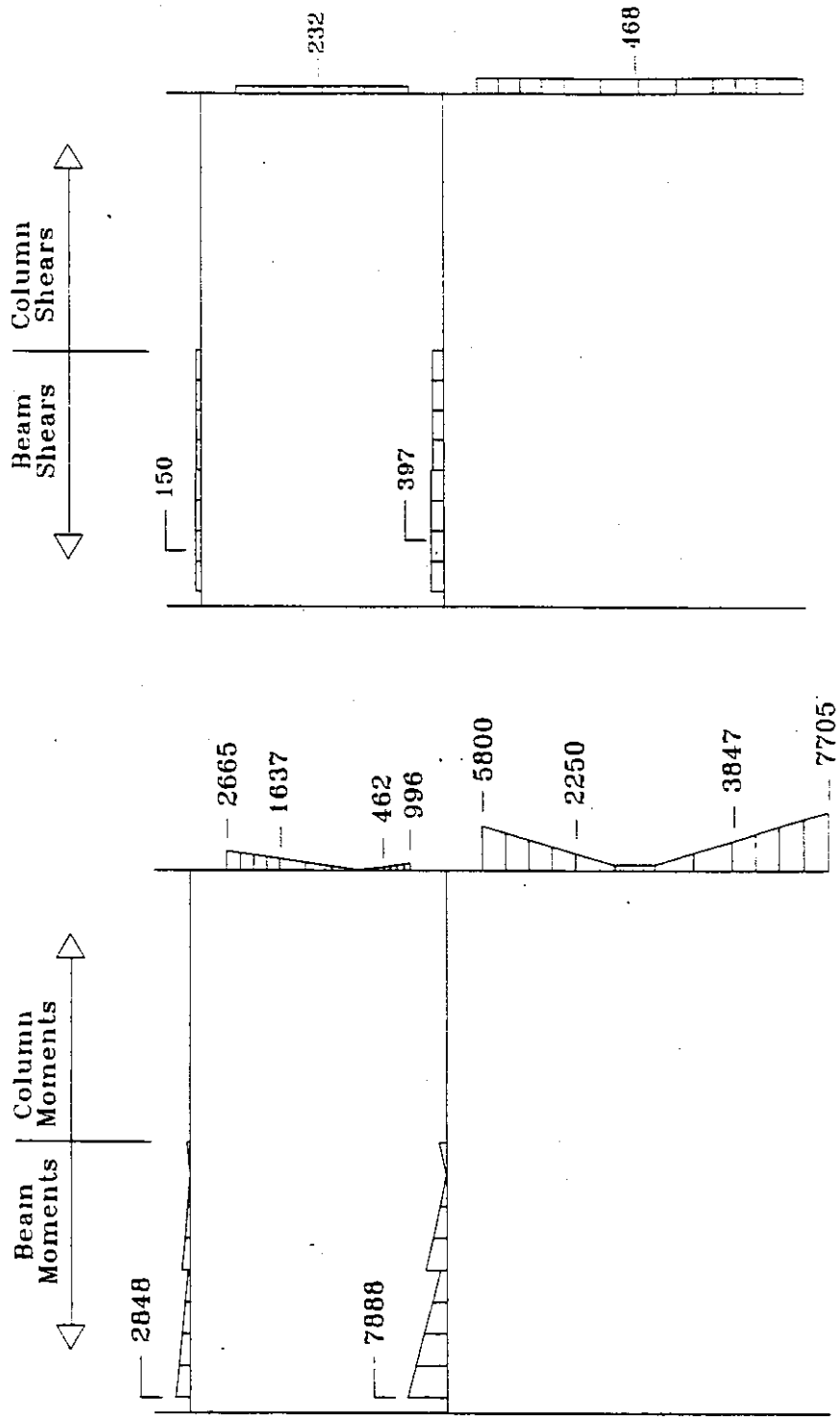
Figure 3.6. Seismic Moment and Shear Diagrams - Exterior Frame

Table 3.2. Story Drifts and Drift Ratios

	Exterior Frame		Interior Frame	
	Transverse	Longitudinal	Transverse	Longitudinal
1st-Story Drift (ft)	0.23	0.26	0.23	0.27
Story Drift Ratio	0.61%	0.69%	0.67%	0.78%
2nd-Story Drift (ft)	0.06	0.08	0.06	0.07
Story Drift Ratio	0.27%	0.36%	0.27%	0.32%
Overall Drift (ft)	0.29	0.34	0.29	0.34
Overall Drift Ratio	0.49%	0.57%	0.51%	0.60%

The computed demands were consistent with those obtained for the WSDOT unit. The transverse seismic demands were generally higher in the SED unit because its mass was 7 percent higher than that of the WSDOT unit, and the spectral accelerations in the transverse direction were the same for both units. For example, the moments in the upper-story columns of the SED unit were 4 percent larger than those in the WSDOT unit. However, the moments in the exterior frame's lower-story columns were 10 percent less in the SED unit than in the WSDOT unit, mainly because the end columns of the SED unit were 3 feet longer. The beam moments of the SED unit were significantly higher (75 percent higher) than in the WSDOT unit for two reasons. First, contributions from the slabs were included in the SED unit's beam moments and not in the WSDOT unit's. Second, there were fewer transverse beams in the SED unit to resist transverse loads.

Figure 3.7 shows the moment and shear forces for an interior transverse frame. The force distributions were similar to those of the exterior frame, but the magnitudes were much larger because of the interior frame's higher stiffness. The forces were also much higher than those of the WSDOT unit's interior frame, up to three times higher for the beams and 25 to 30 percent higher for the columns. The beams and columns of the



b) Seismic Shears (Kips)

a) Seismic Moments (Kip-ft)

Figure 3.7. Seismic Moment and Shear Diagrams - Interior Frame

SED unit's interior frame were larger and stiffer than those of the WSDOT unit, and therefore they attracted more seismic forces.

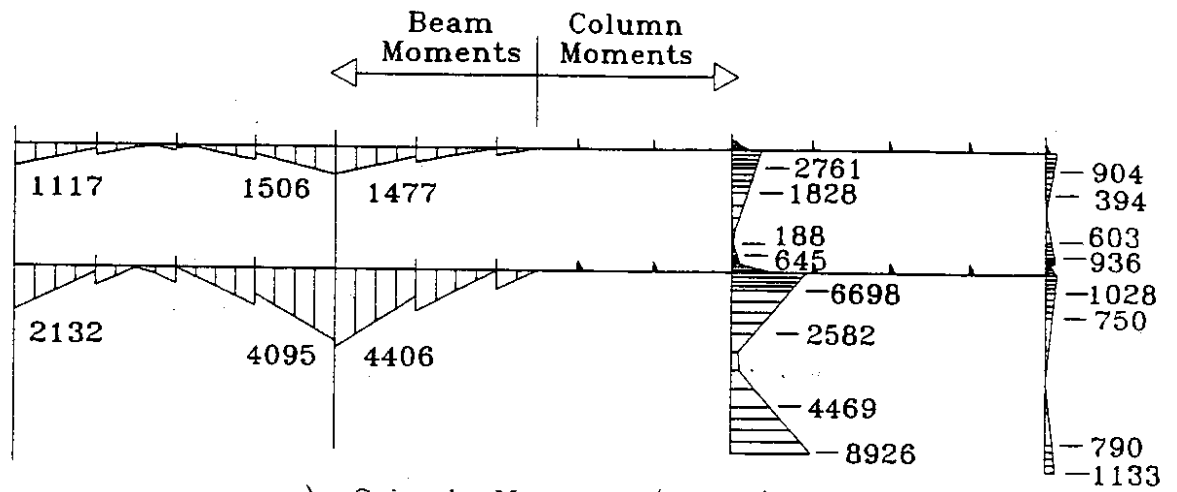
Longitudinal Direction

Figure 3.8 shows the moment and shear forces for a longitudinal frame. The column moments were up to eight times higher in the interior than in the exterior columns. The exterior columns were much more flexible because they were 3 feet longer, and they were bent about their weak axis. The highest moment occurred at the base of the interior columns. The girder moments were over twice as high in the lower-story than in the upper-story. This was expected because the lower-story girders had columns both above and below at the ends. The upper-story girders only had columns below, and therefore, their end restraints were more flexible.

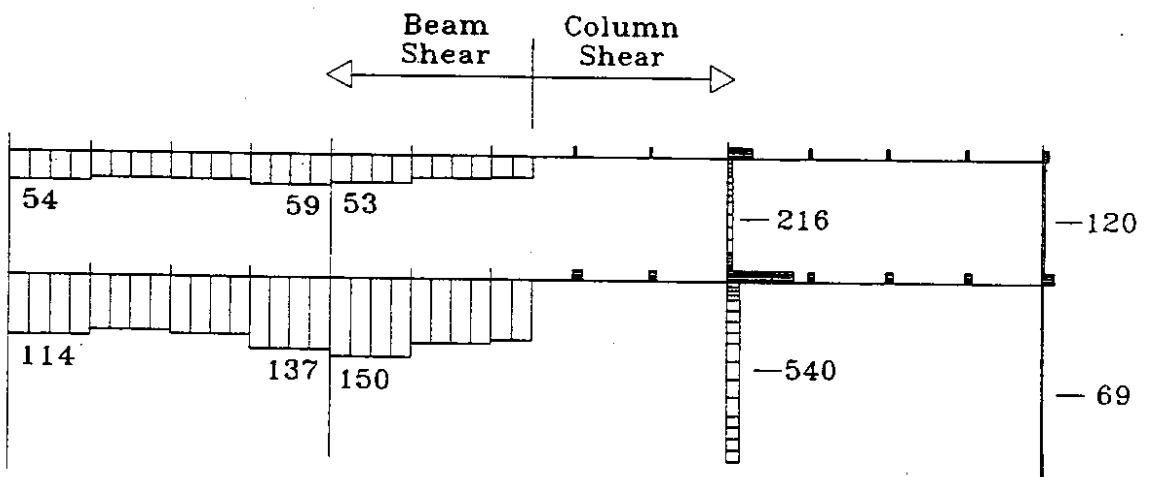
The seismic demands in the longitudinal direction were generally higher in the SED unit than in the WSDOT unit (up to 40 percent higher at the columns). This increase resulted from the SED unit's higher mass and its higher spectral acceleration in the longitudinal direction. One exception was that the forces in the lower-story exterior columns were smaller in the SED unit than in the WSDOT unit. The exterior columns of the SED unit were longer and, consequently, more flexible.

3.5 FLEXURAL CAPACITY-TO-DEMAND RATIOS

In the ATC-6-2 procedure it was necessary to know where yielding occurred to evaluate the column failure modes. Flexural C/D ratios helped identify possible plastic hinging locations. Figure 3.9 shows the locations where the columns were evaluated. The columns were evaluated at their ends (locations 1, 4, 5, and 8), and at intermediate locations where the column capacities dropped significantly (locations 2, 3, 6, and 7). The intermediate evaluation points 2, 3, 6, and 7 were located at bar cut-off points. No allowance was made for bar development. The beams and girders were evaluated at their ends.



a) Seismic Moments (Kip-ft)



b) Seismic Shears (Kips)

Figure 3.8. Seismic Moment and Shear Diagrams - Longitudinal Direction

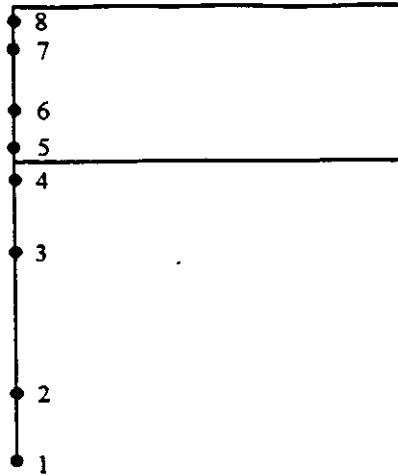


Figure 3.9. Column Analysis Locations

The moment demands have been presented in the previous section. Member capacities were computed using the modified Kent and Park model for confined concrete (Park and Paulay, 1975). Strain hardening of the longitudinal reinforcement was included in the model (Table 4.1). Capacity calculations are discussed in detail in Chapter 4. Both the capacities and demands for the beams included contributions from the slabs.

Transverse Direction

Figure 3.10 shows the flexural C/D ratios for the beams and columns of the typical transverse frames. The right side columns of each frame were subject to compressive axial forces due to seismic loading. The left side columns were subject to tensile axial forces. The calculations of the flexural C/D ratios are presented in Appendix C.

The flexural C/D ratios for both transverse frames were similar. Few values were less than 1.0, indicating that the ductility demands were low in the transverse direction. The lower-story beams had values of r_{eb} ranging from 0.78 to 0.89, while the upper-story values were all greater than 1.0. All column values were greater than 1.0 except at locations 1 and 2, where they varied from 0.83 to 1.09. The difference in values between

Longitudinal Direction

Figure 3.11 shows the flexural C/D ratios for the beams and columns of a longitudinal frame. The column ductility demands were low. The values of r_{ec} were less than 1.0 at interior column locations 1, 2, and 4, where they varied from 0.81 to 0.96. The differences between locations 1 and 2 were again small, and therefore it was not clear which location would yield first. The values of r_{ec} were all greater than 1.0 at the exterior columns because of their relatively high flexibility.

In contrast to the columns, the ductility demands were high for the lower-story girders. The value of r_{eb} at a lower-story girder in positive bending at an interior column was 0.23. These girders had little positive moment reinforcement at these locations, and the demands in the exterior girders were high because the interior girders contributed little to seismic resistance. The values of r_{eb} for the upper-story girders were all greater than or equal to 1.0.

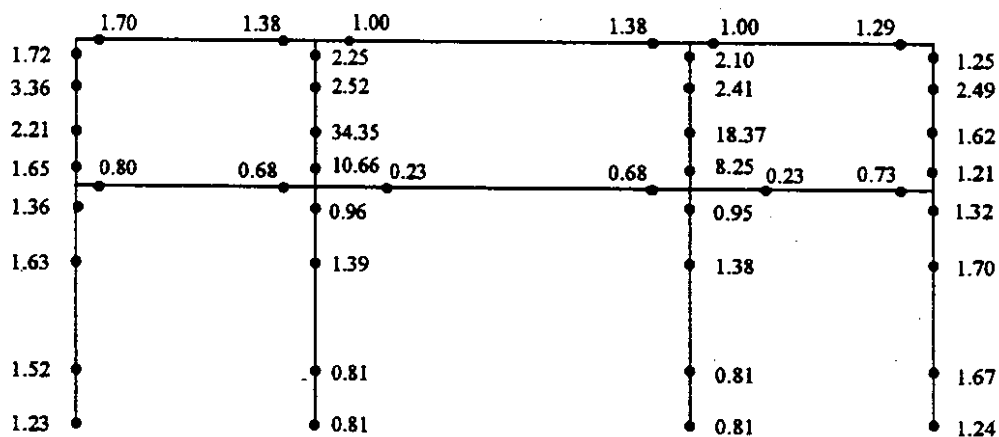


Figure 3.11. Flexural C/D Ratios for a Longitudinal Frame

The flexural C/D ratios were typically higher in the columns of the SED unit's longitudinal frame than those in the WSDOT unit. This was due to the heavier reinforcement of the SED unit's columns. The upper-story, exterior columns of the SED unit were the exception. Their capacity was slightly less than that in the WSDOT unit, and therefore their r_{ec} values were also slightly less. However, the difference was insignificant because the upper-story columns of both units did not yield.

The values of r_{eb} for the exterior girders were significantly less in the SED unit than those for the WSDOT unit. The girders of the WSDOT unit were bigger and more heavily reinforced because they were the only main longitudinal members. In the SED unit, the exterior girders shared the gravity loads with interior girders, and therefore the exterior girders were designed with less capacity. Unfortunately, the exterior girders did not share the seismic loads with the interior girders. The combination of high demands and low capacities resulted in very low values of r_{eb} .

CHAPTER 4

NONLINEAR, STATIC ANALYSIS

The assessment procedure proposed by Priestley, Seible, and Chai (1992) relies on nonlinear, static analyses to determine the lateral force-displacement response of a structure. The nonlinear force-displacement response of each two-dimensional seismic resisting frame of the SED unit is presented in this chapter. Section 4.1 describes the analysis procedure and the two-dimensional, nonlinear model. Sections 4.2 and 4.3 present the force-displacement responses for the transverse and longitudinal frames. Section 4.4 presents the results of plastic-hinge analyses for the SED unit, and section 4.5 compares the responses of the SED and WSDOT units. All the analyses presented in this chapter neglected the effects of other failure modes such as anchorage, splice, shear, joint, and confinement failures. These failure modes and their effects on the response are considered in Chapters 5 through 10.

4.1 DESCRIPTION OF ANALYSIS

The analysis procedure was the same as that used for the WSDOT unit. A companion report, "Seismic Vulnerability of the Alaskan Way Viaduct: WSDOT Typical Unit," (Eberhard et al., 1995) describes the details of the analysis procedure.

The three-dimensional structure was modeled in two dimensions by simplifying it as a set of orthogonal planar frames. Four transverse frames (two interior and two exterior) were assumed to resist the transverse lateral loads, while two longitudinal frames were assumed to resist the longitudinal lateral loads.

Each frame's members were discretized into enough elements to adequately model the varying reinforcement. Moment-curvature ($M-\phi$) relationships were determined for each segment. The segment ends were located approximately 12 inches above or below the bar cut-off points to account for bar development (Figure 4.1). A portion of the slab was assumed to contribute to the flexural resistance of the beams and girders. The

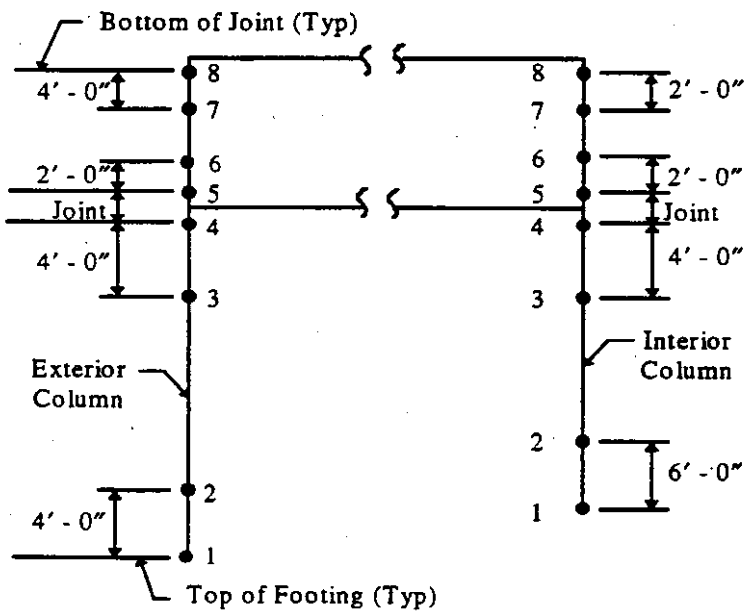


Figure 4.1. Locations of Column Segment Ends

Each two-dimensional frame was subjected to increasing lateral loads applied at the center of mass of each deck; 60 percent of the total lateral load was applied at the upper-deck, and 40 percent was applied at the lower-deck. The lateral loads were increased by 10-kip increments until the ultimate capacity of the frame was reached. The analysis was then restarted at a total lateral load of 100 kips less than the ultimate capacity, and the load was increased by 5-kip increments.

4.2 TRANSVERSE DIRECTION RESPONSE

Figure 4.2 shows the lateral force-displacement relationships for the interior and exterior frames. The total force capacity was found to be 1850 kips (36 percent of the unit's weight) at an upper-deck displacement of 0.6 feet (a 1.1 percent drift ratio). The total ultimate displacement was limited by the displacements of the exterior frames, and therefore, the interior frames did not develop their full lateral force capacities of 740 kips each. At a top-deck displacement of 0.6 feet, the lateral force carried by the interior frame was 640 kips. As expected, the interior frame was stronger than the exterior frame because the interior columns were shorter, wider, and more heavily reinforced at the base. The interior frame was much more ductile because at the location of yielding (6 feet above the footing) the interior column had a lower reinforcement ratio.

The following sections describe the responses of the interior and exterior frames.

Interior Frame Response

Figure 4.3 shows the moment diagrams for the upper- and lower-deck beams of an interior frame. The moments due to dead load only (DL) and due to dead load plus the ultimate lateral-load (DL+740) are plotted along with the capacity envelopes.

Both beams reached their negative moment capacities approximately 6 feet from the face of the right-side column. At this location several negative moment reinforcement bars in both beams were discontinued, resulting in a significant drop in the capacity. The moment in the lower-story beam nearly reached the positive moment capacity at the face

Base Shear-Displacement Curves
Transverse Direction - Fixed Base

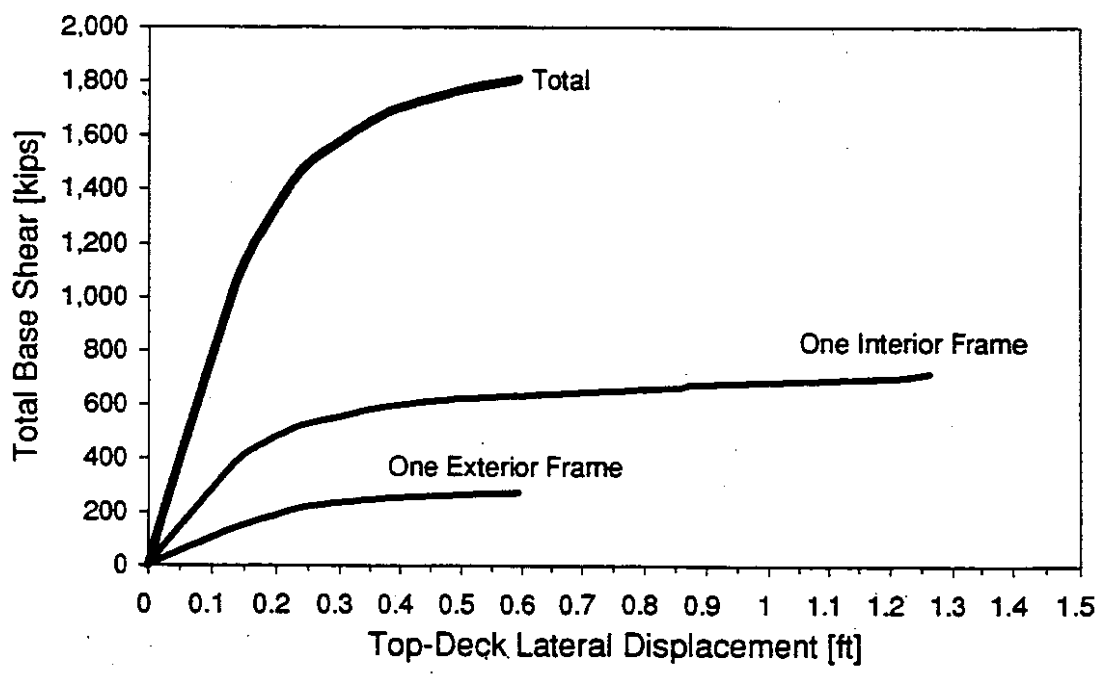
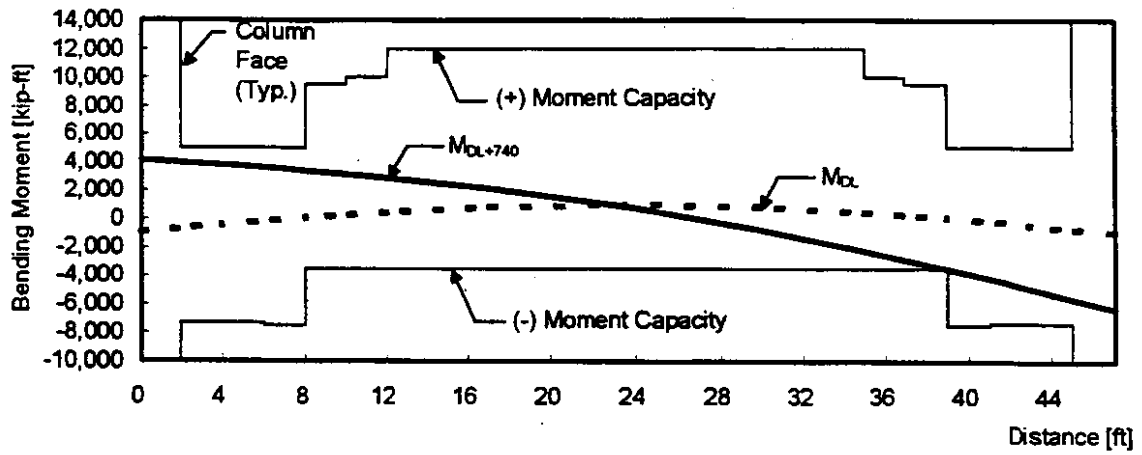
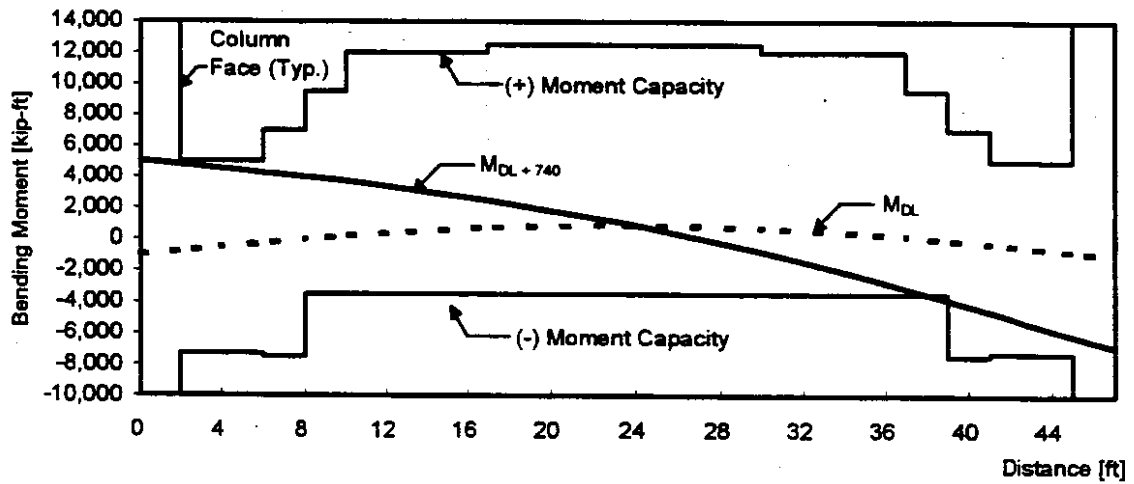


Figure 4.2. Lateral Force-Displacement Relations - Transverse Direction



a) Upper-Story Beam



b) Lower-Story Beam

Figure 4.3. Moment Diagrams for Interior, Transverse Beams

of the left-side column. At the ends of the beams the positive moment reinforcement was minimal because the beams were designed mainly for gravity loads. The left end of the upper-story beam did not reach its ultimate positive moment capacity.

The column moment diagrams corresponding to the ultimate base shear are shown in Figure 4.4 along with the capacity envelopes. The flexural capacities were reached at location 2 in both lower-story columns and at location 7 in the right-side column. The flexural capacity was almost reached at location 3 in both columns. Location 2 was particularly vulnerable because the longitudinal reinforcement had been spliced at that location.

The moment capacity at column location 2 was significantly exceeded because of the element discretization chosen for that location. It is desirable to use short elements within regions of yielding because the finite-element program computes the average moment within the element. In longer elements the difference between the maximum moment and the average moment can be significant. In this case, yielding was anticipated at the column base. Consequently, short elements were used at location 1, while relatively long elements were used at location 2.

Figure 4.5 summarizes the extent of yielding in the columns and beams of an interior frame. Part (a) of this figure shows the ratios of the ultimate flexural capacities (M_U) to the flexural demands corresponding to the ultimate lateral force (M_{740}). A ratio of less than 1 indicates that the ultimate flexural capacity had been exceeded. The ultimate flexural capacity was exceeded in the lower-story columns at location 2 and in the negative moment region of the beams 6 feet from the face of the right-side columns. Part (b) shows the ratios of the yield moments (M_y) to M_{740} . Extensive yielding occurred at column location 2, in both beams 6 feet from the face of the right-side columns and in both beams at the face of the left-side columns. A comparison of Figures 4.5(a) and 4.5(b) shows that the beams yielded first and underwent significant strain hardening before they reached their ultimate capacities. The columns yielded only after the beam reinforcement

began to strain harden. This behavior resulted from the fact that M_u/M_y was large for the beams.

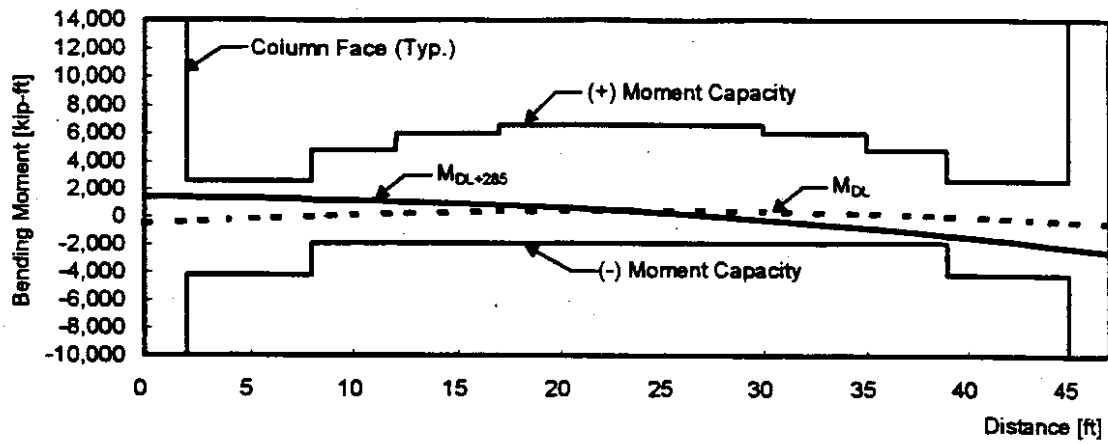
Part (c) shows the ratios of the yield curvatures (Φ_y) to the average curvature demands corresponding to the ultimate lateral force (Φ_{740}). The inverse of this ratio is the curvature ductility demand. The curvature ductility demands were highest in the beams and at column location 2. This figure indicates that the collapse mechanism consisted of plastic hinges in the beams and at location 2 of both columns.

Exterior Frame Response

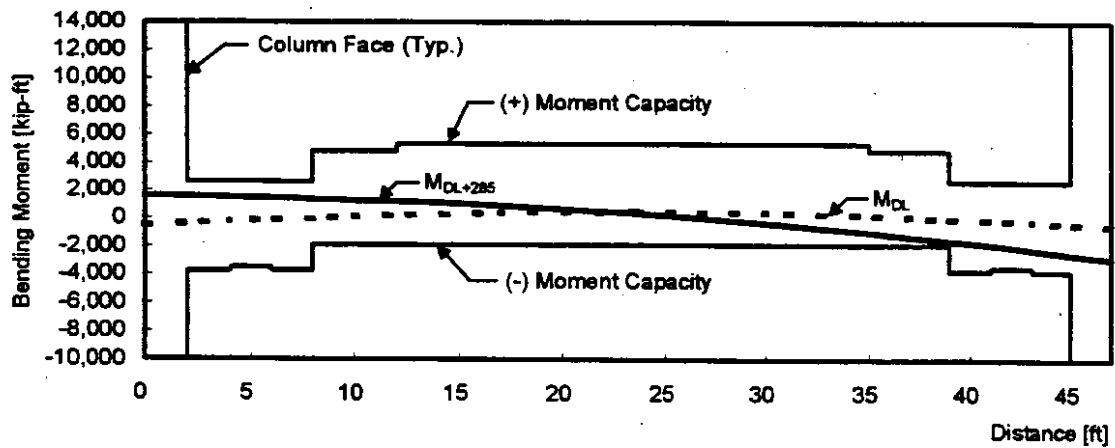
Figure 4.6 shows the moment diagrams for the upper- and lower-story beams of an exterior frame. The moments due to dead load only and due to dead load plus the ultimate lateral load (DL + 285) are plotted along with the capacity envelopes. The beams did not reach their ultimate moment capacities because the analysis stopped when the base of the right column reached its curvature capacity.

The column moment diagrams are shown in Figure 4.7. The ultimate moment capacity was reached at location 1 of the right-side column. The moment at location 2 of the same column was very close to reaching its ultimate capacity. Because of uncertainties in the analysis, it is unclear which location would have actually reached its capacity first. The left-side lower-story column and the upper-story columns did not reach their ultimate capacities.

Figure 4.8 summarizes the flexural demands for the columns and beams of an exterior frame. Part (a) shows that the ultimate flexural capacity was reached at locations 1 and 2 of the right-side column. Part (b) shows that yielding occurred at column locations 1 and 2, in each beam at 6 feet from the face of the right-side columns and in each beam at the face of the left-side columns. Part (c) shows that the curvature ductility demands were highest in the beams and at the base of the columns. The failure mechanism for an exterior frame was similar to that of an interior frame, except that yielding in the interior frames' columns was concentrated at location 2.



a) Upper-Story Beam



b) Lower-Story Beam

Figure 4.6. Moment Diagrams for Exterior, Transverse Beams

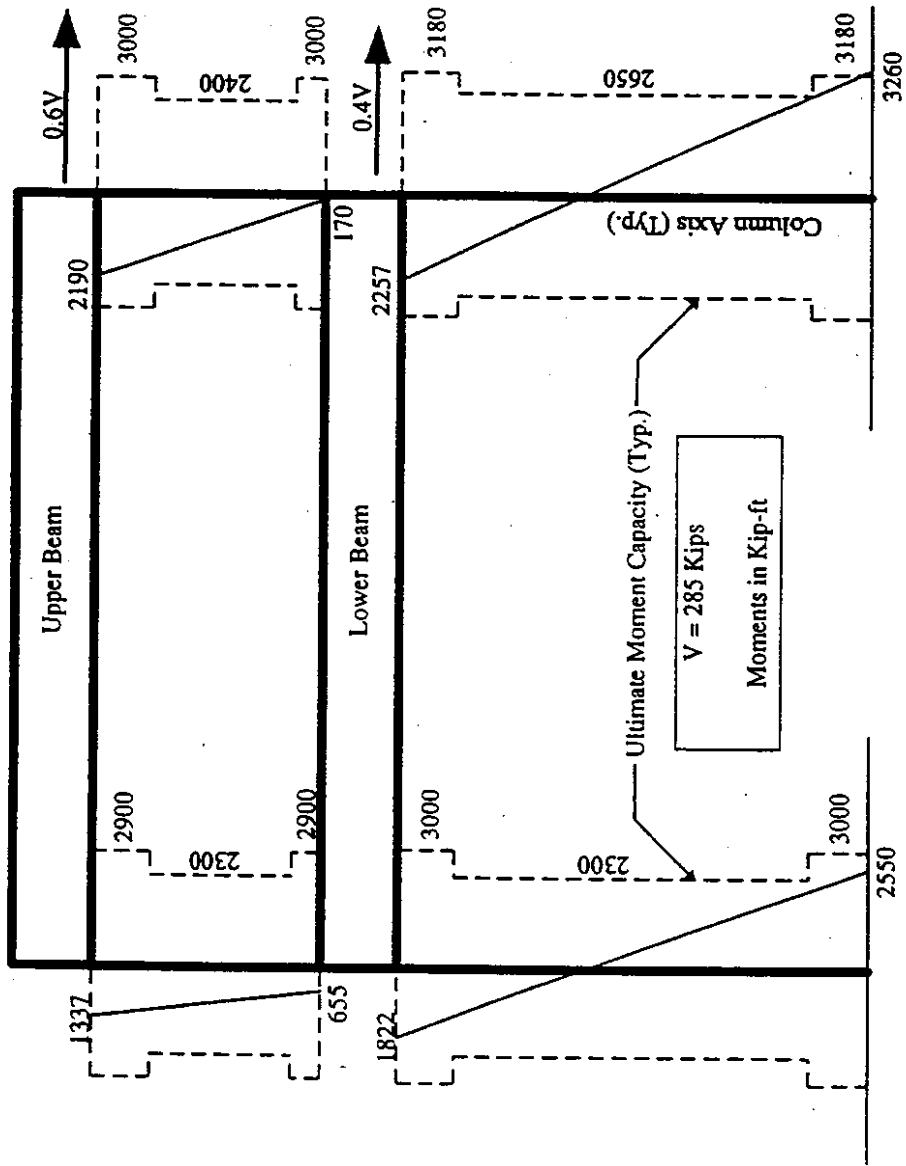


Figure 4.7. Moment Diagrams for Exterior, Transverse Columns

Exterior Bent
Base Shear = 285 Kips

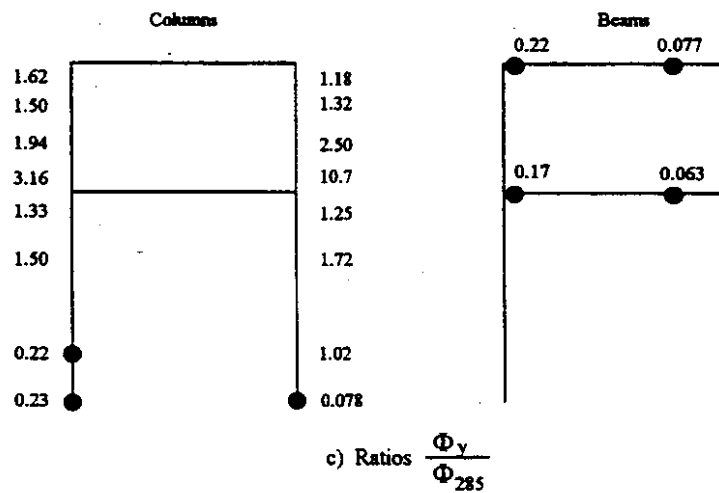
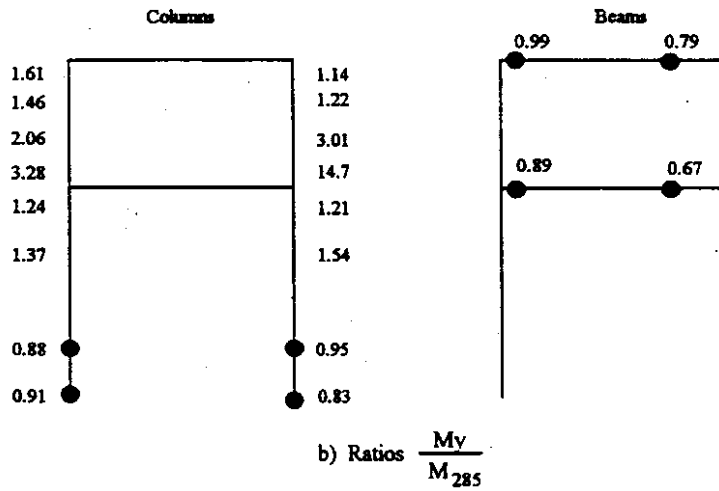
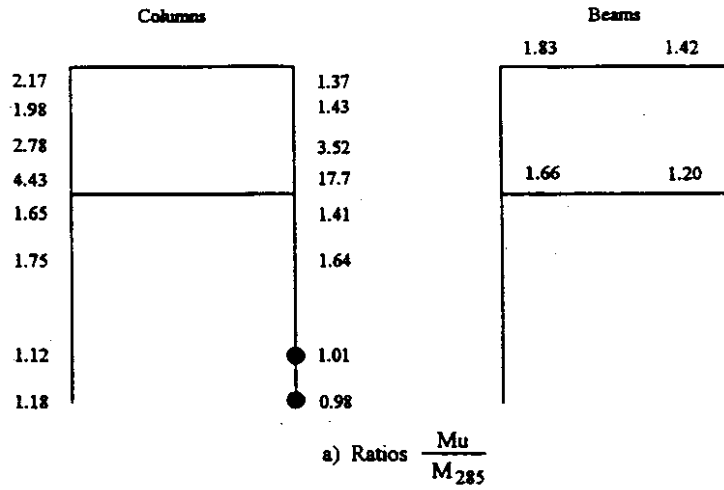


Figure 4.8. Flexural Capacity/Demand Ratios for Exterior Frames

4.3 LONGITUDINAL DIRECTION RESPONSE

The lateral force-displacement relationships for the longitudinal frames are shown in Figure 4.9. The total force capacity was found to be 1500 kips (28 percent of the unit's weight) at an upper-deck displacement of 1.5 feet (a 2.8 percent drift ratio). The total lateral force capacity was 20 percent less in the longitudinal direction than in the transverse direction for two main reasons. First, the girders were relatively weak in comparison to the transverse beams, and second, in the longitudinal direction the exterior columns were bent about their weak axis. The exterior columns were relatively flexible and ductile about their weak axis, and therefore, they did not limit the ultimate lateral displacements as they did in the transverse direction. As a result, the ultimate drift ratio in the longitudinal direction was 2.5 times higher than in the transverse direction.

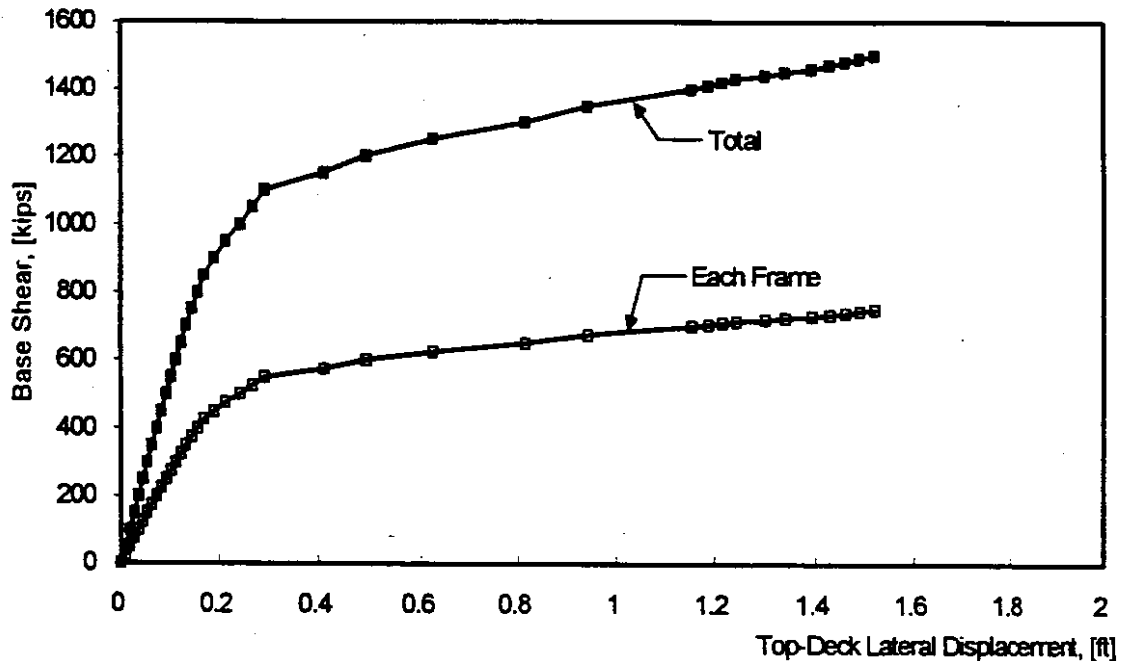


Figure 4.9. Lateral Force-Displacement Relationships for Longitudinal Frames

The moment diagrams corresponding to the ultimate base shear of 1500 kips are shown for the top and bottom girders in Figure 4.10. All girders reached their negative moment capacities at their right ends, while only the two right-side girders reached their positive moment capacities approximately 10 feet from the face of the interior columns. The moments were close to the positive moment capacities in both middle girders 6 feet from the face of the left interior columns and in both left-side girders 2 feet from the face of the exterior columns.

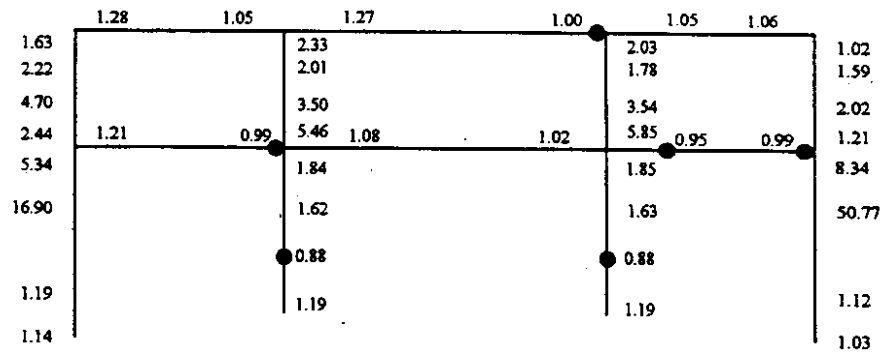
The column moment diagrams corresponding to the ultimate base shear are shown in Figure 4.11. The moment capacities were reached at location 2 of the interior columns. The right-side exterior columns were close to reaching their capacities at locations 1, 2, and 8. All other column locations did not reach their capacities.

Figure 4.12 summarizes the flexural demands for the columns and beams of a longitudinal frame. Part (a) shows that the ultimate capacities were reached at location 2 of both interior columns and at various girder locations. Parts (b) and (c) show that yielding occurred at locations 1 and 2 of each column and in each girder. The highest curvature ductility demands occurred in the girders and at location 2 of the interior columns.

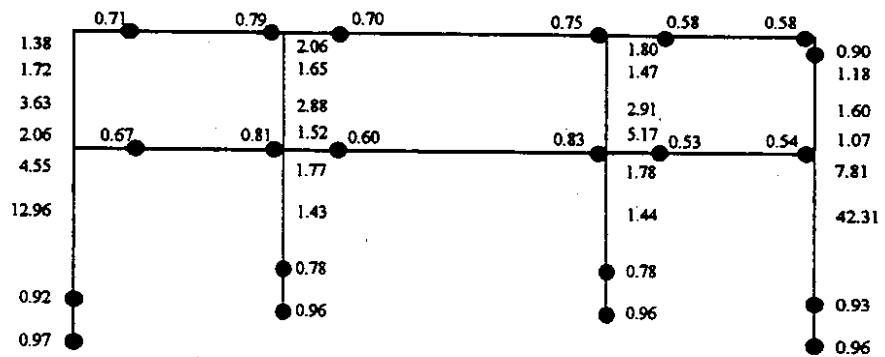
4.4 PLASTIC-HINGE ANALYSIS

Plastic-hinge analyses were conducted to compute the yield and ultimate capacities of each lateral frame. The capacities of each frame were computed using the three failure mechanisms shown in Figure 4.13. Mechanism 1 consisted of plastic hinges at the ends of the lower-story columns. Mechanism 2 consisted of plastic hinges at column locations 2 and 3. Mechanism 3 consisted of plastic hinges in the beams or girders and at either column location 1 or 2, depending on which resulted in the lowest capacity. The hinge locations in the beams and girders were selected on the bases of the results of the nonlinear analyses.

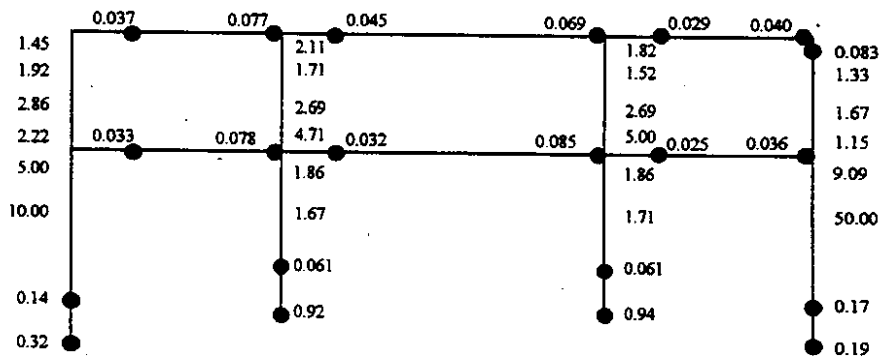
Longitudinal Frame
Base Shear = 750 kips



a) Ratios $\frac{M_u}{M_{750}}$



b) Ratios $\frac{M_v}{M_{750}}$



c) Ratios $\frac{\Phi_v}{\Phi_{750}}$

Figure 4.12. Flexural Capacity/Demand Ratios for Longitudinal Frame

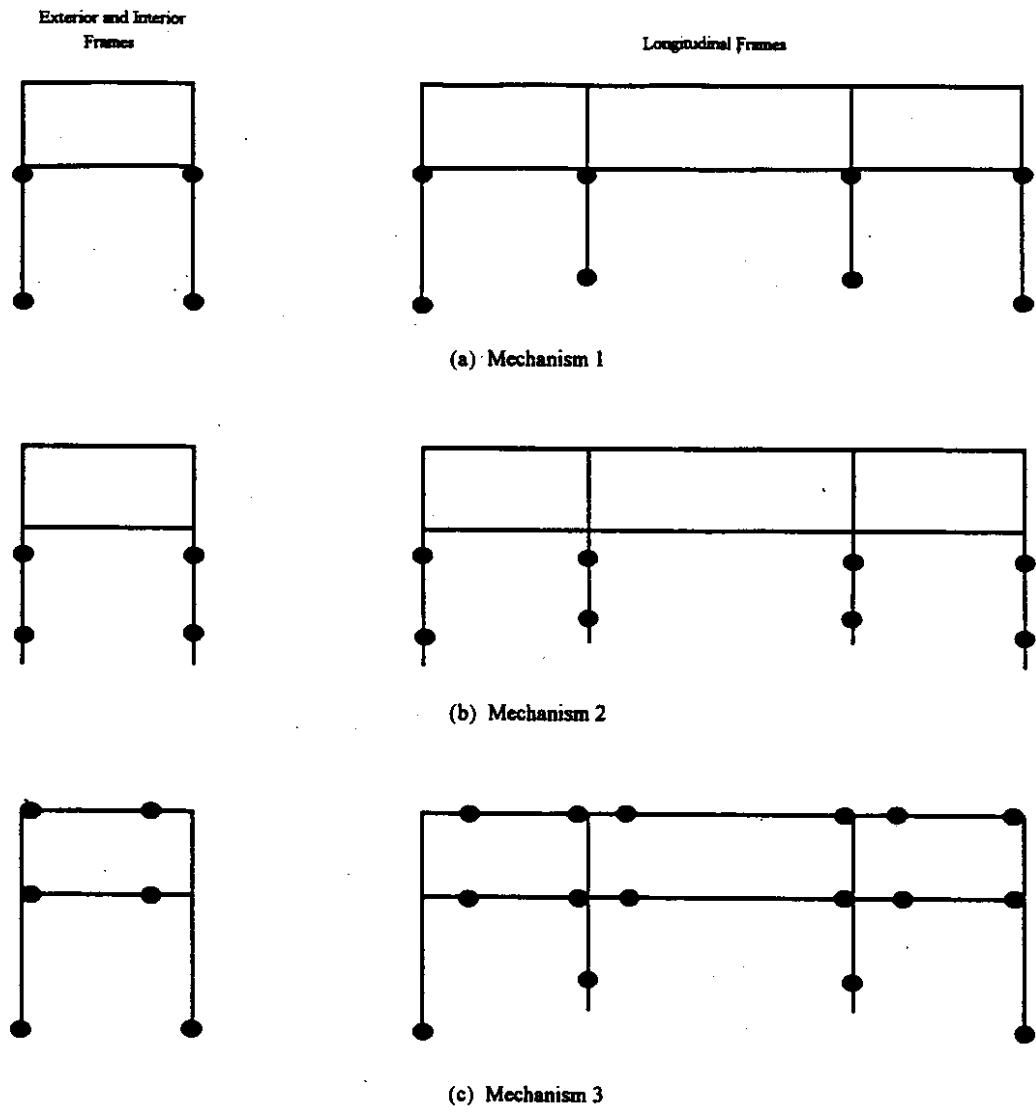


Figure 4.13. Plastic-Hinging Mechanisms 1 thru 3

CHAPTER 5

FLEXURAL DUCTILITY

Structural members must have flexural ductility to withstand the inelastic deformations caused by earthquakes. Flexural ductility is the ability to deform beyond yielding of the longitudinal reinforcement without significant loss of strength. Ductility can be achieved by using properly detailed transverse reinforcement, such as hoops or spirals.

Properly proportioned transverse reinforcement provides confining stresses that enhance the core concrete's compressive strength. The transverse reinforcement also helps prevent the longitudinal reinforcement from buckling after the concrete cover has spalled off. Typically, the concrete cover spalls off between ductility levels 2 to 3.

Older bridges often have too little transverse reinforcement, and it is often inadequately anchored into the column core. Inadequate transverse reinforcement can lead to core crushing and longitudinal reinforcement buckling.

The following sections present flexural ductility evaluations of the typical SED unit that were conducted with both the ATC-6-2 procedure (Section 5.1) and the Priestley et al. (1992) procedure (Section 5.2). Results from both the linear and nonlinear analyses contribute to an evaluation of the global ductility demand imposed on the unit (Section 5.3).

5.1 ATC-6-2 EVALUATION

The ATC-6-2 procedure evaluates the adequacy of confinement by computing the confinement C/D ratio, r_{cc} , at each column location (ATC, 1983). The confinement C/D ratio is defined as the product of the flexural C/D ratio (Chapter 3) and the ductility capacity, μ .

$$r_{cc} = \mu r_{ec} \tag{5.1}$$

The ductility capacity is defined by the following equation:

$$\mu = 2 + 4 \left(\frac{k_1 + k_2}{2} \right) k_3 \quad (5.2)$$

where,

$$k_1 = \frac{A_{sh}(c)}{A_{sh}(d) \left(0.5 + \frac{1.25P}{f_c A_g} \right)} \leq 1 \quad (5.3)$$

$$k_2 = \frac{6}{s/d_b} \leq 1 \text{ or } \frac{0.2}{s/b_{min}} \leq 1, \text{ whichever is smaller} \quad (5.4)$$

k_3 = effectiveness of transverse bar anchorage (ATC, 1983)

P = axial force on column from analysis

A_g = gross section area of column

b_{min} = minimum width of column cross section

$A_{sh}(c)$ = area of existing transverse confinement

$A_{sh}(d)$ = maximum of $30 a h f_c / f_y [A_g / A_c - 1]$
or $0.12 a h f_c / f_y$

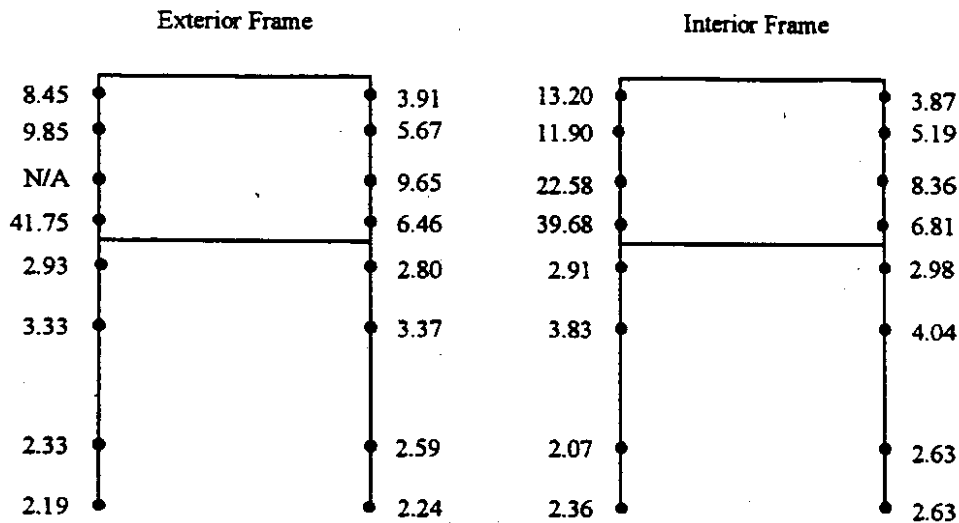
A_c = area of concrete core

h = core dimension of column in direction of shear

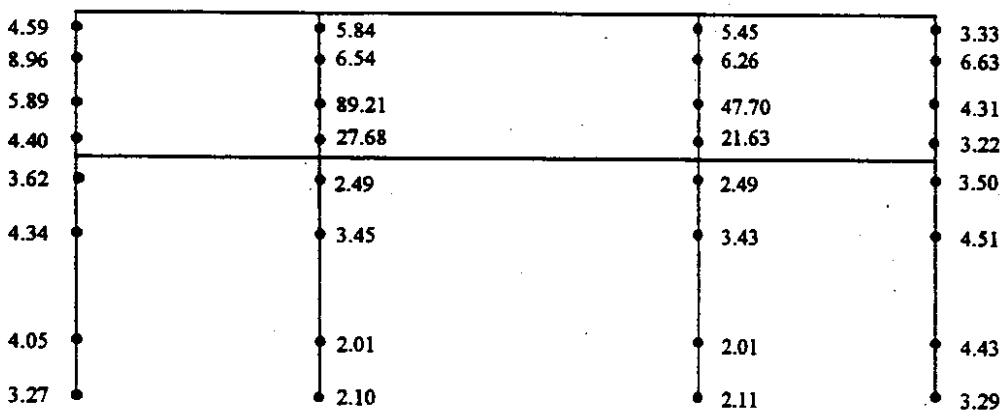
a = vertical spacing of hoops.

According to Equation 5.2, all columns have a minimum ductility of 2, regardless of the size, spacing, and anchorage of the transverse reinforcement. This reflects observations that all columns can achieve a ductility of at least 2 before the concrete cover spalls off (Priestley et al., 1992). It follows that, if r_{ec} exceeds 0.5, the value of r_{cc} will be greater than 1.0.

Figure 5.1 summarizes the values of r_{cc} for each column of the SED unit. All values greatly exceeded 1.0 because the flexural C/D ratios greatly exceeded 0.5 (Section 3.5). The ductility capacities, μ , were found to be relatively low (between 2.4 and 2.7) because the transverse reinforcement was inadequately anchored.



(a) Transverse Frames



(b) Longitudinal Frame

Figure 5.1 ATC-6-2 C/D Ratios for Transverse Confinement, r_{cc}

As discussed in Chapter 3, the flexural C/D ratios were typically larger in the SED unit than in the WSDOT unit, especially at the base of the lower-story columns. The ductility capacities were similar for both units, even though the transverse reinforcement consisted of #4 bars spaced 12 inches in the SED unit and #3 bars with the same spacing in the WSDOT unit. The difference in bar sizes did not affect the results because the bars

were inadequately anchored in both units. As a result, the confinement C/D ratios were typically higher in the SED unit than in the WSDOT unit.

5.2 PRIESTLEY ET AL. (1992) EVALUATION (UCSD)

The Priestley et al. (1992) procedure evaluates the adequacy of confinement by computing a global C/D ratio. The global C/D ratio is the ratio of the equivalent elastic base shear strength (V_E) to the base shear demand (V_D). The values of V_E are determined from the nonlinear force-displacement relationships, and the values of V_D are computed from both the ATC-6 and the site-specific response spectra. The ATC-6 response spectrum is shown in Figure 3.5, and the site-specific response spectrum is shown in Figure 5.2. The effects of transverse reinforcement are accounted for in the nonlinear analyses.

Equivalent Elastic Strength, V_E

The equivalent elastic strength (V_E) of the unit was assumed to be the product of the unit's elastic stiffness and the ultimate displacement at the center of mass (Figure 5.3). This assumption is consistent with the observation that the maximum linear and nonlinear displacements are nearly equal for long-period structures. The elastic stiffness was defined as the line that passes through the origin and the yield point of the force-displacement relationship. The yield base shear was assumed to be 75 percent of the ultimate lateral strength. These criteria were the same as those used to evaluate the WSDOT unit (Eberhard et al., 1995).

Figure 5.3 shows that V_E is sensitive to variations of the ultimate displacement. In turn, Eberhard et al. (1995) found that the ultimate displacement computed with nonlinear analysis was sensitive to the element lengths within the plastic-hinging region. As an alternative to the nonlinear analysis, the ultimate displacement was computed with plastic-hinge analyses similar to those described in Chapter 4. Mechanism 3 (Figure 4.2) was assumed to be the controlling failure mechanism for each frame. The total lateral

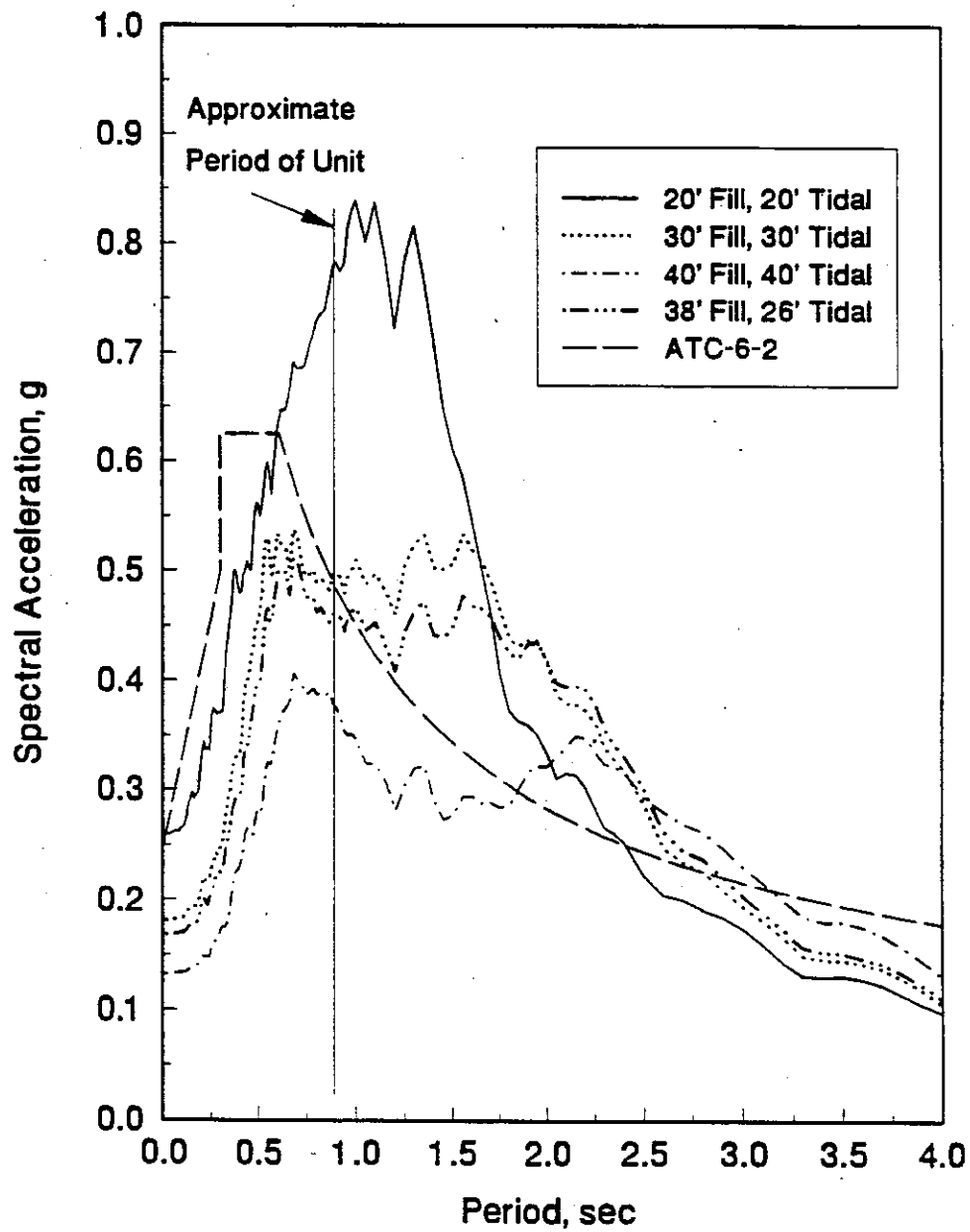


Figure 5.2. Site-specific Response Spectrum

location 2 of the right column. Both plastic analyses predicted displacements that were 25 to 30 percent smaller than the nonlinear displacement. The displacement computed by the Corley method was 15 percent higher than that computed by the Park and Priestley method.

For the exterior frame, all three methods predicted failure at location 1 of the right column. The displacements predicted by both plastic analyses were 30 to 40 percent higher than the nonlinear displacement. The Park and Priestley displacement was 5 percent higher than the Corley displacement.

For the longitudinal frame, the nonlinear method predicted failure at location 2 of the interior columns, whereas the plastic analyses predicted failure at the bottom left girder at the face of the interior column. The plastic-hinge displacements were 35 to 40 percent less than the nonlinear displacement.

To be consistent with the evaluation of the WSDOT unit and with the Priestley et al. (1992) procedure, V_E was computed with the displacements from the Park and Priestley plastic-hinge analysis. The results of the V_E calculations are listed in Table 5.2. The spectral acceleration capacities computed by dividing V_E by the mass are also listed in Table 5.2. The stiffness in the transverse direction was significantly higher than in the longitudinal direction, but the ultimate displacements were very close. As a result, the equivalent elastic strength in the transverse direction was 60 percent higher than in the longitudinal direction.

Base-Shear Demand, V_D

The periods for each direction were computed from the lateral stiffnesses listed in Table 5.2 and from the total mass of the structure. The computed values are listed in Table 5.3. These periods were slightly higher than those computed with the three-

Table 5.1 Computed Displacements

	Parameter	Nonlinear Analysis	Corley	Priestley and Park
Transverse, Interior Frame	Δ_y [in.]	3.0	-	-
	l_p [in.]	-	23.0	18.5
	θ_p [rad]	-	0.0143	0.0111
	Δ_p [in.]	-	6.3	5.1
	Δ_R [in.]	12.0	9.3	8.1
	Failure Location	Right Col. Location 2	Right Col. Location 2	Right Col. Location 2
Transverse, Exterior Frame	Δ_y [in.]	2.2	-	-
	l_p [in.]	-	23.0	24.6
	θ_p [rad]	-	0.0113	0.0123
	Δ_p [in.]	-	5.9	6.4
	Δ_R [in.]	6.2	8.1	8.6
	Failure Location	Right Col. Location 1	Right Col. Location 1	Right Col. Location 1
Longitudinal Frame	Δ_y [in.]	3.4	-	-
	l_p [in.]	-	35.0	29.8
	θ_p [rad]	-	0.014	0.0122
	Δ_p [in.]	-	4.0	5.2
	Δ_R [in.]	14.3	9.2	8.6
	Failure Location	Interior Col. Location 2	Bottom, Left Girder Right Side	Bottom, Left Girder Right Side

Δ_y = Yield Displacement at Center of Mass

l_p = Plastic-Hinge Length

θ_p = Plastic-Hinge Rotation

Δ_p = Plastic Displacement at Center of Mass

Table 5.2 Equivalent Elastic Base-Shear Strengths

Direction	Yield Stiffness [kips/ft]	Yield Displ. [ft.]	Ultimate Displ. [ft.]	Base Shear V_E [kips]	$S_a(c)$ $= V_E/\text{Mass}$ [g]
Transverse	7500	0.19	0.67	5000	0.96
Longitudinal	4020	0.28	0.71	2850	0.55

Table 5.3 Global Capacity-to-Demand Ratios

Direction	Period [sec.]	ATC Spectrum		Site-Specific Spectrum	
		$S_a(D)^{ATC}$ [g]	$\frac{S_a(C)}{S_a(D)^{ATC}}$	$S_a(D)^{Site}$ [g]	$\frac{S_a(C)}{S_a(D)^{Site}}$
Transverse	0.92	0.48	2.00	0.80	1.20
Longitudinal	1.26	0.39	1.41	0.80	0.70

dimensional, linear model (Section 3.3). In the transverse direction, the period computed for the SED unit was 15 percent less than that for the WSDOT unit because of the SED unit's higher stiffness. The opposite was true for the longitudinal direction.

The periods listed in Table 5.3 were used with both the ATC-6-2 and the site-specific response spectra (Section 3.4) to compute the spectral demands. The spectral demands ($S_a(D)$) are listed in Table 5.3.

Global Capacity-to-Demand Ratios

The global C/D ratios are computed as V_E/V_D , which can also be expressed as $S_a(C)/S_a(D)$. These ratios are listed in Table 5.3 for each direction and for each spectrum. The global C/D ratios were 40 to 70 percent higher in the transverse direction than in the longitudinal direction because the spectral capacities were significantly higher

in the transverse direction. The global C/D ratios were 60 to 100 percent lower for the site-specific spectrum than for the ATC-6 spectrum because the spectral demands were greater from the site-specific spectrum.

The flexural ductility appears to be adequate in both directions when considering the ATC-6 spectrum. In contrast, the SED unit appears to be vulnerable to flexural ductility failure in the longitudinal direction when considering the site-specific spectrum.

5.3 GLOBAL DUCTILITY DEMANDS

The global ductility demand can be approximated as the ratio of the base-shear demand to the base-shear corresponding to yield. The base-shear demand was taken as the base-shear from the response spectra (Table 5.3), and the yield base-shear was taken as 75 percent of the base shear capacity. Table 5.4 lists the global ductility demands for both the transverse and longitudinal directions, and for both the ATC-6 and site-specific response spectra.

The global ductility demands were slightly higher in the longitudinal direction than in the transverse direction for both response spectra. The global ductility demands from the site-specific spectrum were 70 to 100 percent higher than those from the ATC-6 spectrum.

Table 5.4 Global Ductility Demands

Direction	Yield Shear $Y_y = 0.75 V_u$ [Kips]	ATC Spectrum		Site-Specific Spectrum	
		V_{D}^{ATC} [Kips]	V_D/V_y	V_{D}^{Site} [Kips]	V_D/V_y
Transverse	1390	2490	1.79	4150	3.00
Longitudinal	1125	2020	1.80	4150	3.69

CHAPTER 6

SHEAR

Shear failures are undesirable because they are typically brittle and catastrophic. Current design methods attempt to avoid shear failures by ensuring that a member's shear capacity is greater than its flexural capacity, and therefore, that the member yields in flexure rather than failing in shear. For older bridges, there are many situations in which members could fail in shear before they would yield.

The shear vulnerabilities of the SED unit's columns were evaluated by computing capacity-to-demand ratios for each column with both the ATC-6-2 and the Priestley et al. (1994) procedures. In each procedure, the shear demands were computed using limit analyses. The shear capacities for both procedures were computed with the same general equation.

$$V_n = V_c + V_s + V_p \quad (6.1)$$

The shear capacity, V_n , was computed as the sum of the shear strength provided by the concrete, V_c , the shear strength provided by the transverse reinforcement, V_s , and shear strength provided by axial loads, V_p . The equations for V_c , V_s , and V_p are different for each procedure, and they are provided in the following sections. Nonetheless, in both procedures, the total shear capacity varies with the degree of displacement ductility, as shown in Figure 6.1. The initial shear strength, V_i , is constant up to the ductility level μ_i , and it decreases linearly to a final value, V_f , at a ductility level μ_f . Three scenarios are possible: first, if the shear demands exceed the initial capacity, the member will fail in a brittle manner (case A); second, if the shear demands are less than V_i , but greater than V_f , the member will fail in a combination of shear and flexure (case B); and third, if the shear demands are less than V_f , the member will not fail in shear regardless of the flexural ductility demand (case C).

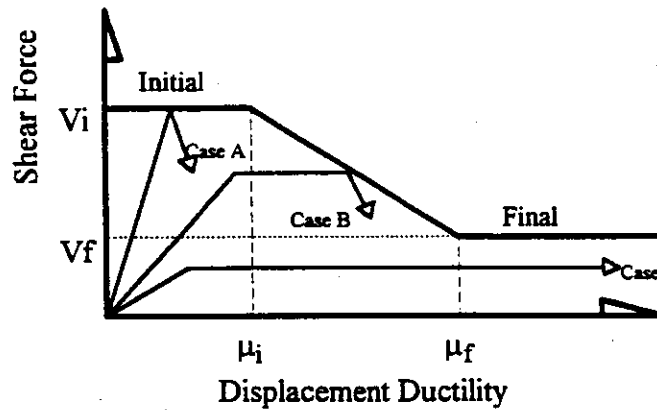


Figure 6.1. Variation of Shear Resistance with Ductility

6.1 ATC-6-2 EVALUATION

The computation of the shear capacity-to-demand ratio, r_{cv} , begins by determining whether the column yields. If the column does not yield ($r_{ec} > 1.0$), r_{cv} is defined as the ratio of the column's initial shear capacity, $V_i(c)$, to the elastic shear demand, $V_e(d)$. The value of $V_i(c)$ is the sum of the resistance provided by the concrete (V_c), steel (V_s), and axial load (V_p).

$$V_i(c) = V_c + V_s + V_p \quad (6.2)$$

where,

$$V_c = 2\sqrt{f_c} b d \quad (6.3)$$

$$V_s = (A_v f_y d)/s \quad (6.4)$$

$$V_p = (P/1000A_g) \sqrt{f_c} b d \quad (6.5)$$

If r_{cv} is less than 1.0, the column may fail suddenly in shear before any flexural yielding has occurred.

If the column was predicted to yield ($r_{ec} < 1.0$), then the three shear cases (A, B, and C) are possible. To determine which case applies, the maximum shear force resulting from plastic hinging in the column, $V_u(d)$, must be determined. According to ATC-6, $V_u(d)$ is equal to $1.3(M_{u1} + M_{u2})/L$, where M_{u1} and M_{u2} are the ultimate moments at the hinge locations and L is the distance between the hinges. The values of M_{u1} and M_{u2}

were determined using the procedures in Section 4.8.2 of "Seismic Design Guidelines" (ATC, 1981). The basic steps of these procedures are listed below.

- 1) Determine the plastic moment capacities at the hinge locations using the axial loads corresponding to dead load.
- 2) Compute the shear forces corresponding to the above values and sum them to obtain the maximum base shear for the bent.
- 3) Apply the maximum base shear laterally at the center of mass and determine the corresponding axial loads in the columns.
- 4) Combine the axial loads from step 3 with the gravity loads and determine the revised plastic moment capacities at the hinge locations.
- 5) Compute the maximum base shear corresponding to the new moments and compare it to the previous value. If it is not within 10 percent of the previous value, repeat steps 3-5.

The models used to compute M_{u1} and M_{u2} included the effects of strain hardening. Therefore, the over strength-factor of 1.3 in the equation for $V_u(d)$ was ignored for these analyses.

If $V_u(d)$ exceeds the initial shear strength of the column (case A), the column may fail in a brittle manner before the plastic hinges form. The C/D ratio for shear case A is computed using the elastic demands as follows:

$$r_{cv} = V_i(c)/V_e(d) \quad (6.6)$$

If $V_u(d)$ is less than $V_i(c)$, but greater than the final shear strength of the column, $V_f(c)$, the column may fail in shear after some flexural yielding has occurred (case B). The final shear strength of the column, $V_f(c)$, is the sum of the resistances provided by the transverse reinforcement and the axial load. The resistance provided by the concrete is neglected. If the transverse reinforcement is inadequately anchored, its resistance is neglected also. The resistance provided by the axial load is considered only when the axial stress exceeds 10 percent of the concrete's compressive strength. The value of r_{cv} for shear case B is computed as follows:

$$r_{cv} = \mu r_{ec} \quad (6.7)$$

where,

$$\mu = 2 + \left[0.75 \frac{L_c}{b_c} \right] \left[\frac{V_i(c) - V_u(d)}{V_i(c) - V_f(c)} \right] \quad (6.8)$$

and,

$$\begin{aligned} L_c &= \text{distance between hinges} \\ b_c &= \text{width of column in the direction of shear} \\ L_c/b_c &< 4.0 \end{aligned}$$

If $V_u(d)$ is less than $V_f(c)$, the column will not fail in shear, regardless of the ductility demand (case C). The C/D ratio for shear case C is computed as follows:

$$r_{cv} = (2 + 0.75 L_c/b_c) r_{ec} \quad (6.9)$$

For the typical SED unit, the value of $V_f(c)$ for all column locations was taken to be zero because the transverse reinforcement was inadequately anchored and the resistance provided by the axial load was neglected. Therefore, shear case C was not possible in these analyses.

Transverse Direction

Figure 6.2 lists the values of r_{cv} for the exterior and interior transverse frames. The values were computed at the possible plastic-hinge locations of the columns. The plastic-hinge locations were determined with plastic analyses.

For the exterior frame, yielding was predicted only at location 1 of both lower-story columns. The shear analyses indicated that shear case B applied at these two locations. The ductility demands were found to be very low ($\mu = 2.7-2.8$), and as a result, the shear C/D ratios greatly exceeded 1.0 ($r_{cv} = 2.4-2.7$). At location 4 of the same columns, the C/D ratios ($r_{cv} = 1.3-1.5$) were significantly less than the values at location 1, even though the capacities and demands were virtually the same. The only difference was that the values of r_{ec} were slightly less than 1.0 at location 1, and they were slightly greater than 1.0 at location 4. This discrepancy was an artifact of the ATC-6-2 procedure.

Yielding was not predicted in the exterior frame's upper-story columns, and the elastic shear demands were less than the initial shear capacities. Consequently, the values of r_{CV} were all greater than 1.0. Nonetheless, the shear demands associated with plastic hinging, $V_u(d)$, were much greater than the initial shear capacities, and shear case A would apply if the demands increased enough.

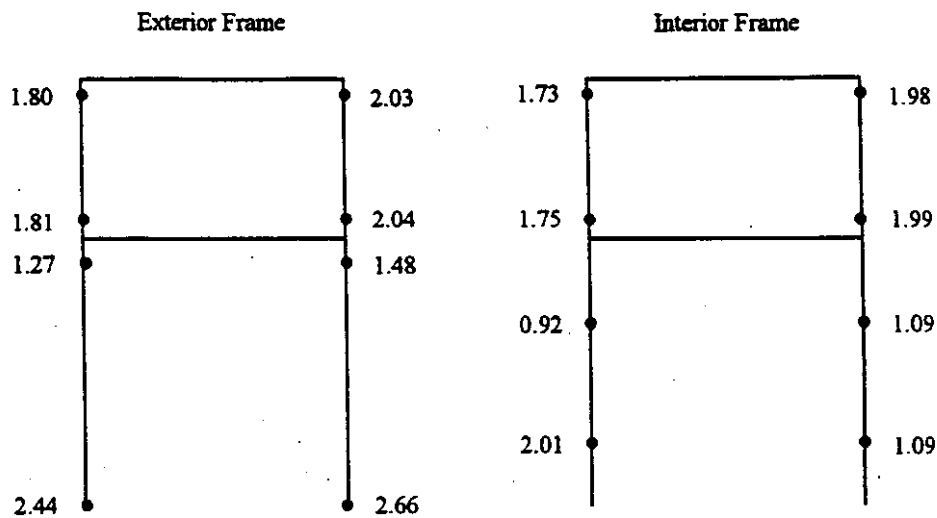


Figure 6.2. Shear C/D Ratios for Transverse Frames

For the interior frame, yielding was predicted only at location 2 of the tension-side, lower-story column (Figures 3.9 and 3.10). As in the exterior frame, shear case B applied; the ductility demand was low ($\mu = 2.4$); and the value of r_{CV} was much greater than 1.0 ($r_{CV} = 2.0$). At location 3 of the same column, the capacities and demands were nearly the same as at location 2, but yielding was not predicted. Because the elastic shear demand was greater than the initial shear capacity, column location 3 was predicted to fail in a brittle manner ($r_{CV} = 0.9$). Again, this demonstrated an inconsistency with the ATC-6-2 procedure.

The results for the interior frame's upper-story columns were nearly the same as those for the exterior frame.

Longitudinal Direction

Figure 6.3 lists the values of r_{CV} for the exterior and interior columns of a typical longitudinal frame.

For the exterior columns, no yielding was predicted, and all elastic shear demands were less than the initial shear capacities. Therefore, all values of r_{CV} exceeded 1.0. The values of r_{CV} for the exterior, upper-story columns were less than those for the exterior, lower-story columns. This is because the elastic analysis predicted higher shear demands in the stiff, upper-story columns than those predicted for the more flexible lower-story columns. For all the exterior column locations, the ultimate shear capacities, $V_u(d)$, as determined from limit analyses, were less than the initial shear capacities, $V_i(c)$; therefore, shear case B would apply if the shear demands increased enough.

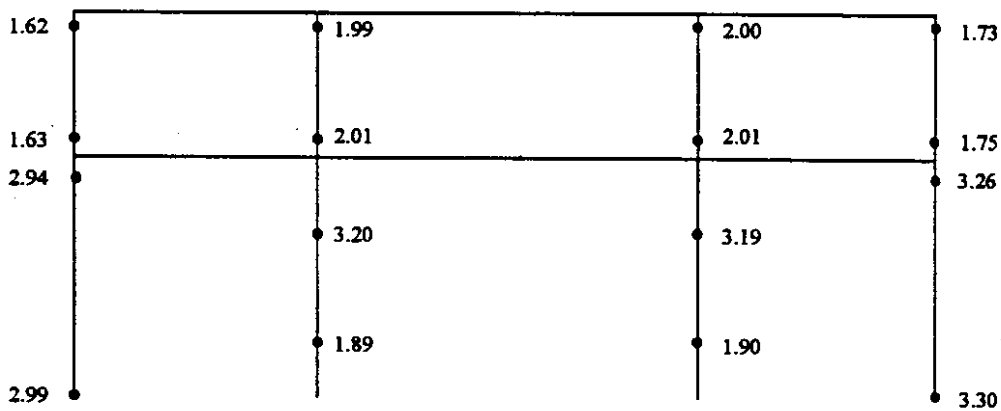


Figure 6.3. Shear C/D Ratios for Longitudinal Frame

Yielding was predicted at all four locations of the lower-story, interior columns. Shear case B applied at each location. The values of r_{CV} were greater than 1.0 ($r_{CV} = 1.9 - 3.2$) because the ductility demands were low ($\mu = 2.3$).

The upper-story, interior columns were not predicted to yield, and the elastic shear demands were much less than the initial shear capacities. Therefore, the values of r_{CV}

were all greater than 1.0 ($r_{CV} = 2.0$). For these columns, $V_u(d)$ was much greater than $V_i(c)$, and therefore, shear case A would apply if the demands increased enough.

6.2 PRIESTLEY ET AL. (1994) EVALUATION (UCSD)

The Priestley et al. (1994) shear evaluation procedures are similar to those of ATC-6-2. The shear demands are computed the same way, by using plastic-hinge analyses of the columns. The ultimate moments at the hinge locations are the same as those used in the two-dimensional, nonlinear analyses and include the effects of axial load and strain hardening. The general equation for the total shear capacity (Equation 6.1) is the same for both procedures, but the individual contributions, V_c , V_s , and V_p , are computed differently. The initial resistance provided by the concrete, V_{ci} , is assumed to be constant up to a ductility level of 2.0, at which point it decreases linearly to a final resistance, V_{cf} , at a ductility level of 4.0.

$$V_{ci} = 3.5\sqrt{f_c} 0.8 A_g \quad (6.10)$$

$$V_{cf} = 1.2\sqrt{f_c} 0.8 A_g \quad (6.11)$$

The shear capacities were first computed assuming that the resistances provided by the transverse reinforcement, V_s , and the axial load, V_p , are constant for all levels of ductility.

$$V_s = (A_v f_{yt} D') / (s \tan 30) \quad (6.12)$$

$$V_p = P \tan \alpha \quad (6.13)$$

where

A_v = area of transverse reinforcement

f_{yt} = yield stress of transverse reinforcement

D' = distance from outside of hoop to outside of hoop in the direction of shear

s = hoop spacing

α = angle of axial load with the column axis

Because the transverse reinforcement is inadequately anchored, the final shear capacities were computed again neglecting the contributions of the transverse reinforcement ($V_s = 0$).

The results of the analyses for both the exterior and interior frames in both the transverse and longitudinal directions are given in Table 6.1. Capacity-to-demand ratios are listed for the initial shear capacity (up to a ductility level of 2), for the final shear capacity (at a ductility level of 4) assuming that the transverse reinforcement is properly anchored, and for the final shear capacity assuming that the transverse reinforcement is ineffective ($V_s = 0$).

According to the results summarized in Table 6.1, the shear strength of the lower-story columns appears adequate for displacement ductilities below 2. When the contribution of the transverse reinforcement was included in the shear capacities, "Case B" shear failure was predicted for the lower-story, interior columns in the transverse direction at a displacement ductility of 4 ($C/D = 0.92$). The other lower-story columns, except for the exterior columns in the longitudinal direction, were predicted to be marginally adequate ($C/D = 1.03 - 1.06$). The lower-story, exterior columns in the longitudinal direction were found to be adequate for all levels of ductility demand ($C/D = 1.65$).

When the contribution of the transverse reinforcement was neglected ($V_s = 0$), the C/D ratios were reduced by 20 to 40 percent. "Case B" shear failure was predicted for all the lower-story columns, except for the exterior columns in the longitudinal direction. The minimum C/D ratio for the lower-story columns was 0.58.

"Case A" shear failure was predicted in the upper-story columns, but it is unlikely they would reach their ultimate shear demands because the demands would be limited by the lower-story columns. Therefore, shear failure would be unlikely in the upper-story columns.

6.3 COMBINED EVALUATION

The results from both procedures were similar. Both procedures identified the lower-story, interior columns as being vulnerable to shear failure, although they predicted different ductilities. The ATC-6-2 procedure predicted these columns would fail before

Table 6.1. Priestly et al. (1994) Shear Evaluation for Columns

Frame	Level	Beam's Axial Force	Column Dimensions				Bottom Moment [k-ft]	Top Moment [k-ft]	Axial Load [kips]	Initial Concrete Capacity [kips]	Final Concrete Capacity [kips]	Compr. Block Depth ϕ [in.]	Tangent of Angle α	Axial Load Contrib. V_p [kips]	Total Initial Capacity [kips]	Total Final Capacity [kips]	Shear at Plastic Capacity [kips]	Initial C/D Ratio (mu-sf)	Final C/D Ratio (mu-sf)	Final C/D Ratio (mu-sf) (V _s =0)
			Length		D'															
			e1	e2	e1	e2														
Exterior Frame	Bottom	comp	32.1	4	2	43	3180	3180	545	258	88	12	0.08	55	401	233	188	2.02	1.17	0.72
	Top	tens	32.1	4	2	43	3000	3000	218	258	88	12	0.08	20	387	188	187	1.88	1.08	0.68
Transverse Direction	Bottom	comp	15.8	4	2	43	3000	3000	278	258	88	12	0.18	53	349	231	380	1.85	0.81	0.37
	Top	tens	15.8	4	2	43	2900	2900	103	258	88	12	0.18	20	348	187	357	1.00	0.84	0.29
Exterior Frame	Bottom	comp	32.1	2	4	19	1410	1410	488	258	88	6	0.05	22	318	148	84	3.82	1.70	1.25
	Top	tens	32.1	2	4	19	1350	1350	243	258	88	6	0.05	11	307	139	84	2.85	1.65	1.18
Interior Frame	Bottom	comp	15.8	2	4	19	1280	1280	119	258	88	6	0.09	11	307	139	162	1.88	0.88	0.65
	Top	tens	15.8	2	4	19	1280	1280	119	258	88	6	0.09	11	307	139	162	1.88	0.88	0.65
Transverse Direction	Bottom	comp	17.1	4	4	43	4000	4000	1340	512	178	12	0.18	238	637	501	488	1.79	1.07	0.48
	Top	tens	17.1	4	4	43	3900	3900	450	512	178	12	0.18	74	678	339	374	1.81	0.91	0.37
Interior Frame	Bottom	comp	15.8	4	4	43	6280	6280	830	512	178	12	0.18	120	722	345	781	0.81	0.48	0.27
	Top	tens	15.8	4	4	43	6000	6000	210	512	178	12	0.18	40	645	308	759	0.85	0.40	0.28
Transverse Direction	Bottom	comp	17.1	4	4	43	3500	3500	950	512	178	12	0.18	187	788	432	408	1.88	1.08	0.44
	Top	tens	17.1	4	4	43	3500	3500	824	512	178	12	0.18	84	758	429	408	1.85	1.03	0.41
Interior Frame	Bottom	comp	15.8	4	4	43	8000	8000	452	512	178	12	0.18	84	844	352	759	0.81	0.48	0.34
	Top	tens	15.8	4	4	43	8000	8000	484	512	178	12	0.18	81	833	348	759	0.80	0.48	0.34

flexural yielding ($V_i(c) < V_e(d)$), whereas the Priestley et al. (1994) procedure predicted that failure would occur after yielding ($2.0 < \mu < 4.0$). In addition, the Priestley et al. (1992) procedure found that when the shear resistance of the transverse reinforcement is neglected, the lower-story, exterior columns would fail in shear before developing their flexural capacities.

Both procedures determined that the upper-story columns would fail before they yielded in flexure, but shear failure is unlikely because the shear demands would be limited by the lower-story columns.

CHAPTER 7

ANCHORAGE

Inadequate anchorage of longitudinal reinforcement can lead to a sudden loss of flexural strength. In older bridges, the anchorage of the vertical column reinforcement into the footings and cap beams is often inadequate. Also, the beam positive-moment reinforcement often does not have a hook, and the anchorage length into the joints is too short.

The typical SED unit was evaluated for anchorage failure with both the ATC-6-2 and Priestley et al. (1992) procedures. The results are presented in the following sections. The evaluations were performed at the following locations:

- the longitudinal column reinforcement anchored into the top cap beams; these bars were not hooked at their ends
- the longitudinal reinforcement of beams and girders anchored into the exterior columns; the anchorage depths were limited, and most of the positive-moment bars were not hooked
- the bottom, longitudinal reinforcement of the exterior girders at interior column joints; these bars were discontinuous through the interior columns and had no hooks at their ends.

Anchorage failure was not anticipated at the footings because the longitudinal column bars were welded to steel frames that were embedded 3.75 feet into the footings. The frames were made of heavy angle members and were specified to develop the full tensile capacity of the column bars.

7.1 ATC-6-2 EVALUATION

Procedures for evaluating failure of the longitudinal column reinforcement anchored into the footings and cap beams are provided by ATC-6-2. Even though ATC-

6-2 does not require such an evaluation for beams, the procedures were also applied to the anchorage of the longitudinal beam and girder reinforcement.

The procedure begins by comparing the provided effective anchorage length of the longitudinal reinforcement, $\lambda_a(c)$, to the required effective anchorage length, $\lambda_a(d)$. If $\lambda_a(c)$ is less than $\lambda_a(d)$, the anchorage C/D ratio, r_{ca} , is a function of r_{ec} .

$$r_{ca} = \frac{\lambda_a(c)}{\lambda_a(d)} r_{ec} \quad (7.1)$$

If $\lambda_a(c)$ is greater than or equal to $\lambda_a(d)$, r_{ca} depends on the reinforcement details and the location of the anchorage. For this case, where the anchorage is evaluated at the cap beams, r_{ca} is equal to 1.0.

For straight reinforcement, the effective anchorage length, $\lambda_a(c)$, is taken as the embedded depth; for hooked reinforcement, it is taken as the embedded depth up to the hook. The required anchorage length, $\lambda_a(d)$, for straight bars is

$$\lambda_a(d) = \frac{k_s d_b}{\sqrt{f'c} \left(1 + \frac{2.5c}{d_b} + k_{tr} \right)} \geq 30d_b \quad (7.2)$$

where,

$$k_s = \text{reinforcing steel constant} = \frac{f_y - 11000}{4.8}$$

d_b = bar diameter [in.]

$f'c$ = concrete compression strength [psi]

f_y = yield stress of steel [psi]

c = lesser of the reinforcement's clear cover or 1/2 its spacing [in.]

$$k_{tr} = [A_{tr}(c)f_{yt}/600] s d_b < 2.5$$

A_{tr} = area of transverse reinforcement [in.²]

f_{yt} = yield stress of transverse reinforcement

s = spacing of transverse reinforcement

Square deformed bars were used as the main longitudinal reinforcement in the SED unit. The nominal bar diameter (d_b) was approximated as the nominal diameter of the equivalent round bar.

The required anchorage length for hooked bars is

$$\lambda_a(d) = \frac{k_m 1200 d_b f_y}{60000 \sqrt{f_c}} \geq 15d_b \quad (7.3)$$

where,

$k_m = 0.7$ for bars #11 and smaller

$k_m = 1.0$ for bars #13 and greater

Equations 7.2 and 7.3 show that $\lambda_a(d)$ can not be less than 30 bar diameters for straight bars and 15 bar diameters for hooked bars.

In all cases, $\lambda_a(d)$ was limited to the minimum value of 30 bar diameters for straight bars and 15 bar diameters for hooked bars. Table 7.1 lists the values of $\lambda_a(d)$ for each bar size based on these minimum values.

Columns

Table 7.2 lists the results of the evaluation for column bar anchorage into the cap beams. All columns had the same size reinforcement and anchorage lengths at their tops. Consequently, the values of $\lambda_a(c)/\lambda_a(d)$ were the same for all columns ($\lambda_a(c)/\lambda_a(d) = 0.85$). Although the anchorage lengths were insufficient ($\lambda_a(c) < \lambda_a(d)$), the flexural ductility demands were small, and all values of r_{ca} exceeded 1.0. The value of r_{ca} for the exterior column bars in the longitudinal frame was slightly greater than 1.0 ($r_{ca} = 1.06$), indicating that the anchorage length at this location was marginal.

Table 7.1. Required Embedment Lengths

Square Bar Size	Equivalent Round Bar Diameter [in.]	ATC-6-2 $\lambda_a(d)$		Priestley et al. (1992)
		Straight Bars (30d _b) [in.]	Hooked Bars (15d _b) [in.]	λ_{smin} [in.]
1" x 1"	1.128 (#9)	33.9	16.9	11.7
2" x 2"	2.257 (#18)	67.7	33.9	23.4

Table 7.2. ATC-6-2 Anchorage Evaluation for Column Bars into Cap Beams

Column Location			$\lambda_a(c)$ in.	$\lambda_a(d)$ in.	$\lambda_a(c)/\lambda_a(d)$	r_{ec}	r_{ca}
Transverse Frame	Exterior	Comp. Tens.	57.5	67.7	0.85	1.64	1.39
			57.5	67.7	0.85	3.54	3.01
	Interior	Comp. Tens.	57.5	67.7	0.85	1.49	1.26
			57.5	67.7	0.85	5.08	4.31
Longitudinal Frame	Exterior	Comp. Tens.	57.5	67.7	0.85	1.25	1.06
			57.5	67.7	0.85	1.72	1.46
	Interior	Comp. Tens.	57.5	67.7	0.85	2.10	1.79
			57.5	67.7	0.85	2.25	1.91

Table 7.3. ATC-6-2 Anchorage Evaluation for Transverse Beams

Beam Location		Bar Location	End of Bar	$\lambda_a(c)$ [in.]	$\lambda_a(d)$ [in.]	$\lambda_a(c)/\lambda_a(d)$	r_{ec}	r_{ba}
Exterior Frame	Lower-story	Bottom	Straight	44.0	67.7	0.65	0.79	0.51
		Top	Hooked	46.0	33.9	1.36	0.89	1.00
	Upper-story	Bottom	Straight	44.0	67.7	0.65	2.51	1.63
		Top	Hooked	46.0	33.9	1.36	2.15	1.00
Interior Frame	Lower-story	Bottom	Straight	44.0	67.7	0.65	0.79	0.51
		Top	Hooked	46.0	33.9	1.36	0.78	1.00
	Upper-story	Bottom	Straight	44.0	67.7	0.65	3.52	2.29
		Top	Hooked	46.0	33.9	1.36	1.71	1.00

Transverse Beams

Table 7.3 lists the values of r_{ba} for the longitudinal reinforcement at the ends of the transverse beams. The top bars for both the interior and exterior beams had 90-degree hooks at their ends, were 2-inch square bars, and had 46 inches of effective anchorage. The anchorage depths were found to be sufficient ($\lambda_a(c)/\lambda_a(d) = 1.36$), and therefore, the values of r_{ba} were set equal to 1.0.

The bottom bars were all straight, 2-inch square bars with 44 inches of effective anchorage into the columns. These anchorage lengths were found to be insufficient ($\lambda_a(c)/\lambda_a(d) = 0.65$). For the upper-story beams, the flexural ductility demands were low, and as a result, all values of r_{ba} for these beams were greater than 1.0. For the lower-story beams, the flexural ductility demands were relatively high, and as a result, the values of r_{ba} were much less than 1.0 ($r_{ba} = 0.51$).

Longitudinal Girders

Table 7.4 lists the values of r_{ba} for the exterior girder's top and bottom reinforcement. This reinforcement was anchored into the exterior columns, and it was discontinuous at the interior columns.

Table 7.4. ATC-6-2 Anchorage Evaluation for Longitudinal Girders

Girder Location		Bar Location	End of Bar	$\lambda_a(c)$ [in.]	$\lambda_a(d)$ [in.]	$\lambda_a(c)/\lambda_a(d)$	r_{ec}	r_{ba}
Exterior Column	Lower-story	Bottom	Straight	22.0	33.9	0.65	0.80	0.52
		Bottom	Hooked	22.0	16.9	1.30	0.80	1.00
		Top	Hooked	20.0	16.9	1.18	0.73	1.00
	Upper-story	Bottom	Straight	22.0	33.9	0.65	1.70	1.10
		Bottom	Hooked	22.0	16.9	1.30	1.70	1.00
		Top	Hooked	20.0	16.9	1.18	1.29	1.00
Interior Column	Lower-story	Bottom	Straight	21.0	33.9	0.62	0.23	0.14
	Upper-story	Bottom	Straight	21.0	33.9	0.62	1.00	0.62

At the exterior columns, all the top bars and two bottom bars were 1-inch square bars with hooks at the ends. The anchorage lengths of these were found to be sufficient. The other two bottom bars were 1-inch square bars but were straight at their ends. The anchorage lengths for these were insufficient ($\lambda_a(c)/\lambda_a(d) = 0.65$), and the ductility demands in positive bending were high. Therefore, the resulting value of r_{ba} for the straight bottom bars was much less than 1.0 ($r_{ba} = 0.52$).

At the interior columns, the bottom, 1-inch square bars were anchored 21 inches straight into the columns. These anchorage lengths were found to be insufficient ($\lambda_a(c)/\lambda_a(d) = 0.62$). In addition, the positive-moment ductility demands in the lower-story, exterior girders at the interior columns were very high. The resulting value of r_{ba} was very low ($r_{ba} = 0.14$). The value of r_{ba} for the upper-story girders was also less than 1.0 ($r_{ba} = 0.62$) because of high ductility demands and insufficient anchorage lengths.

7.2 PRIESTLEY ET AL. (1992) EVALUATION (UCSD)

The Priestley et al. (1992) procedure distinguishes between two types of anchorage, confined and unconfined. Anchorage confinement can result from adequately anchored transverse reinforcement or from clamping forces provided by the flexural reinforcement of an adjacent member. The clamping force may become ineffective if the adjacent member's reinforcement yields.

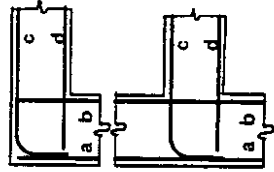
The development of confined anchorage is limited by the shearing strength of the concrete surrounding the anchored reinforcement. The average bond stress associated with this limit, μ_u , has been determined from tests (Priestley et al., 1992) and is as follows:

$$\mu_u = 18\sqrt{f_c} \quad (7.4)$$

If the ultimate tensile stress of the reinforcement, f_u , is assumed to be 1.5 times the yield stress, f_y , then the minimum anchorage length required to develop the reinforcement bar, λ_{smin} , can be written as follows:

Table 7.5. Priestly et al. (1992) Anchorage Evaluation

TRANSVERSE DIRECTION												
Frame	Deck Level	Moment	Bar ID	Bar #	Location	Condition	s (in.)	Length, l _s (in.)	T _s (kips)	T _u (kips)	T _s /T _u Ratio	l _s /l _{smin} Ratio
Interior	Top Level	(-)	a	18	Column/Ext	-	Welded to hooked ends of top bars in beam	6.8	48	95.9	258.4	0.37
		(+)	b	18	Column/Int	d yields						
	Bottom Level	(-)	c	18	Beam/Top	d doesn't yield						
		(+)	d	18	Beam/Bot	b yields	Hooked Bar	7.4	45	97.9	258.4	0.38
Exterior	Top Level	(-)	c	18	Beam/Top	b doesn't yield						
		(+)	d	18	Beam/Bot	b yields	Hooked Bar	7.4	45	97.9	258.4	0.38
	Bottom Level	(-)	a	18	Column/Ext	b doesn't yield						
		(+)	b	18	Column/Int	d yields	Welded to hooked ends of top bars in beam	8.5	48	119.9	258.4	0.46
Exterior	Top Level	(-)	c	18	Beam/Top	d doesn't yield						
		(+)	d	18	Beam/Bot	b yields	Hooked Bar	9.5	45	125.7	258.4	0.49
	Bottom Level	(-)	c	18	Beam/Top	b doesn't yield						
		(+)	d	18	Beam/Bot	b yields	Hooked Bar	9.5	45	125.7	258.4	0.49
LONGITUDINAL DIRECTION												
Column	Deck Level	Moment	Bar ID	Bar #	Location	Condition	s (in.)	Length, l _s (in.)	T _s (kips)	T _u (kips)	T _s /T _u Ratio	l _s /l _{smin} Ratio
Exterior	Top Level	(-)	a	18	Column/Ext	-		8	48	112.9	258.4	0.44
		(+)	b	18	Column/Int	d yields		8	48	112.9	258.4	0.44
	Bottom Level	(-)	c	9	Girder/Top	d doesn't yield						
		(+)	d	9	Girder/Bot	b yields	Hooked Bar	3	22	19.4	64.6	0.30
Interior	Top Level	(-)	c	9	Girder/Top	b doesn't yield						
		(+)	d	9	Girder/Bot	b yields	Hooked Bar	3	22	19.4	64.6	0.30
	Bottom Level	(-)	c	9	Girder/Top	b doesn't yield						
		(+)	d	9	Girder/Bot	a or b yield	Bars are continuous	9	21	55.6	64.6	0.86
Interior	Top Level	(-)	c	9	Girder/Top	a or b don't yield						
		(+)	d	9	Girder/Bot	a or b yield	Bars are continuous	9	21	55.6	64.6	0.86
	Bottom Level	(-)	c	9	Girder/Top	a or b don't yield						
		(+)	d	9	Girder/Bot	a or b don't yield						



Columns

The columns' type-b bars that were anchored into the top cap beams would be confined by the cap beams' or girders' type-d bars as long as the type-d bars did not yield or slip. Assuming that the beam or girder reinforcement did not yield, the anchorage of the columns' type-b bars would be adequate ($\lambda_s/\lambda_{smin} = 2$). If the cap beams' reinforcement did yield, and confinement of the anchorage was lost, then the anchorage lengths would be insufficient ($T_s/T_u = 0.4 - 0.5$). The flexural demands in the upper-story members were found to be small (Chapters 3 and 4) and it is unlikely that the upper-story cap beams would yield. Therefore, anchorage failure is unlikely for the columns' type-b bars.

The type-a bars in the transverse direction were welded to the hooks of the cap beams' type-c bars, and they were not in danger of pulling out. In the longitudinal direction, the columns' type-a bars were unconfined because of inadequate transverse reinforcement. The anchorage lengths of these bars were not sufficient to develop the bars' ultimate tensile capacities ($T_s/T_u = 0.4$). These anchorage lengths were also not sufficient to develop the bars' yield capacities, T_y ($T_s/T_y = 0.8$). Therefore, anchorage failure could occur before the bars yielded. Even though the flexural demands were small for the upper-story members, the columns' type-a bars in the longitudinal direction might be vulnerable to anchorage failure.

Transverse Beams

The type-c bars for the transverse beams were hooked into the columns, and their anchorage appeared to be adequate. The type-d bars were not hooked, but they would be confined by the columns' type-b bars so long as the type-b bars did not yield. The plastic hinges were expected to form in the beams (Chapters 3 and 4), and therefore, the columns were unlikely to yield. Given that fact, the type-d bars of the transverse beams appeared to be adequate for both the upper and lower stories and for both the interior and exterior frames ($\lambda_s/\lambda_{smin} = 2$).

Longitudinal Girders

As in the transverse beams, the type-c bars for the longitudinal girders were hooked into the columns, and their anchorage appeared to be adequate. For the type-d bars, half were hooked and half were not. These bars were confined by the columns' type-b bars. The girders were much weaker than the columns, and therefore, the columns would be unlikely to yield. Therefore, it appeared that the anchorage lengths for both the hooked and straight bars were adequate ($\lambda_s/\lambda_{smin} = 2$).

At the interior columns, the girders type-d bars were discontinuous through the columns. Again, it is unlikely that the column reinforcement would yield, and therefore, they would provide confinement for the girders' type-d bars. It appeared that the anchorage for these bars would also be adequate ($\lambda_s/\lambda_{smin} = 2$).

7.3 COMBINED ASSESSMENT

Both procedures predicted similar results for the column bars anchored into the cap beams. The ATC-6-2 procedure predicted that the tensile capacity of the type-b bars could not be developed ($\lambda_a(c)/\lambda_a(d) = 0.85$), but the anchorage was adequate because the flexural demands were small. The Priestley et al. (1992) procedure predicted that the full capacity could be developed in the type-b bars as long as the cap beam reinforcement did not yield. The cap beam reinforcement would be unlikely to yield because the flexural demands were small. Both procedures also predicted that the type-a bars in the longitudinal direction might be vulnerable to anchorage failure. The type-a bars in the transverse direction were not evaluated because they were welded to the cap beams' type-c bars.

The Priestley et al. (1992) procedure found that all the type-c and type-d bars of the beams and girders were adequately anchored because the column longitudinal bars provided confinement. While it is certain that the longitudinal girders would yield before the columns, it is not as certain that the transverse beams would do the same. The results

for the different plastic hinge mechanisms in the transverse direction were close, and there was uncertainty in the procedures. Therefore, it was not certain whether the transverse beams would yield before the columns. If the columns did yield before the transverse beams, the beam anchorage might be inadequate ($T_s/T_u = 0.38-0.49$). The ATC-6-2 procedure does not include the effects of confinement provided by adjacent members, and therefore, anchorage failure was predicted for the straight bars of the lower-story beams and girders where the flexural demands were high.

CHAPTER 8

SPLICES

Lap splices can fail if splices are too short, if they are located in plastic hinging zones, or if they have inadequate transverse reinforcement. Lap splice failure can result in reduced flexural and shear capacities.

In many older bridges (including the typical WSDOT unit) the columns' longitudinal bars are spliced directly above the footings. This location is typically a potential plastic-hinging zone, and the splice lengths are typically inadequate (20 bar diameters for the WSDOT unit). Therefore, the lap splices directly above the footings in many older bridges are vulnerable to failure.

Unlike many older bridges, the typical SED unit does not have lap splices directly above the footings. In fact, lap splices are used sparingly throughout the SED unit. Most of the columns' longitudinal bar splices are staggered and are welded with sufficient weld lengths to develop the tensile capacities of the reinforcement. Lap splices are used only in the interior, lower-story columns, as shown in Figure 8.1. The splices are located 7 feet above the footings (column location 2) and 6.5 feet below the bottom of the lower-story joints (column location 3). Only eight of twelve bars at these locations are lap spliced. The other four bars, which are the corner bars, are weld spliced near mid-height of the columns. The two bars within each lap splice differ in size; those coming up from the footings and those coming down from the lower-story joints are 2-inch square bars. These bars are spliced to 1-inch square bars.

Although these lap splices are located away from the footings and the joints, they are located in potential plastic-hinging zones. Their failure could result in reduced moment and shear capacities for the interior, lower-story columns. The potential for lap splice failure was investigated, as described in the following sections, with both the ATC-6-2 and Priestley et al. (1992) procedures.

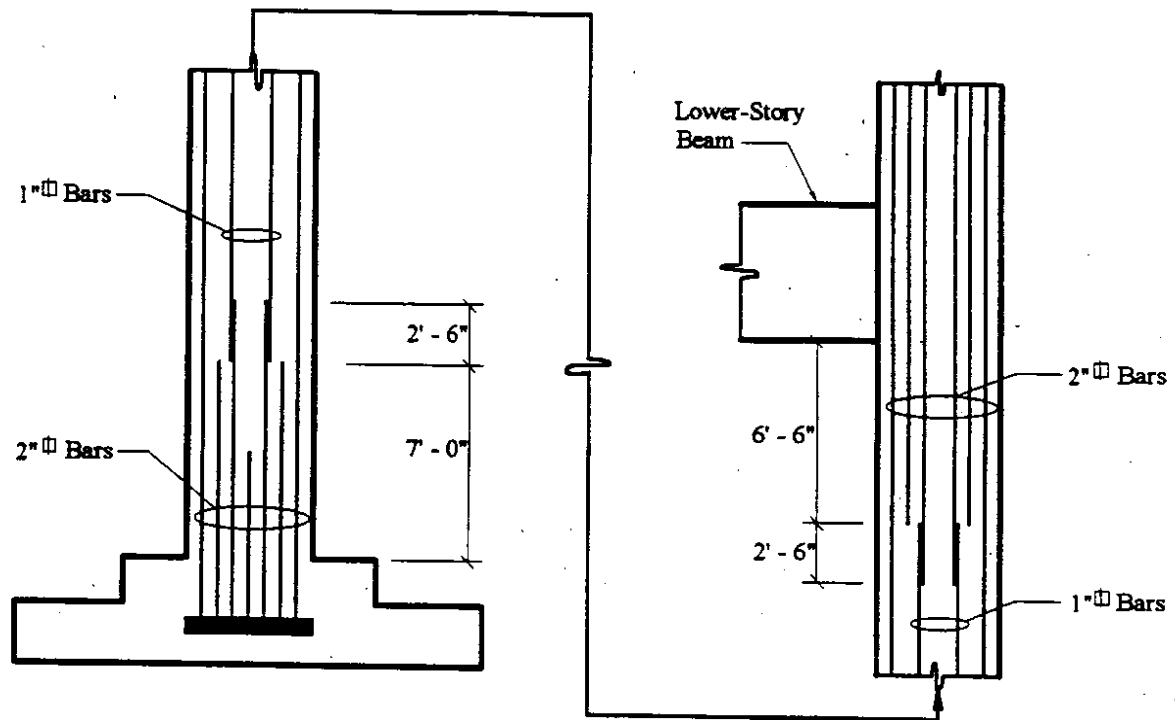


Figure 8.1. Lap Splices for Interior, Lower-Story Columns

All the longitudinal bars in the exterior columns and the four corner bars in the interior columns are weld spliced. Each of these bars are weld spliced near mid-height of both the upper- and lower-story columns, and the splices are staggered. The flexural demands at mid-height of the columns are small, and therefore, the welded splices are not likely to fail.

8.1 ATC-6-2 EVALUATION

According to ATC-6-2, if a lap splice is not located within a potential plastic-hinge zone and the splice length is sufficient, then splice failure is unlikely to occur. A lap splice length, λ_s , is sufficient when it is greater than the minimum lap splice length, λ_{smin} . The equation for λ_{smin} is as follows:

$$\lambda_{smin} = 1860 \cdot d_b / \sqrt{f'_c} \quad (8.1)$$

where,

d_b = bar diameter [in.]

f'_c = concrete compressive strength [psi]

For the SED unit's columns, for which $f'c$ was assumed to be 6300 psi, the value of λ_{smin} was approximately $24 \cdot d_b$. If λ_s is less than λ_{smin} and the splice is located outside potential plastic-hinge locations, then the splice C/D ratio, r_{cs} , is

$$r_{cs} = (\lambda_s / \lambda_{smin}) \cdot r_{ec} \quad (8.2)$$

If a lap splice is located within a potential plastic-hinge zone, and the splice length is inadequate ($l_s < l_{smin}$), the splice C/D ratio is

$$r_{cs} = \frac{A_{tr}(c)}{A_{tr}(d)} \left[\frac{(6/s)\lambda_s}{\lambda_{smin}} \right] r_{ec} < \frac{A_{tr}(c)}{A_{tr}(d)} r_{ec} \quad (8.3)$$

where,

$A_{tr}(c)$ = cross-sectional area of transverse reinforcement

$A_{tr}(d)$ = area of transverse reinforcement required to prevent splice failure

$$= \frac{s f_y A_b}{l_s f_{yt}} \quad (8.4)$$

s = spacing of transverse reinforcement [in.]

f_y = yield stress of spliced reinforcement [ksi]

A_b = area of spliced bar [in^2]

f_{yt} = yield stress of transverse reinforcement [ksi]

The factor $6/s$ should not be greater than 1.0, and λ_{smin} should not be less than $30 \cdot d_b$.

Also, if λ_s is greater than λ_{smin} , then r_{cs} does not have to be less than $0.75 \cdot r_{ec}$.

The following assumptions were made to implement the ATC-6-2 procedure:

- The bar diameter for square bars was assumed to be the diameter of a round bar with equivalent cross-sectional area.
- The area of the spliced bars, A_b , was assumed to be the larger of the two spliced bars.

- All the bars at locations 2 and 3 were assumed to be lap spliced, even though only eight of twelve bars were actually spliced.

Table 8.1 presents the results of the evaluation. All of the splices had the same bar sizes, splice lengths, minimum splice length requirements, transverse reinforcement, and transverse reinforcement requirements. The values of r_{CS} varied because some splices were in potential plastic-hinge zones, while some were not, and because r_{ec} varies according to the column locations and directions.

Table 8.1. ATC-6-2 Column Splice C/D Ratios, r_{CS}

Bar Size	Equivalent Bar Diam. [in.]	A_b [in. ²]	λ_s [in.]	s [in.]	$A_{tr}(c)$ [in. ²]	$A_{tr}(c)/A_{tr}(d)$	$6/s$	λ_s/λ_{smin}
2" x 2"	2.257	4.0	30	12	0.20	0.125	0.5	0.44

			r_{ec}	r_{CS}
Column Location 2	Trans.	Comp. Tens.	1.06	0.029
	Long.	Comp. Tens.	0.83	0.023
Column Location 3	Trans.	Comp. Tens.	0.81	0.022
	Long.	Comp. Tens.	0.81	0.022
Column Location 2	Trans.	Comp. Tens.	1.63	0.720
	Long.	Comp. Tens.	1.54	0.680
Column Location 3	Trans.	Comp. Tens.	1.38	0.610
	Long.	Comp. Tens.	1.39	0.610

In both the transverse and longitudinal directions, the splices at column location 2 were within possible plastic-hinge zones; the area and spacing of the confining reinforcement was inadequate; and the splice lengths were inadequate. All of these deficiencies together resulted in very low values of r_{CS} ($r_{CS} = 0.02 - 0.03$).

The splices at column location 3 in both directions were not within possible plastic-hinging zones (Chapter 3). Therefore, the values of r_{CS} were determined using Equation 8.2 and were a function of the splice length, the required splice length, and r_{ec} .

These splices were also found to be vulnerable ($r_{CS} = 0.6 - 0.7$), but to a lesser degree than the splices at column location 2.

8.2 PRIESTLEY ET AL. (1992) EVALUATION (UCSD)

The Priestley et al. (1992) procedure for evaluating splice failure resembles the procedure for evaluating anchorage failure. The type of splice is again classified as confined or unconfined. The SED unit's splices were all classified as unconfined because of inadequate transverse reinforcement and because there were no adjacent members whose reinforcement might provide confinement.

Unconfined splice failure is characterized by the formation of longitudinal cracks between the bars and along the surface inside the rows of bars. The maximum resistance that can be developed along these cracks, T_b , is given in Equation 8.6.

$$T_b = f_t \cdot p \cdot \lambda_s \quad (8.6)$$

where,

f_t = concrete resistance, assumed equal to $4\sqrt{f_c}$ [psi]

p = perimeter of crack surface around spliced bar [in.]

$$= 2(c + d_b) + s/2$$

λ_s = length of splice [in.]

c = concrete cover [in.]

d_b = diameter of spliced bars [in.]

s = spacing of spliced bars [in.]

The splices are evaluated by comparing T_b to the bar's yield capacity, T_y , and to the bar's ultimate capacity, T_u . If T_b is greater than T_u , the splice is unlikely to fail. If T_b is less than T_u but is greater than T_y , the splice may survive beyond the yield moment but will have limited ductility and may not survive repeated load reversals. If T_b is less than T_y , the splice will fail before the yield moment is reached.

The results of the Priestley et al. (1992) splice evaluation are presented in this section. To be consistent with the evaluation of the typical WSDOT unit, the concrete cover, c , was conservatively assumed to be 1.0 inches.

The splices at both column locations 2 and 3 and in both the longitudinal and transverse directions were identical, according to the Priestley et al. (1992) procedure, because they all had the same bars sizes, bar spacing, splice lengths, and material properties. Table 8.2 lists the results of the evaluation. Table 8.2 shows that T_b was less than T_y ($T_b/T_y = 0.88$), and therefore, these splices would likely fail before the yield moment was reached.

Table 8.2. Priestley et al. (1992) Splice Evaluation

s [in.]	p [in.]	λ_s [in.]	T_b [kips]	T_y [kips]	T_u [kips]	T_b/T_y	T_b/T_u
14	13.5	30	128	145	260	0.88	0.49

8.3 COMBINED ASSESSMENT

Both procedures revealed that the splices at locations 2 and 3 of the interior columns were inadequate. While the Priestley et al. (1992) procedure found that the vulnerabilities were the same at both locations 2 and 3, the ATC-6-2 procedure found that the splices at location 2 were much more vulnerable than those at location 3.

Both procedures are probably overly conservative because not all the bars at column locations 2 and 3 were lap spliced. While the flexural and shear capacities of the interior, lower-story columns would likely decrease if the lap splices failed, the reductions would be less than if all the bars had been spliced at the same locations.

CHAPTER 9

JOINTS

Joint-shear failure was a major source of damage to double-deck bridges during the 1989 Loma Prieta earthquake. Nonetheless, ATC-6-2 does not provide procedures for evaluating joint-shear failure. Priestley et al. (1992) provide evaluation procedures that compare a joint's principle tensile stress to its tensile capacity. For joints with little shear reinforcement, the tensile capacity is conservatively approximated as $3.5\sqrt{f'_c}$. In a simpler assessment procedure proposed by Thewalt and Stojadinovic (1992), a joint's nominal shear stress is compared to a limiting value. For joints with little shear reinforcement, Thewalt and Stojadinovic recommend that the nominal shear stress be limited to $3.5\sqrt{f'_c}$ (psi).

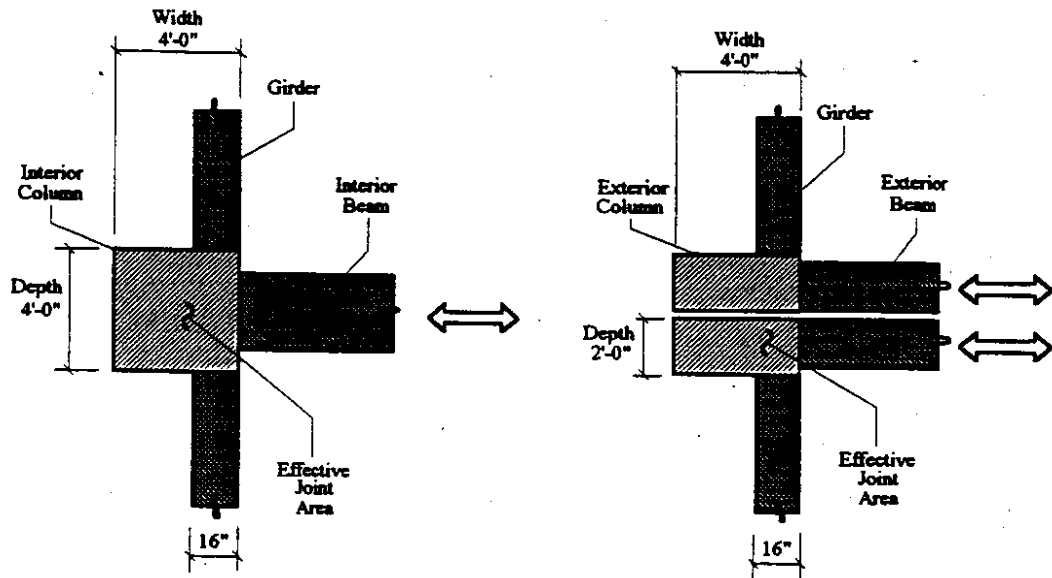
The joints of the typical WSDOT unit were evaluated using both the tensile and shear stress criteria (Eberhard et al. 1995). Both methods produced similar results, and therefore, only the simpler nominal shear stress method was used to evaluate the joints of the typical SED unit.

9.1 EFFECTIVE JOINT AREAS

The area over which the horizontal shear forces effectively act is referred to as the "effective joint area." In the transverse direction, where the beams are slightly narrower than the columns, the entire column cross-section was assumed to be effective in resisting the horizontal shear (Figure 9.1).

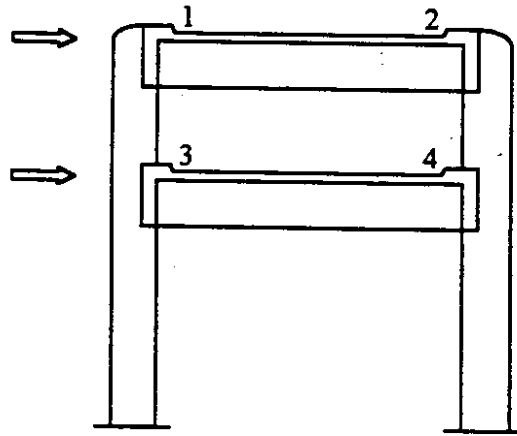
In the longitudinal direction, where the exterior girders are significantly narrower than the columns, it would have been unconservative to assume that the entire cross-sectional area of the column would resist the horizontal shear. On the other hand, it would have been overly conservative to assume that the effective width was equal to the girder width. Therefore, the effective width was determined following the procedures used in the evaluation of the WSDOT unit. The boundary of the effective area was

approximated by a line extending from the girder's exterior face at 45 degrees through the column. The effective width was calculated to be the girder width plus either 1/2 the protruding column dimension, or 1/2 the column depth, whichever was less (Figure 9.2).



a) Plan View Interior Joint

b) Plan View Exterior Joint



c) Joint Designations

Figure 9.1. Effective Joint Areas and Designations - Transverse Direction

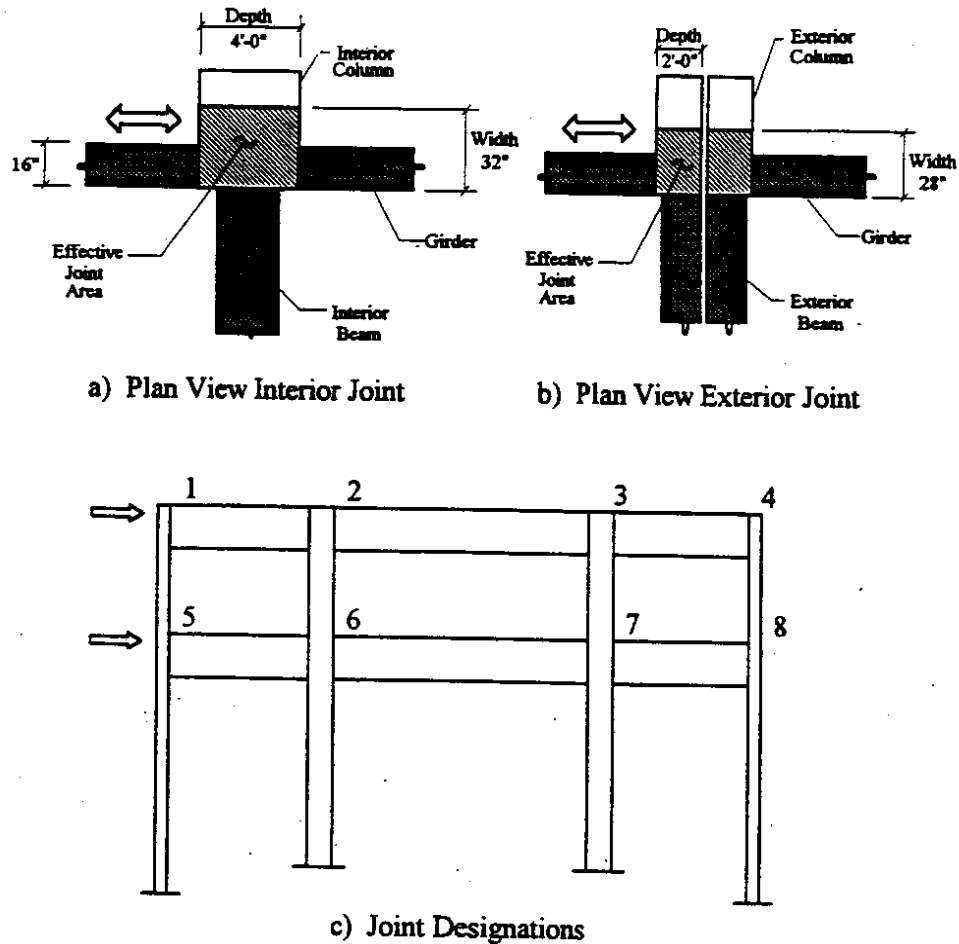


Figure 9.2. Effective Joint Areas and Designations - Longitudinal Direction

9.2 EVALUATION

The joint-shear stress, v , was computed with the following equation:

$$v = V/(b_j \cdot d_j) \text{ [psi]} \quad (9.1)$$

where,

V = joint-shear force [lbs]

b_j = effective joint width [in.]

d_j = effective joint depth [in.]

Each joint was evaluated using three values of joint-shear force. First, the ultimate joint-shear force, V_{ult} , was computed with the following equation:

$$V_{ult} = (M_{ult}^L + M_{ult}^R)/z \quad (9.2)$$

where,

M_{ult}^L = beam's or girder's ultimate moment capacity at left of the joint

M_{ult}^R = beam's or girder's ultimate moment capacity at right of the joint

z = effective lever arm of the beams or girders

M_{ult} for each beam for girder was computed as the product of the tensile reinforcement's area, A_{st} , the tensile reinforcement's ultimate tensile stress, f_{su} , and the effective lever arm, z .

$$M_{ult} = A_{st} \cdot f_{su} \cdot z \quad (9.3)$$

The ultimate strength of the tensile reinforcement, f_{su} , was assumed to be 1.3 times greater than the reinforcement's yield strength, f_y , and the value of A_{st} included the effective slab reinforcement for negative beam or girder moments.

The second set of shear forces was derived from the results of the nonlinear analyses (Chapter 4). The third set of shear forces was again computed using Equation 9.2, except the effects of the slab reinforcement were ignored. In each of the three cases, the maximum joint forces were limited by the columns' capacity to resist the unbalanced beam or girder moments.

Table 9.1 lists the results of the joint-shear evaluation for both the transverse and longitudinal directions and for all three values of joint-shear stress. The evaluation revealed that almost all the joints were vulnerable to joint-shear failure, even given the less conservative values of v_{non} and v_{ult} with no slab reinforcement. The exterior, longitudinal joints at locations 4 and 8 would likely be adequate if the slab reinforcement was ignored. Most of the slab bars were anchored at their ends with 180 degree hooks, and they would likely contribute to the moment capacities of the beams, and girders. Therefore, it would be unconservative to ignore the slab reinforcement in the joint-shear analyses. In addition, joints 4 and 8 would likely be vulnerable when the forces reversed direction (see joints 1 and 5).

Chapter 7 revealed that the anchorage of the positive moment reinforcement of some beams and girders might be vulnerable to anchorage failure, and thus the positive moment capacities of these members might be less than the capacities used for these joint-shear evaluations. Therefore, anchorage failure would decrease a joints' vulnerability to shear failure when it was subjected to a beam's or girder's positive bending moment. On the other hand, the negative moment reinforcement (including the top slab reinforcement) was adequately anchored and would likely cause joint-shear failure when it was in tension. Therefore, all the joints were vulnerable to shear failure.

Table 9.1. Joint-Shear C/D Ratios

Joint Location			Slab Reinf. Included				No Slab Reinf.	
			$\frac{v_{ult}(d)}{\sqrt{f'c}}$	C/D (1)	$\frac{v_{non}(d)}{\sqrt{f'c}}$	C/D (1)	$\frac{v_{ult}(d)}{\sqrt{f'c}}$	C/D (1)
Transverse Direction	Int. Frame	1	4.5	0.78	4.6	0.77	4.5	0.78
		2	7.2	0.49	6.4	0.54	6.7	0.52
		3	4.5	0.78	5.5	0.64	4.5	0.78
		4	9.1	0.38	7.0	0.50	7.9	0.44
	Ext. Frame	1	4.5	0.78	3.3	1.07	4.5	0.78
		2	6.9	0.51	5.1	0.68	5.7	0.61
		3	4.5	0.78	3.6	0.97	4.5	0.78
		4	9.0	0.39	5.8	0.60	7.2	0.48
Longitudinal Direction		1	3.8	0.92	3.6	0.96	3.8	0.92
		2	5.4	0.65	4.2	0.83	4.6	0.76
		3	5.4	0.65	4.9	0.72	4.6	0.76
		4	4.5	0.78	5.5	0.63	2.9	1.22
		5	3.8	0.92	4.0	0.86	3.8	0.92
		6	6.6	0.53	5.4	0.64	5.9	0.60
		7	6.6	0.53	5.6	0.62	5.9	0.60
		8	4.6	0.75	5.9	0.59	2.9	1.22

(1) $v(c) = 3.5\sqrt{f'c}$
 $f'c = 5400$ psi

CHAPTER 10

PILE-SUPPORTED FOOTINGS

The unit selected for this evaluation (Bents 109 thru 112) is supported by footings with the geometries shown in Figure 10.1. The footings along the west side of the unit were typical for both the east and west sides of the typical 184-foot units, while the footings along the east side were used only for this particular unit to avoid an obstruction. Both the west- and east-side footings were evaluated in this chapter, but the results for the west-side footings are more important because they represent the majority of the footings along the City-of-Seattle Designed section.

The four footings vary in plan dimensions as shown in Figure 10.1. The footings are 2.5-feet thick and the pedestals are 2.0-feet thick (Figure 10.2). The footings are reinforced with a bottom mat of steel. The reinforcement ratios vary from 0.3 to 0.6 percent in the transverse direction and from 0.1 to 0.8 percent in the longitudinal direction. The reinforcing bars have 180° hooks at both ends.

The footings are supported on 14-inch diameter cast-in-place concrete piles. The number of piles at each footing varies from fourteen at an exterior footing to twenty at an interior footing. The piles are embedded 12 inches into the footings, but no steel connects the piles to the footings.

The seismic vulnerability of each footing was evaluated in the transverse direction only. Each footing was evaluated for flexural and shear failures near the face of the columns and near the face of the pedestal. Each column-to-footing joint was also evaluated for joint shear failure.

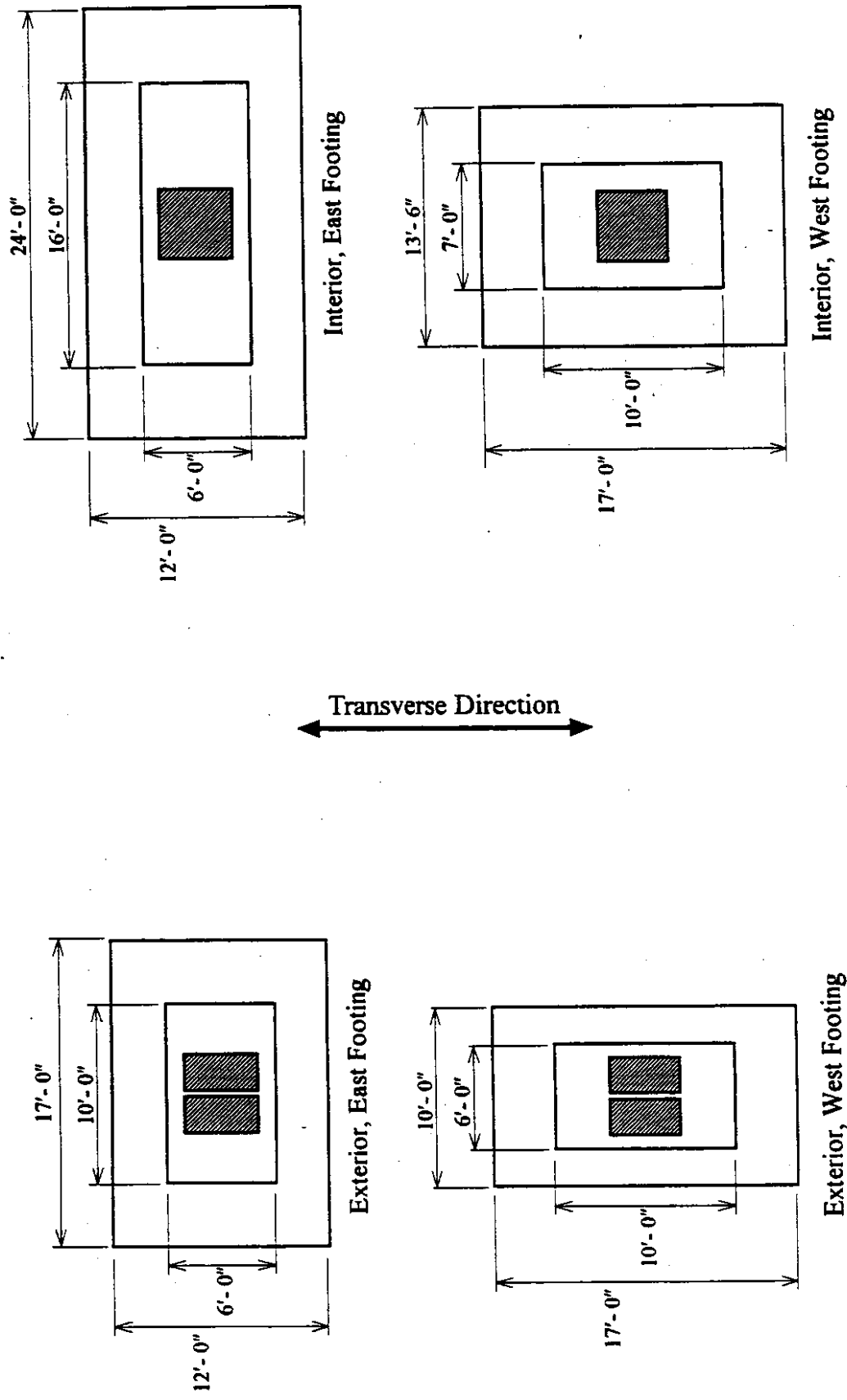


Figure 10.1. Footing Configurations and Plan Dimensions

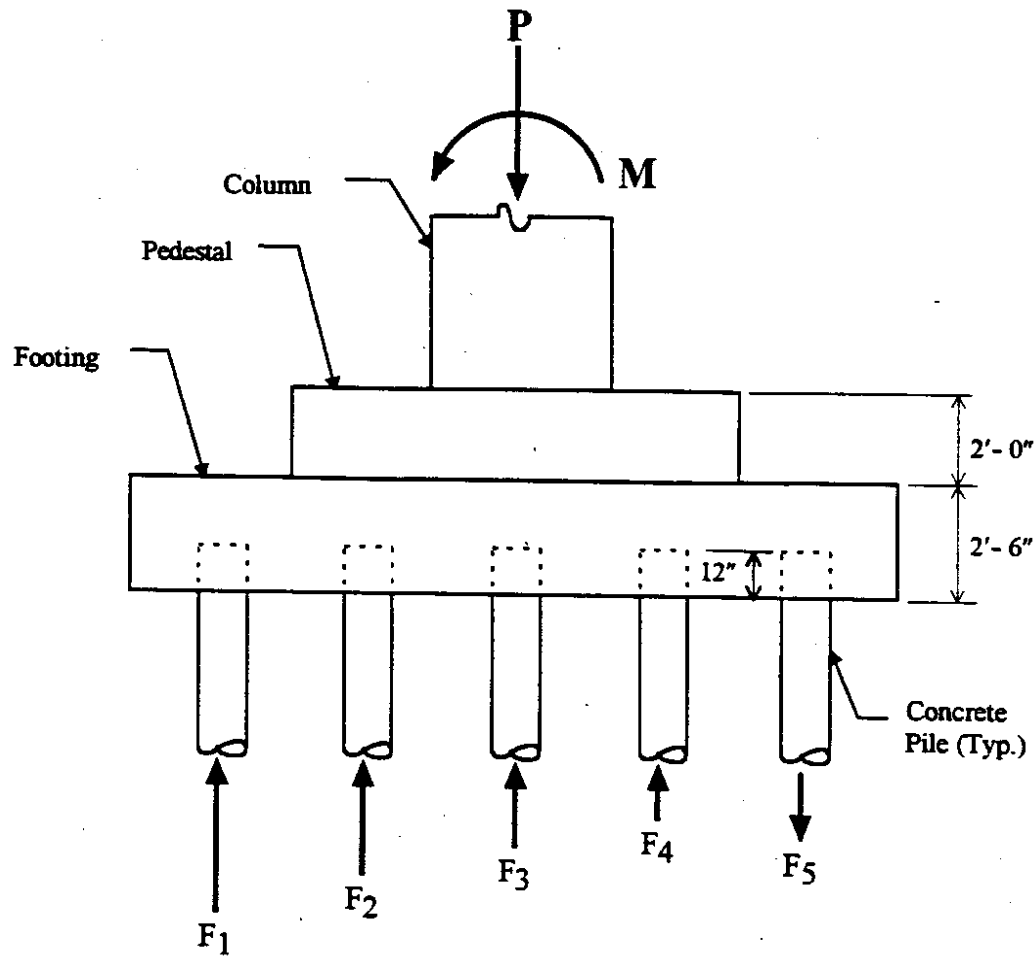


Figure 10.2. Typical SED Unit Footing

10.1 PILE FORCES

To compute the footing internal forces, it was necessary to determine the pile axial forces. The assumptions made to estimate the pile forces for the WSDOT unit were repeated for this evaluation and are listed below (Eberhard et al., 1995).

- The footings were rigid.
- The soil resistance beneath the footings was neglected.
- The pile stiffnesses were linear.

- The applied transverse moments were equal to the flexural capacity of an interior column, or were equal to twice the flexural capacity of an exterior column.
- The applied axial loads included the gravity and seismic axial forces from the columns, the weight of the footings, and the weight of the soil above the footings.

To find an upper-bound of the tensile forces in the piles, it was assumed the pile-to-footing connections were infinitely strong in tension. The applied footing loads and the resulting pile forces are listed in Table 10.1. Tensile forces were present in the last row of piles for each footing, including the compression-side footings. The magnitudes ranged from 23 to 85 kips of tensile force per pile. In comparison, the pile's tensile strength would be 77 kips if the concrete tensile strength were 500 psi.

Table 10.1. Pile Forces - Assuming Connections Have Tensile Capacity

		Exterior Frame				Interior Frame			
		West		East		West		East	
		Comp.	Tens.	Comp.	Tens.	Comp.	Tens.	Comp.	Tens.
Ultimate Moment [k-ft]		6360	6000	6360	6000	7800	6700	7800	6700
Column Axial Load [kips]		1380	640	1421	681	1540	620	1592	672
Pile Forces [kips/pile] (# of Piles/Row)	Row 1	-220(3)	-160(3)	-243(5)	-182(5)	-188(4)	-127(4)	-203(7)	-140(7)
	Row 2	-159(3)	-103(3)	-102(4)	-49(4)	-133(4)	-79(4)	-80(6)	-34(6)
	Row 3	-98(2)	-46(2)	40(5)	85(5)	-77(4)	-31(4)	44(7)	73(7)
	Row 4	-38(3)	11(3)	-	-	-21(4)	17(4)	-	-
	Row 5	23(3)	69(3)	-	-	34(4)	65(4)	-	-

Note: + Tension, - Compression

The pile-to-footing connections would not likely develop the tensile forces listed in Table 10.1. As a lower-bound on the pile tensile resistance, the connections were assumed to have no tensile capacity, and the pile forces were reevaluated. Table 10.2 lists the results. For the tension-side footings and for one compression-side footing (the east-side footing of an interior bent), all but the first row of piles failed in tension. As a consequence, the footings would likely "rock" within the first few load reversals. Once these piles pulled out of a footing, the maximum footing moment was limited to the

product of the column axial force and the moment arm between the column centerline and the centerline of the outside row of piles.

Either the east- or west-side footings could initially be subject to the seismic compressive forces. Therefore, each footing was evaluated using the compression-side loads.

Table 10.2. Pile Forces - Assuming Connections Have No Tensile Capacity

		Exterior Frame				Interior Frame			
		West		East		West		East	
		Comp.	Tens.	Comp.	Tens.	Comp.	Tens.	Comp.	Tens.
Ultimate Moment [k-ft]		6360	4470 ⁽¹⁾	6360	3060 ⁽¹⁾	7800	4340 ⁽¹⁾	7150 ⁽¹⁾	3020 ⁽¹⁾
Column Axial Load [kips]		1380	640	1421	681	1540	620	1592	672
Pile Forces [kips/pile] (# of Piles/Row)	Row 1	-231(3)	-213(3)	-283(5)	-136(5)	-214(4)	-155(4)	-227(7)	-96(7)
	Row 2	-158(3)	0	-2(4)	0	-128(4)	0	0	0
	Row 3	-86(2)	0	0	0	-42(4)	0	0	0
	Row 4	-14(3)	0	-	-	0	0	-	-
	Row 5	0	0	-	-	0	0	-	-

⁽¹⁾ Max. Moment limited by pile pull out

Note: + Tension, - Compression

10.2 FLEXURE

Each footing was evaluated for flexural failure by computing flexural capacity-to-demand ratios near the face of the pedestal and near the face of the column. The flexural demands were computed from the compression-side pile forces listed in Table 10.2. The footing yield and ultimate flexural capacities were computed by assuming a rectangular compressive stress distribution for the concrete (ACI 318-89, 1989). The effective width, b_e , was taken as the sum of the column's width and twice the footing's effective depth as recommended by Priestley et al. (1992). The compressive strength of the concrete was taken as 1.5 times the specified strength of 3600 psi and the ultimate concrete strain was taken to be 0.005. The reinforcement properties are listed in Table 4.1.

The capacities, demands, and C/D ratios for each footing are listed in Table 10.3. The C/D ratios predict that the west footings will not reach their ultimate capacities, but

they are likely to yield near the column face. In contrast, the east footings are likely to exceed their ultimate capacities near the face of the pedestal.

Table 10.3. Footing Flexural C/D Ratios - Transverse Direction

Location		Exterior Frame		Interior Frame	
		West	East	West	East
Face of Pedestal	Md (kip-ft)	1383	2120	1715	2352
	My (kip-ft)	1677	1107	1992	1107
	<i>CD</i>	1.21	0.52	1.16	0.47
	Mu (kip-ft)	2528	1959	3008	1959
	<i>CD</i>	1.83	0.92	1.75	0.83
Face of Column	Md (kip-ft)	4171	3533	5060	3920
	My (kip-ft)	3276	2114	3908	2114
	<i>CD</i>	0.79	0.60	0.77	0.54
	Mu (kip-ft)	5251	3751	6181	3751
	<i>CD</i>	1.26	1.06	1.22	0.96

10.3 SHEAR

Shear failure was evaluated in a similar manner as the flexural evaluation. Capacity-to-demand ratios were computed for both the section near the face of the pedestal and the section near the face of the column. The shear demands were computed with the compression-side pile forces from Table 10.2. The shear capacities were estimated with the following equation (ACI-ASCE Committee 426, 1974):

$$V_c = (0.85 + 120\rho_w)\sqrt{f'_c} (b_e d) \quad (10.1)$$

where

$$0.85 + 120\rho_w \leq 2.4.$$

The computed shear demands, capacities, and C/D ratios are listed in Table 10.4. The C/D ratios indicate that all the footings are likely to fail in shear. All the west footings had C/D ratios close to 0.55 at both cross-sections. The C/D ratios for the east footings were 50 percent lower than those of the west footings, and were lowest at the footing cross-section.

Table 10.4. Footing Shear C/D Ratios - Transverse Direction

Location		Exterior Frame		Interior Frame	
		West	East	West	East
Face of Pedestal	Vd (kips)	692	1413	858	1568
	Vc (kips)	389	370	467	370
	<i>C/D</i>	0.56	0.26	0.54	0.24
Face of Column	Vd (kips)	1167	1413	1371	1568
	Vc (kips)	616	619	748	619
	<i>C/D</i>	0.53	0.44	0.55	0.39

10.4 COLUMN-TO-FOOTING JOINTS

The column-to-footing joints were evaluated for shear failure by computing *C/D* ratios for the maximum tensile stress within the joint. The maximum tensile stress demands were computed from the state of stress created by the vertical shear and vertical compressive stresses from the columns' flexural and axial forces. The tensile stress capacity was assumed to be $3.5\sqrt{f'_c}$, which is the stress at which the joint begins to deteriorate (Priestley et al., 1992).

The footing's vertical joint shear force generated by the column moment was taken as the column's ultimate moment capacity divided by its effective depth. The joint shear area was assumed to be the footing's effective depth times its effective width. The footing's effective width was taken as the sum of the column width and the footings effective depth.

The joints' vertical compressive forces were equal to the column axial forces from the non-linear analyses, and included the effects of gravity and seismic loads. Both cases where the seismic loads add and subtract from the gravity loads were considered in this evaluation. The compressive force area was assumed to be a rectangular area with side dimensions equal to the columns' plan dimensions plus the footings effective depth.

The results of the joint shear evaluation, listed in Table 10.5, indicate that the joints are vulnerable to shear failure. The maximum tensile stresses ranged from $4.3 \sqrt{f'c}$ to $5.6 \sqrt{f'c}$, and the C/D ratios ranged from 0.62 to 0.81.

Table 10.5. Column-To-Footing Joint Shear C/D Ratios

	Exterior Frame				Interior Frame			
	West		East		West		East	
	Comp.	tens.	Comp.	tens.	Comp.	tens.	Comp.	tens.
Column Axial Force (kips)	1170	430	1170	430	1340	420	1340	420
Effective Joint Area (in. ²)	9480	9480	9700	9700	9430	9430	9700	9700
Comp. Stress (psi)	123	45	121	44	142	45	138	43
Max. Col. Moment (k-ft.)	6360	6000	6360	6000	7800	6700	7800	6700
Effective Col. Depth (in.)	41	41	41	41	41	41	41	41
Joint Shear Force (kips)	1861	1758	1861	1758	2283	1961	2283	1961
Effective Joint Width (in.)	97.5	97.5	98.5	98.5	97	97	98.5	98.5
Effective Joint Depth (in.)	49.4	49.4	50.5	50.5	49.1	49.1	50.5	50.5
Vert. Jt. Shear Stress (psi)	387	365	374	353	479	412	459	394
Max. Jt. Shear Stress (psi)	392	365	379	354	484	412	484	395
f_{max} (psi)	330	343	319	332	413	390	395	373
$f_{max}/\sqrt{f'c}$	4.5	4.7	4.3	4.5	5.6	5.3	5.4	5.1
C/D	0.78	0.75	0.81	0.78	0.62	0.66	0.65	0.69

CHAPTER 11

RECOMMENDATIONS

The typical SED unit's geometry and reinforcing details combine to make it vulnerable to a number of seismic failure modes. The vulnerabilities, the consequences of failure, and possible retrofit measures for each failure mode are discussed in Section 11.1. Section 11.2 prioritizes the failure modes based on their likelihood, consequence and cost of suppressing them. Section 11.3 discusses and contrasts the main differences between the typical SED and WSDOT units.

11.1 VULNERABILITIES

The results from both the ATC-6-2 procedure and Priestley et al. (1992) procedure (UCSD) were combined to assess the seismic vulnerabilities of the typical SED unit. Two response spectra were considered: a soft-soil response spectrum from ATC-6 with a peak ground acceleration of 0.25g, and a site-specific response spectrum. Column shear, anchorage, splice, joint shear and footing failures were found to be possible failure modes. Each of these failure modes, their consequences of failure, and possible retrofit ideas are discussed in the following paragraphs.

Column Shear Failure

Both assessment procedures predicted that the lower-story, interior columns were vulnerable to shear failure. The UCSD procedure found that these columns would fail in shear after they yield in flexure, while the ATC-6-2 procedure found that these columns would fail in shear before they yield. In addition, the UCSD procedure found that the lower-story, exterior columns were vulnerable in the transverse direction.

Column shear failure must be prevented because it can cause the structure to collapse suddenly. Possible retrofits include full-height steel, fiberglass, or carbon fiber jackets. If the retrofit measures increase the strength of the lower-story columns enough,

the demands in the upper-story columns could increase to the point where the upper-story columns are vulnerable to shear failure.

Anchorage Failure

The Priestley et al. (1992) procedure predicted that the transverse beam's positive moment reinforcement that is anchored into the columns may be slightly vulnerable to pull-out. The ATC-6-2 procedure predicted that all the lower-story beams' and girders' positive moment reinforcement are vulnerable to anchorage failure, but the ATC-6-2 procedure does not include the effects of confinement provided by the column reinforcement. Therefore, the Priestley et al. (1992) procedure is probably more realistic.

Anchorage failure of the beams' positive moment reinforcement could lead to a loss of flexural strength in the beams, but would not likely lead to collapse.

Splice Failure

Lap splices were only used at locations 2 and 3 of the lower-story, interior columns. Even though these splices are located away from the column bases and the lower-story joints, they are, unfortunately, located where the column capacities decrease sharply and where plastic hinges are likely to form. Both assessment procedures found these splices to be vulnerable.

Lap splice failure can lead to decreased flexural and shear capacities of the lower-story, interior columns and can lead to permanent structural damage or even collapse. Fortunately, the retrofit measures for insufficient lap splices would be the same as for column shear. The same column jackets used to prevent column shear would also prevent lap splice failure.

The welded splices located near mid-height of the lower-story columns in both the interior and exterior bents are not likely to fail for two reasons: first, the splices are located near the columns' inflection points where the flexural demands are small, and second, the splices are staggered.

Joint Shear Failure

All the joints of the typical SED unit have no shear reinforcement and were found to be vulnerable to joint shear failure. Joint shear can lead to collapse of the structure. Possible retrofits include prestressing the joints or encasing them in carbon fiber wraps. Although not considered in this study, the joints in the outrigger bents are likely to be particularly vulnerable. Their vulnerability should be investigated.

Footing Failure

The footings were found to be vulnerable to shear and joint shear failures. The consequences of footing failure may include permanent vertical, lateral, and rotational displacements that could render the structure unserviceable. It is unlikely that a footing failure will result in collapse. Retrofits for the footings would likely be expensive and difficult to design because of the degree of soil liquefaction expected (Kramer et al., 1995).

11.2 RETROFIT PRIORITIES

A priority rating scheme similar to one used to for the evaluation of the WSDOT unit (Eberhard et al., 1995) is presented in this section.

For each failure mode, relative ratings ranging from 1 to 4 are assigned for the likelihood of failure, the consequence of failure, and the cost of retrofitting. A rating of "1" indicates that a failure mode is likely to occur, the consequence of failure is severe, and the cost of retrofitting is relatively low. These three ratings are considered together to assign the retrofit priority rating. The priority ratings range from 1 to 4, with a rating of "1" being the highest priority.

The ratings are listed in Table 11.1. The consequence and cost ratings are the same as those used in the evaluation of the WSDOT unit. Therefore, the differences in the retrofit priorities between the SED and WSDOT units are due to differences in the likelihood of failure.

Table 11.1. Priority Ratings for Retrofit Measures

Location	Failure Mode	Likelihood	Consequence	Cost	Priority
Columns	Flexure	4	4	2	1
	Shear	1	1	2	
Joints	Diagonal Tension	1	1	3	1
	Anchorage	3	3	3	
Lower-Story Lap Splices	Flexure	2	2	1	2
	Shear	?	1	1	
Pile Supported footings	Shear	1	2	3	3
	Joint Shear	2	2	3	
	Anchorage	-	-	-	
Upper-Story Lap Splices	Flexure	-	-	-	N/A
	Shear	-	-	-	

The highest retrofit priorities for the SED unit are for joint and column shear failures, both with priority ratings of "1." Next on the retrofit priority list are the lower-story lap splices. Finally, footing failure is last on the priority list with a rating of 3.

11.3 COMPARISON WITH TYPICAL WSDOT UNIT

The typical SED and WSDOT units have similar span lengths, bent widths, bent elevations, column sizes, and weights. Consequently, both typical units have similar mode shapes and periods of vibration. For a response spectrum analysis using the same response spectrum, both typical units have similar spectral accelerations and relative drift ratios. On the other hand, the seismic vulnerabilities of each typical unit are quite different, and these differences stem mainly from differences in reinforcement details, material properties, and horizontal framing members.

The following sections discuss the important differences between the two typical units and the effects they have on each failure mode. The order in which the failure modes are discussed below follows the order in which they appear in Table 11.1.

Columns

The SED columns are less vulnerable in flexure than the WSDOT columns for two reasons. First, the SED columns have higher flexural capacities than the WSDOT columns because they are more heavily reinforced. Second, the plastic hinges form beam/column failure mechanisms in the SED frames that distribute the flexural yielding throughout the frames. The WSDOT frames fail with lower-story mechanisms that concentrate the flexural deformation at the lower-story columns.

The downside of having higher flexural capacities is that the SED unit's lower-story columns are more vulnerable to shear failure than those of the WSDOT unit. Because the consequences of shear failure are so great, column retrofits for both the SED and WSDOT units were given an overall priority rating of "1."

Joints

The joints of both the WSDOT and SED units were found to be vulnerable to shear failure, and both were assigned retrofit priority ratings of "1." In the transverse direction, the joint shear stresses in the SED unit were higher than those of the WSDOT unit. The opposite was true in the longitudinal direction. The difference occurred because of differences in the horizontal framing systems. The SED unit has strong transverse beams and relatively weak longitudinal girders, while the opposite is true for the WSDOT unit.

Lower-Story Lap Splices

The lower-story longitudinal bars of the WSDOT unit are lap spliced to the footing bars directly above the footings where the flexural demands are highest. These splices were found to be vulnerable and were assigned a retrofit priority of "1" for the WSDOT section (Eberhard et al., 1995). In contrast, the lower-story column bars of the SED unit are spliced at locations 2 and 3 in the interior columns only (Chapter 8). These splice locations are away from the footings and the highest flexural demands. In addition, only two-thirds of the longitudinal bars are lap spliced at each location. Unfortunately, the

splices are located where the column capacities drop significantly and where plastic hinges are likely to form. These splices were also found to be vulnerable, but they are less likely to fail than the lower-story lap splices of the WSDOT unit. Consequently, the SED unit splices were assigned a retrofit priority of “2.”

Footings

The footings of the SED and WSDOT units differ in appearance; the SED footings have a pedestal while the WSDOT footings have a uniform thickness. Both are reinforced with a bottom mat of steel only. Both footings were found to be vulnerable to shear failure, and both column-to-footing joints were found to be vulnerable to joint shear failure.

The most important difference between the SED and WSDOT footings is the anchorage of the vertical column reinforcement into the footings. The WSDOT column bars are hooked outward into the footings and are vulnerable to anchorage failure. The SED column bars are welded to “grillages” that are embedded into the footings. Although the effectiveness of the “grillages” was not evaluated, they provide more anchorage than an outwardly hooked bar.

Upper-Story Lap Splices

The WSDOT unit’s upper-story column reinforcement is lap spliced directly above the lower-story deck. Even though the likelihood of failure is small, the consequences of failure are severe enough to warrant a retrofit priority rating of “2.”

In contrast, there are no lap splices in the SED unit’s upper-story columns. Some bars are spliced with welds, but they are located at the columns’ inflection points where the force demands are likely to be small. These splices are not likely to fail.

ACKNOWLEDGMENTS

The writers are grateful for the support of colleagues at the University of Washington. In particular, Associate Professor S.L. Kramer and Dr. N. Nadarajah developed the site-specific response spectra for the viaduct. This report was prepared with the assistance of TRAC staff members S. MacLaughlin, A. O'Brien, and R. Porter.

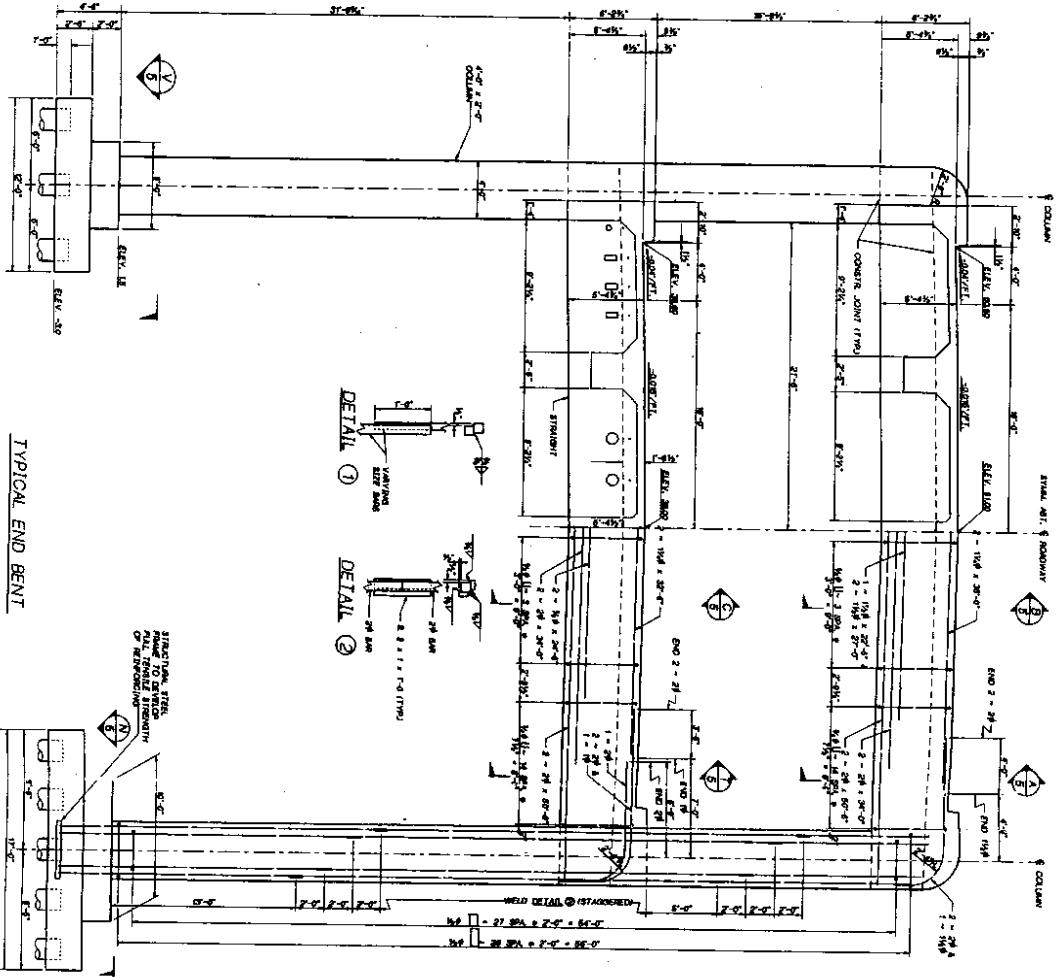
This project was funded by the Washington State Department of Transportation. Senior Structural Engineer Timothy Moore served as technical contact. Structural plans were reproduced by Detailer D. Pulse.

REFERENCES

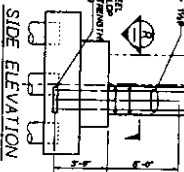
- American Concrete Institute. (1989). *Building Code Requirements for Reinforced Concrete (ACI-319-89)*. American Concrete Institute. Detroit.
- Applied Technology Council. (1981, October). *Seismic Design Guidelines For Highway Bridges (ATC-6)*. Redwood City, California.
- Applied Technology Council. (1983, August). *Seismic Retrofitting Guidelines for Highway Bridges (ATC-6-2)*. Redwood City, California.
- Brown, C. B., Eberhard, M. O., Kramer, S. L., Roeder, C. W., and Stanton, J. F. (1992, April). "Preliminary Investigation of the Seismic Vulnerability of the Alaskan Way Viaduct." WA-RD 265.1. Washington State Department of Transportation, Olympia.
- Corley, W. G. (1966, October). Rotational Capacity of Reinforced Concrete Beams. *Journal of the Structural Division, ASCE*. pp. 121-146.
- Dodson, J., Rochelle, S. G., and Stoddard, R. B. (1990, May). "Earthquake Analyses of the Alaskan Way Viaduct." Executive Summary. Washington State Department of Transportation, Olympia.
- Eberhard, M. O., De la Colina, J., and Ryter, S. (1995, June). "Seismic Vulnerability of the Alaskan Way Viaduct: WSDOT Typical Unit." WA-RD 363.1. Washington State Department of Transportation, Olympia.
- Kramer, S. L. and Eberhard, M. O. (1995, July). "Seismic Vulnerability of the Alaskan Way Viaduct: Summary Report." WA-RD 363.4. Washington State Department of Transportation, Olympia.
- Hershman, M. J., Heikkala, S., and Tobin, C. (1981). *Seattle's Waterfront: "A Walker's Guide to the History of Elliott Bay."* Institute for Marine Studies, University of Washington, Seattle.
- Kent, C. D., and Park, R. (1971, July). "Flexural Members with Confined Concrete." *Journal of the Structural Division, ASCE*. pp. 1969-1990.
- Kramer, S. L., Sivaneswaran, N., and Tucker, K. N. (1995, July). "Seismic Vulnerability of the Alaskan Way Viaduct: Geotechnical Engineering Aspects." WA-RD 363.2. Washington State Department of Transportation, Olympia.
- McLean, D. I. 1994. "Seismic Retrofitting of Bridge Substructures." Report to be published by Washington State Department of Transportation, Olympia.
- Park, R., and Paulay, T. (1975). *"Reinforced Concrete Structures."* John Wiley and Sons, Inc. New York, N.Y. 769 pp.
- Priestley, M. J. N., Seible, F., and Chai, Y. H. (1992, August). "Design Guidelines for Assessment Retrofit and Repair of Bridges for Seismic Performance." Report No. SSRT-92/01. Department of Applied Mechanics and Engineering Sciences. University of California, San Diego.

- Priestley, M. J. N., Seible, F., and Uang, C.-M. (1994, February). "The Northridge Earthquake of January 17, 1994," Report No. SSRP-94/06. Department of Applied Mechanics and Engineering Sciences. University of California, San Diego.
- Priestley, M. J. N., and Park, R. (1987, January-February). "Strength and Ductility of Concrete Bridge Columns Under Seismic Loading." *ACI Structural Journal*. pp. 61-76.
- Ryter, S. (1994, March). Seismic Vulnerability of the Alaskan Way Viaduct. *In partial fulfillment of the requirements for the degree of Master of Science in Civil Engineering*. University of Washington, Seattle.
- Thewalt, C., and Stojadinvic, B.. (1992, July). "Behavior and Retrofit of Bridge Outrigger Beams." *Proceedings, 10th World Conference on Earthquake Engineering*. Madrid, Spain
- Wilson, E. L., and Habibullah, A. (1988). Sap90 5.04 Owners Manual. Computers and Structures, Inc., Berkeley, California.

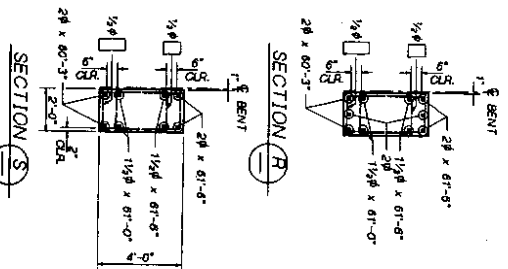
Appendix A
Structural Drawings of Typical SED Unit



TYPICAL END BENT



SIDE ELEVATION



PROJECT NO.	109 & 112
DATE	4-27-55
REVISION	
BY	
CHECKED BY	
DESIGNED BY	
BRIDGE PROJECT NO.	
BRIDGE NO.	
SECTION	

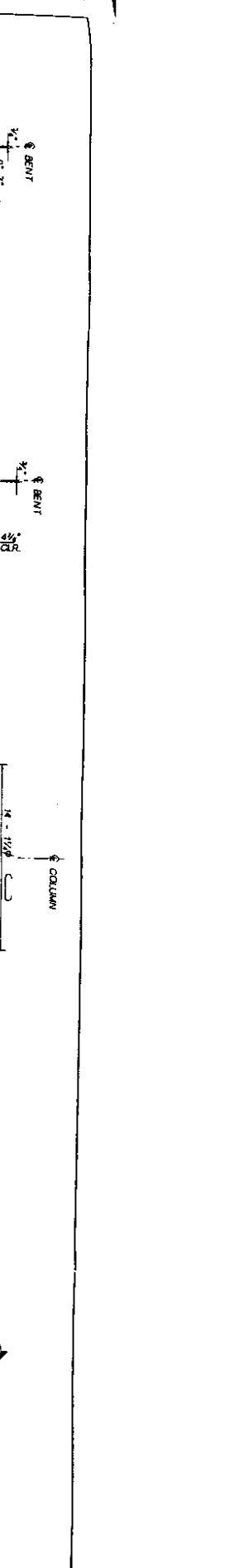
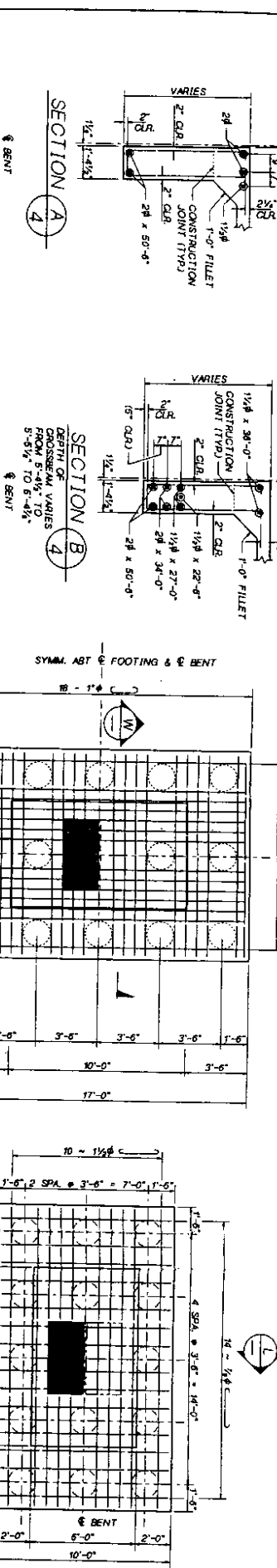
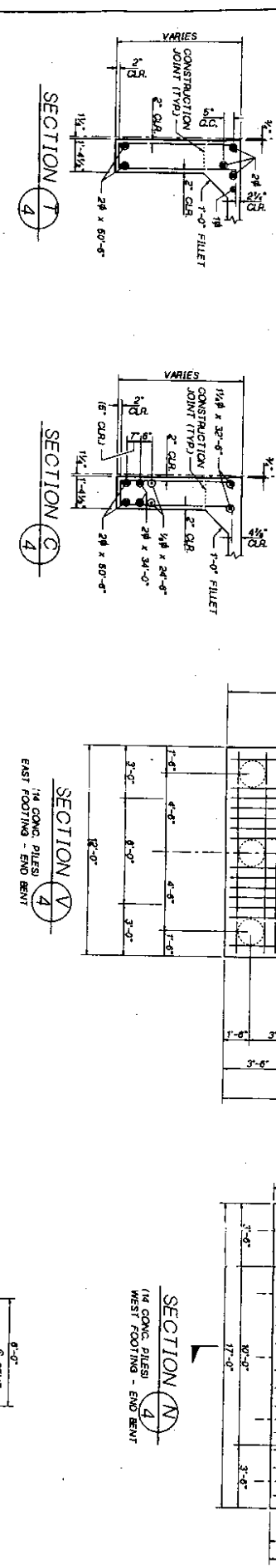
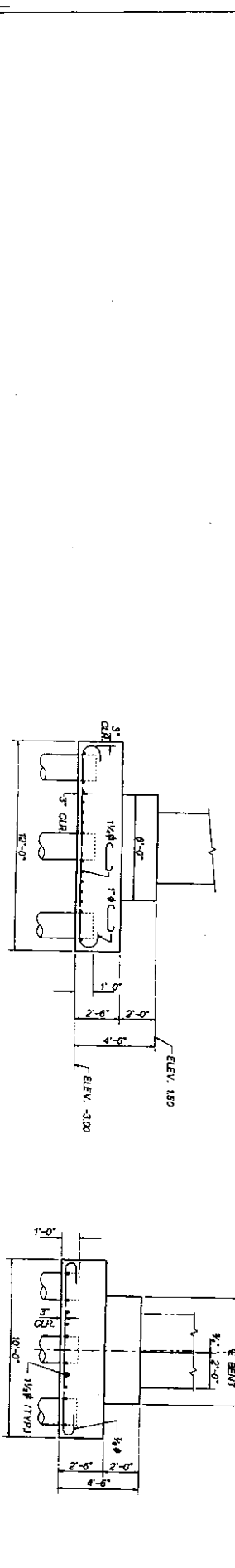
NO.	10
W.A.S.H.	
JOB NUMBER	
DATE	

WASHINGTON STATE
Department of Transportation

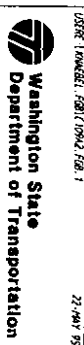
CITY OF SEATTLE
ALASKAN WAY VIADUCT
END BENTS
BENTS 109 & 112

PROJECT NO.	DATE	BY	CHKD.	APP'D.
10	1/21/55	WASH		
11				
12				
13				
14				
15				
16				
17				
18				
19				
20				
21				
22				
23				
24				
25				
26				
27				
28				
29				
30				
31				
32				
33				
34				
35				
36				
37				
38				
39				
40				
41				
42				
43				
44				
45				
46				
47				
48				
49				
50				

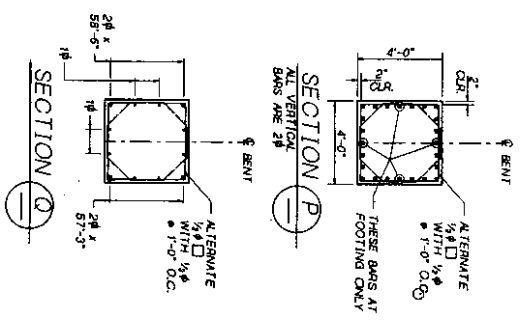
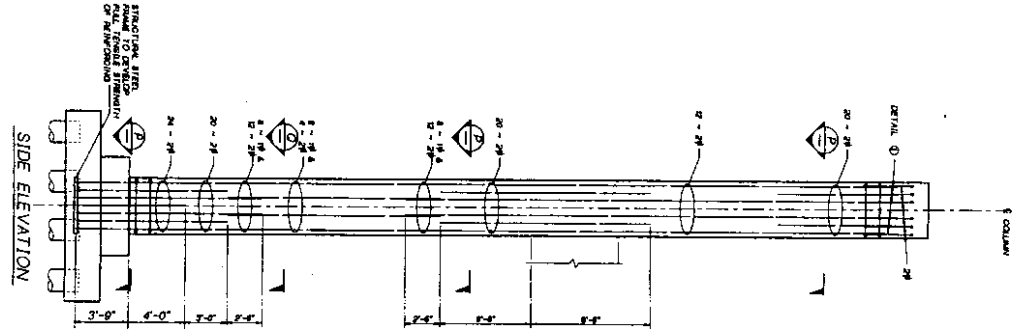
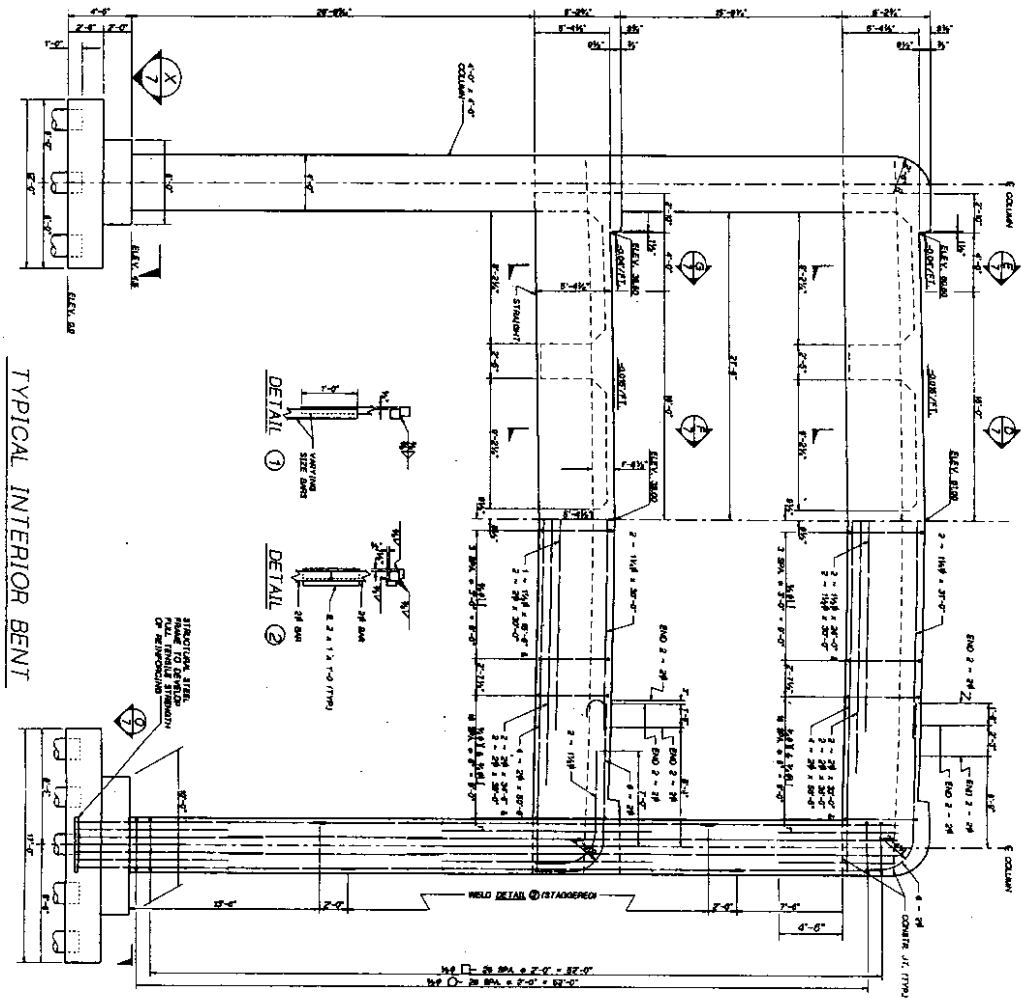
PROJECT NO. 10
 DATE 1/21/55
 BY WASH
 CHECKED BY
 DRAWN BY
 APPROVED BY
 TITLE
 PROJECT NAME
 CITY OF SEATTLE
 ALASKAN WAY VIADUCT
 END BENT DETAILS



SECTION T
 SECTION A
 SECTION B
 SECTION C
 SECTION V
 SECTION W
 SECTION L
 SECTION 4



CITY OF SEATTLE
 ALASKAN WAY VIADUCT
 END BENT DETAILS



Project Name	101 WASH
Job Number	101 WASH
Scale	AS SHOWN
Revision	
Drawn By	
Checked By	
Approved By	

Sheet No.	101 WASH 0
Sheet Count	101 WASH 0
Sheet Title	101 WASH 0

Washington State Department of Transportation

22-441 95

CITY OF SEATTLE
ALASKAN WAY VIADUCT
INTERIOR BENT
BENTS 110 & 111

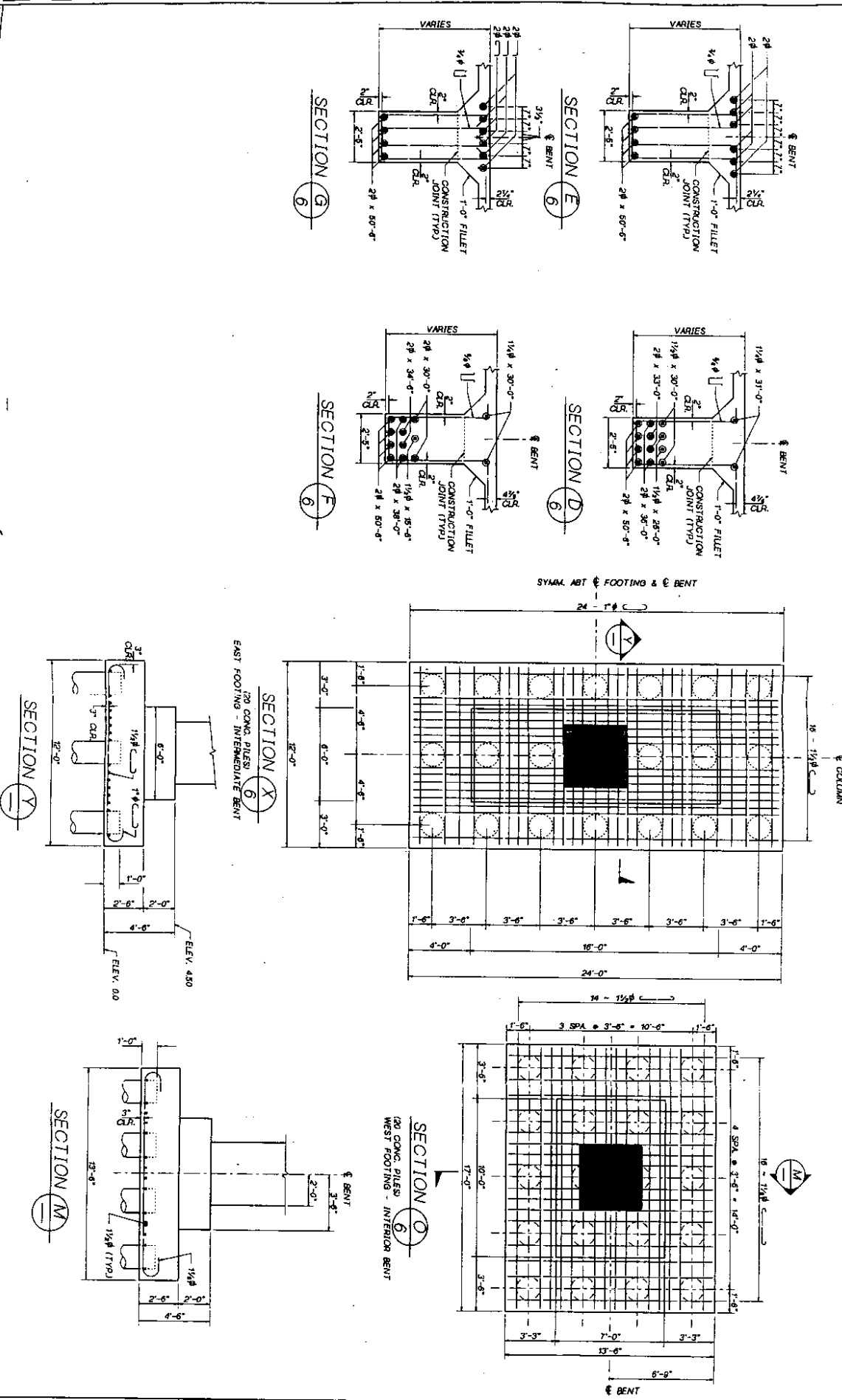
DESIGNED BY	CHALLENGER
CHECKED BY	CHALLENGER
IN CHARGE	CHALLENGER
DATE	10/11/95

NO.	DATE	BY	REVISION
1	10/11/95	CHALLENGER	ISSUE FOR CONSTRUCTION

PROJECT	INTERIOR BENT
LOCATION	ALASKAN WAY VIADUCT
DATE	10/11/95


Washington State Department of Transportation
 27 7441 95

CITY OF SEATTLE
 ALASKAN WAY VIADUCT
 INTERIOR BENT DETAILS



USGS (NUMBER): 480170962 (201)
 27 7441 95

Appendix B

Calculations of ATC-6-2 Flexural C/D Ratios

Table B.1. Column Flexural C/D Ratios (Transverse Direction)

Location		Seismic Moment Kip-ft	Seismic Axial Force Kips	Gravity Moment Kip-ft	Gravity Axial Force Kips	Total Moment Kip-ft	Total Axial Force Kips	Moment Capacity Kip-ft	Capacity/ Demand
Exterior Frame	1	3289	240	83	343	3372	583	3170	0.94
	2	2377	240	48	337	3206	103	2940	0.92
						2425	577	2640	1.09
	3	1735	240	108	310	2329	97	2280	0.98
						1843	550	2620	1.42
	4	2526	240	139	304	1627	70	2270	1.40
						2665	544	3140	1.18
	5	633	79	465	161	2387	64	2930	1.23
						1098	240	2980	2.71
	6	285	79	297	158	168	82	2940	17.50
						582	237	2360	4.05
	7	770	79	218	148	-12	79	2280	N/A
						988	227	2350	2.38
	8	1319	79	491	142	552	69	2280	4.13
						1810	221	2970	1.64
						828	63	2930	3.54
Interior Frame	1	7705	550	270	953	7975	1503	8050	1.01
	2	3847	550	65	933	7435	403	6800	0.91
						3912	1483	4140	1.06
	3	2250	550	259	901	3782	383	3140	0.83
						2509	1451	4100	1.63
	4	5800	550	451	883	1991	351	3070	1.54
						6251	1433	7110	1.14
	5	996	146	1389	461	5349	333	6010	1.12
						2385	607	6200	2.60
	6	462	146	975	455	-393	315	6000	N/A
						1437	601	4630	3.22
	7	1637	146	666	433	-513	309	4460	N/A
						2303	579	4610	2.00
	8	2665	146	1487	423	971	287	4450	4.58
						4152	569	6170	1.49
						1178	277	5980	5.08

Table B.2. Column Flexural C/D Ratios (Longitudinal Direction)

Location	Seismic Moment	Seismic Axial Force	Gravity Moment	Gravity Axial Force	Total Moment	Total Axial Force	Moment Capacity	Capacity/Demand	
	Kip-ft	Kips	Kip-ft	Kips	Kip-ft	Kips	Kip-ft		
Exterior Columns	1	1133	149	31	343	1164	492	1440	1.24
	2	790	149	18	337	1102	194	1350	1.23
						808	486	1350	1.67
	3	750	149	40	310	772	188	1170	1.52
						790	459	1340	1.70
	4	1028	149	52	304	710	161	1160	1.63
						1080	453	1430	1.32
	5	936	57	162	161	976	155	1330	1.36
						1098	218	1330	1.21
	6	603	57	106	158	774	104	1280	1.65
						709	215	1150	1.62
	7	394	57	67	148	497	101	1100	2.21
						461	205	1150	2.49
	8	904	57	159	142	327	91	1100	3.36
						1063	199	1330	1.25
						745	85	1280	1.72
Interior Columns	1	8926	13	29	953	8955	966	7240	0.81
	2	4469	13	9	933	8897	940	7220	0.81
						4478	946	3620	0.81
	3	2582	13	21	901	4460	920	3600	0.81
						2603	914	3590	1.38
	4	6698	13	39	883	2561	888	3570	1.39
						6737	896	6430	0.95
	5	645	7	82	461	6659	870	6400	0.96
						727	468	6000	8.25
	6	188	7	57	455	563	454	6000	10.66
						245	462	4500	18.37
	7	1828	7	43	433	131	448	4500	34.35
						1871	440	4500	2.41
	8	2761	7	93	423	1785	426	4500	2.52
						2854	430	6000	2.10
						2668	416	6000	2.25

Table B.3. Beam and Girder Flexural C/D Ratios

Member	Deck	Location		Seismic	Gravity	Total	Moment	Capacity/
				Moment	Moment	Moment	Capacity	Demand
				Kip-ft	Kip-ft	Kip-ft	Kip-ft	
Exterior Girder	Bottom	at Ext Col	+	2132	-234	1898	1520	0.80
			-			-2366	-1725	0.73
	Top	at Int Col	+	4095	-750	3345	760	0.23
			-			-4845	-3300	0.68
		at Ext Col	+	1117	-222	895	1520	1.70
			-			-1339	-1725	1.29
Cross- Beam Ext Frame	Bottom	at Int Col	+	1506	-745	761	760	1.00
			-			-2251	-3100	1.38
Cross- Beam Int Frame	Bottom	at Ext Col	+	3782	-490	3292	2600	0.79
			-			-4272	-3800	0.89
	Top	at Ext Col	+	1495	-458	1037	2600	2.51
Cross- Beam Int Frame	Bottom		-			-1953	-4200	2.15
		at Int Col	+	7888	-1523	6365	5000	0.79
	Top		-			-9411	-7300	0.78
		At Int Col	+	2848	-1429	1419	5000	3.52
		-			-4277	-7300	1.71	



Appendix C

Calculations of ATC-6-2 C/D Ratios for All Failure Modes

Table C.1. Column Confinement C/D Ratios (Transverse Direction)

Location	Comp Tension	θ in.	F _{cm} in.	h _c in.	b _c in.	A _c in. ²	N _y in.	345000 psi A _{st} (c) in. ²	A _{st} (t) in. ²	Axial Load Max kips	k ₁	b _m in.	c _b in.	k ₂	k ₃ (in.)	u _{eff} in.	k ₃ (ft)	u	Iterater	Rec	Rec
Exterior Frame	Comp	12	44	44	20	880	1132	0.4	0.43	563	0.07	24	1893	0.40	0.40	2.84	0.41	2.31	0.41	0.84	2.74
	Tension	12	44	44	20	880	1132	0.4	0.43	100	0.06	24	1893	0.40	0.40	2.84	0.41	2.31	0.41	0.84	2.74
	Comp	18	44	44	20	880	1132	0.4	0.43	377	0.07	24	1893	0.40	0.40	2.84	0.41	2.31	0.41	0.84	2.74
	Tension	18	44	44	20	880	1132	0.4	0.43	97	0.06	24	1893	0.40	0.40	2.84	0.41	2.31	0.41	0.84	2.74
	Comp	12	44	44	20	880	1132	0.4	0.43	550	0.07	24	1893	0.40	0.40	2.84	0.41	2.31	0.41	0.84	2.74
	Tension	12	44	44	20	880	1132	0.4	0.43	70	0.06	24	1893	0.40	0.40	2.84	0.41	2.31	0.41	0.84	2.74
	Comp	18	44	44	20	880	1132	0.4	0.43	544	0.07	24	1893	0.40	0.40	2.84	0.41	2.31	0.41	0.84	2.74
	Tension	18	44	44	20	880	1132	0.4	0.43	64	0.06	24	1893	0.40	0.40	2.84	0.41	2.31	0.41	0.84	2.74
Interior Frame	Comp	12	44	44	20	880	1132	0.4	0.43	240	0.08	24	1893	0.40	0.40	2.84	0.41	2.31	0.41	0.84	2.74
	Tension	12	44	44	20	880	1132	0.4	0.43	22	0.08	24	1893	0.40	0.40	2.84	0.41	2.31	0.41	0.84	2.74
	Comp	18	44	44	20	880	1132	0.4	0.43	237	0.08	24	1893	0.40	0.40	2.84	0.41	2.31	0.41	0.84	2.74
	Tension	18	44	44	20	880	1132	0.4	0.43	79	0.08	24	1893	0.40	0.40	2.84	0.41	2.31	0.41	0.84	2.74
	Comp	12	44	44	20	880	1132	0.4	0.43	227	0.08	24	1893	0.40	0.40	2.84	0.41	2.31	0.41	0.84	2.74
	Tension	12	44	44	20	880	1132	0.4	0.43	21	0.08	24	1893	0.40	0.40	2.84	0.41	2.31	0.41	0.84	2.74
	Comp	18	44	44	20	880	1132	0.4	0.43	241	0.08	24	1893	0.40	0.40	2.84	0.41	2.31	0.41	0.84	2.74
	Tension	18	44	44	20	880	1132	0.4	0.43	21	0.08	24	1893	0.40	0.40	2.84	0.41	2.31	0.41	0.84	2.74

Table C.3. Column Shear C/D Ratios (Transverse Direction)

Location	Comp. Tension	Mo1		Mo2		L	Vc(d)	Vc(d)	Vc(d)	b	d	Av	Av	Asd/Load	e	VI	Ac	VI	Column Status	LoBo	Resuff	Key	Reo	Rev
		Kip-ft	Kip-ft	Kip-ft	Kip-ft																			
Ea Trans Columns	1	3170	3140	32.1	32.1	32.1	182	182	24	45	1080	0.4	533	13	0.00	17.2	0.00	CRS B	4	3.82	U	0.04	2.81	
	2	3540	3530	32.1	32.1	32.1	182	182	24	45	1080	0.4	533	13	0.00	17.2	0.00	CRS B	4	3.82	U	0.04	2.81	
	3	3140	3170	32.1	32.1	32.1	182	182	24	45	1080	0.4	544	13	0.00	17.2	0.00	CRS B	4	3.82	U	0.04	2.81	
	4	3530	3540	32.1	32.1	32.1	182	182	24	45	1080	0.4	544	13	0.00	17.2	0.00	CRS B	4	3.82	U	0.04	2.81	
	5	3090	3070	32.1	32.1	32.1	182	182	24	45	1080	0.4	44	13	0.00	17.2	0.00	CRS B	4	3.82	U	0.04	2.81	
Ea Trans Columns	6	3110	3110	32.1	32.1	32.1	182	182	24	45	1080	0.4	307	13	0.00	17.2	0.00	CRS B	4	3.82	U	0.04	2.81	
	7	3110	3110	32.1	32.1	32.1	182	182	24	45	1080	0.4	311	13	0.00	17.2	0.00	CRS B	4	3.82	U	0.04	2.81	
	8	3110	3110	32.1	32.1	32.1	182	182	24	45	1080	0.4	311	13	0.00	17.2	0.00	CRS B	4	3.82	U	0.04	2.81	
	9	3110	3110	32.1	32.1	32.1	182	182	24	45	1080	0.4	311	13	0.00	17.2	0.00	CRS B	4	3.82	U	0.04	2.81	
	10	3110	3110	32.1	32.1	32.1	182	182	24	45	1080	0.4	311	13	0.00	17.2	0.00	CRS B	4	3.82	U	0.04	2.81	
Ea Trans Columns	11	4090	4090	37.1	37.1	37.1	241	241	48	105	1160	0.4	1033	13	0.00	17.2	0.00	CRS B	4	3.82	U	0.04	2.81	
	12	3190	3190	37.1	37.1	37.1	241	241	48	105	1160	0.4	433	13	0.00	17.2	0.00	CRS B	4	3.82	U	0.04	2.81	
	13	4090	4090	37.1	37.1	37.1	241	241	48	105	1160	0.4	1071	13	0.00	17.2	0.00	CRS B	4	3.82	U	0.04	2.81	
	14	3190	3190	37.1	37.1	37.1	241	241	48	105	1160	0.4	461	13	0.00	17.2	0.00	CRS B	4	3.82	U	0.04	2.81	
	15	4090	4090	37.1	37.1	37.1	241	241	48	105	1160	0.4	671	13	0.00	17.2	0.00	CRS B	4	3.82	U	0.04	2.81	
Ea Trans Columns	16	3190	3190	37.1	37.1	37.1	241	241	48	105	1160	0.4	711	13	0.00	17.2	0.00	CRS B	4	3.82	U	0.04	2.81	
	17	3190	3190	37.1	37.1	37.1	241	241	48	105	1160	0.4	711	13	0.00	17.2	0.00	CRS B	4	3.82	U	0.04	2.81	
	18	3190	3190	37.1	37.1	37.1	241	241	48	105	1160	0.4	711	13	0.00	17.2	0.00	CRS B	4	3.82	U	0.04	2.81	
	19	3190	3190	37.1	37.1	37.1	241	241	48	105	1160	0.4	711	13	0.00	17.2	0.00	CRS B	4	3.82	U	0.04	2.81	
	20	3190	3190	37.1	37.1	37.1	241	241	48	105	1160	0.4	711	13	0.00	17.2	0.00	CRS B	4	3.82	U	0.04	2.81	

Table C.5. Anchorage C/D Ratios (Transverse Direction)

Location		End of Bar	la(c) (in.)	la(d) (in.)	la(c)/la(d)	rec	ra
Top of Exterior Columns	+	Straight	57.5	67.7	0.85	1.64	1.39
	-	Straight	57.5	67.7	0.85	3.54	3.01
Top of Interior Columns	+	Straight	57.5	67.7	0.85	1.49	1.27
	-	Straight	57.5	67.7	0.85	5.08	4.31
Lower-Story Exterior Beams	Bottom	Straight	44.0	67.7	0.65	0.79	0.51
	Top	Hooked	46.0	33.9	1.36	0.89	1.00
Upper-Story Exterior Beams	Bottom	Straight	44.0	67.7	0.65	2.51	1.63
	Top	Hooked	46.0	33.9	1.36	2.15	1.00
Lower-Story Interior Beams	Bottom	Straight	44.0	67.7	0.65	0.79	0.51
	Top	Hooked	46.0	33.9	1.36	0.78	1.00
Upper-Story Interior Beams	Bottom	Straight	44.0	67.7	0.65	3.52	2.29
	Top	Hooked	46.0	33.9	1.36	1.71	1.00